TOHOKU
UNIVERSITY

CORE RESEARCH CLUSTER

The 4th Symposium for The Core Research Cluster for Materials Science and the 3rd Symposium on International Joint Graduate Program in Materials Science

"Create New Value of Materials Science through Broad Collaboration"

2020

PROGRAM
SPEAKERS CVs
ABSTRACTS
POSTER ABSTRACTS

Tohoku University

The 4th Symposium for The Core Research Cluster for Materials Science and the 3rd Symposium on International Joint Graduate Program in Materials Science

November 16 (Mon) - 18 (Wed), 2020

As of October 28, 2020

DAY 1	Nov. 16 (Mon)	
JST	Core Research Cluster for Materials Science	GP-MS
9:00	9:00-9:10 Opening Remarks: OHNO Hideo, President of Tohoku University	
9:10	9:10-9:55 Plenary Session ① Chair: KOTANI Motoko ・Byeong-Joo Lee (Pohang University of Science and Technology)	
9:20		
9:30		
9:40		
9:50		
9:55	9:55-10:00 Remarks: YAMAGUCHI Masahiro, Head of the Division for International Joint Graduate School Programs, Tohoku University	
10:00	10:00-10:10 Break (10 min.)	
10:10	10:10-11:40 <Materials Science> Session 1 Chair: FURUHARA Tadashi 1-A. OHTANI Hiroshi (Tohoku University) 1-B. MATSUBAE Kazuyo (Tohoku University) 1-C. ABE Eiji (The University of Tokyo)	
10:20		
10:30		
10:40		
10:50		
11:00		
11:10		
11:20		
11:30		
11:40	Lunch (11:40-13:00)	
11:50		
12:00		
12:10		
12:20		
12:30		
12:40		
12:50		
13:00	13:00-14:30 <Materials Science> Session 2 Chair: YOSHIMI Kyosuke 2-A. Qiang Charles Feng (University of Science and Technology Beijing) 2-B. OHMURA Takahito (National Institute for Materials Science) 2-C. NOMURA Naoyuki (Tohoku University)	
13:10		
13:20		
13:30		
13:40		
13:50		
14:00		14:00-16:00 <GP-MS> Student Session 1 Chair: KOSABA Takumi 1-A. Ying Jin (University of Science and Technology Beijing) 1-B. HIROMOTO Sachiko (National institute for Materials Science) 1-C. KOSABA Takumi (Tohoku University)
14:10		
14:20		
14:30	14:30-14:50 Break (20 min.)	
14:40		
14:50	14:50-16:20 <Materials Science> Session 3 Chair: HIRANO-IWATA Ayumi 3-A. KURIYAGAWA Tsunemoto (Tohoku University) 3-B. UMETSU Mitsuo (Tohoku University) 3-C. Yi-tao Long (Nanjing University)	
15:00		
15:10		
15:20		
15:30		
15:40		
15:50		
16:00		16:00-16:40 Break(40min.)
16:10		
16:20	16:20-16:40 Break (20 min.)	
16:30		
16:40	16:40-17:25 Plenary Session ② Chair: FURUHARA Tadashi ・Dierk Raabe (Max-Planck-Institut für Eisenforschung GmbH)	
16:50		
17:00		
17:10		
17:20		
17:30	17:25-18:10 Plenary Session ③ Chair: ORIMO Shin-ichi ・Hans-Joachim Freund (Fritz-Haber-Institut der Max-Planck-Gesellschaft)	
17:40		
17:50		
18:00		

TOHOKU
UNIVERSITY

The 4th Symposium for The Core Research Cluster for Materials Science and the 3rd Symposium on International Joint Graduate Program in Materials Science

November 16 (Mon) - 18 (Wed), 2020

CORE RESEARCH CLUSTER

DAY 2	Nov. 17 (Tue)	
JST	Core Research Cluster for Materials Science	GP-MS
10:00	10:00-11:30 <Materials Science> Session 4 Chair: ORIMO Shin-ichi 4-A. MIZUGUCHI Masaki (Nagoya University) 4-B. EINAGA Mari (Osaka University) 4-C. AKAGI Kazuto (Tohoku University)	
10:10		
10:20		
10:30		
10:40		
10:50		
11:00		
11:10		
11:20		
11:30	Lunch (11:30-13:00)	
11:40		
11:50		
12:00		
12:10		
12:20		
12:30		
12:40		
12:50		
13:00	Poster Session (13:00-15:00)	Poster Session (13:00-15:00)
13:10		
13:20		
13:30		
13:40		
13:50		
14:00		
14:10		
14:20		
14:30		
14:40		
14:50		
15:00		
15:10		
15:20		
15:30		
15:40		
15:50		
16:00		
16:10		
16:20		
16:30		
16:40		
16:50		
17:00		17:00-19:00 <GP-MS> Student Session 2 Chair: YAMAGUCHI Mina 2-A. Andreas Klein (Technical University Darmstadt) 2-B. Holger Fritze (Technical University of Clausthal) 2-C. Matthias T. Elm (Justus Liebig University Gießen) 2-D. TAKAMURA Hitoshi (Tohoku University) 2-E. YAMAGUCHI Mina (Tohoku University)
17:10		
17:20		
17:30		
17:40		
17:50		
18:00		
18:10		
18:20		
18:30		
18:40		
18:50		
19:00		19:00-19:10 Break (10 min.)
19:10		19:10-21:10 <GP-MS> Student Session 3 Chair: KURISU Minoru 3-A. Peter Walde (ETH) 3-B. Dora Tang (Max Planck Institute) 3-C. Kate Adamala (University of Minnesota) 3-D. KURISU Minoru (Tohoku University)
19:20		
19:30		
19:40		
19:50		
20:00		
20:10		
20:20		
20:30		
20:40		
20:50		
21:00		

The 4th Symposium for The Core Research Cluster for Materials Science and the 3rd Symposium on International Joint Graduate Program in Materials Science

November 16 (Mon) - 18 (Wed), 2020

DAY 3	Nov. 18 (Wed)	
JST	Core Research Cluster for Materials Science	GP-MS
8:30		
8:40		
8:50		
9:00	9:00-10:30 <Materials Science> Session 5 Chair: FUKUMURA Tomoteru 5-A. MURAKAMI Shuichi (Tokyo Institute of Technology) 5-B. FUJIWARA Kozo (Tohoku University) 5-C. TSUDA Kenji (Tohoku University)	9:00-10:30 <GP-MS> GP-MS Session Chair: SAITO Riichiro A. Shengxi Huang (Pennsylvania State University) B. Lianming Tong (Peking University) C. Teng Yang (Institute of Metal Research, Chinese Academy of Sciences)
9:10		
9:20		
9:30		
9:40		
9:50		
10:00		
10:10		
10:20		
10:30	10:30-10:50 Break (20 min.)	10:30-10:50 Break (20 min.)
10:40		
10:50	10:50-11:10 Poster Award Ceremony	
11:00		
11:10	11:10-11:20 Closing Remarks: NAGASAKA Tetsuya, Dean of Graduate School of Engineering, Tohoku University	

The 4th Symposium for The Core Research Cluster for Materials Science and the 3rd Symposium on International Joint Graduate Program in Materials Science
"Create New Value of Materials Science through Broad Collaboration"

Program & Abstracts

As of October 28, 2020

November 16 (Mon)

Opening Remarks	**9:00 - 9:10** **OHNO Hideo** (President of Tohoku University) 2

Plenary Session 1 9:10-9:55		
Chair: KOTANI Motoko (Director, Core Research Cluster for Materials Science) 3		
Plenary Session 1	**9:10-9:55**	**Byeong-Joo Lee** (Pohang University of Science and Technology) "Solute-dislocation binding: understanding the mechanism for room temperature ductility of Mg alloys" 4

Remarks	**9:55 -10:00** **YAMAGUCHI Masahiro** (Head, Division for International Joint Graduate School Programs) 6

---------- Parallel Session ----------

Session 1 10:10- 11:40		
Chair: FURUHARA Tadashi (Director, IMR) 7		
Session 1-A	**10:10-10:40**	**OHTANI Hiroshi** (IMRAM) "Electron Theory Calculation of Thermodynamic Properties of Alloys and Its Application to Theoretical Phase Diagrams" 8
Session 1-B	**10:40-11:10**	**MATSUBAE Kazuyo** (Graduate School of Environmental Studies) "Resource logistics approach on critical resources for future society" 10
Session 1-C	**11:10-11:40**	**ABE Eiji** (The University of Tokyo) "Kink Strengthening of Mille-feuille Structures in Mg Alloys" 12

Session 2 13:00- 14:30		
Chair: YOSHIMI Kyosuke (Professor, Graduate School of Engineering) 15		
Session 2-A	**13:00-13:30**	**Qiang Charles Feng** (University of Science and Technology Beijing) “Development of γ′-strengthened Co-base superalloys with improved comprehensive performances” 16
Session 2-B	**13:30-14:00**	**OHMURA Takahito** (National Institute for Materials Science) “Characterization of Dislocation Motions in Metallic Materials by TEM In-situ Straining and Nanoindentation” 18
Session 2-C	**14:00-14:30**	**NOMURA Naoyuki** (Graduate School of Engineering) “Challenges of composite powder fabrication for additive manufacturing”.. 20

Student Session 1 14:00- 16:00	
Chair: KOSABA Takumi (Graduate School of Engineering)	
Student Session 1-A	**Ying Jin** (University of Science and Technology Beijing) “High-throughput Characterization Methods for Corrosion Research” 22
Student Session 1-B	**HIROMOTO Sachiko** (National institute for Materials Science) “Calcium Phosphate Coating of Mg/Mg alloys for Biomedical Use” 24
Student Session 1-C	**KOSABA Takumi** (Graduate School of Engineering) “Effect of Anodizing on Galvanic Corrosion Prevention of Pure aluminum Coupled to Pure iron and stainless steel”..................... 26

Session 3 14:50- 16:20		
Chair: HIRANO-IWATA Ayumi (Professor, AIMR/RIEC) 27		
Session 3-A	**14:50-15:20**	**KURIYAGAWA Tsunemoto** (Graduate School of Biomedical Engineering) “Future of High Value Manufacturing (Introduction of Bio-Medical Applications for the Super Aging Society)” ... 28
Session 3-B	**15:20-15:50**	**UMETSU Mitsuo** (Graduate School of Engineering) “Protein-based molecular evolution for nano-bioengineering” 30
Session 3-C	**15:50-16:20**	**Yi-tao Long** (Nanjing University) “Electrochemistry Confined Nanopore: Design and Application in Single Molecule Sensing” 32

November 17 (Tue)

November 18 (Wed)

Poster Award Ceremony 10:50-11:10

Poster Presentation (Materials Science)

Project Introduction of the Core Research Cluster for Materials Science

Poster Presentations
(International Joint Graduate Program in Materials Science)

Solute-dislocation binding: understanding the mechanism for room temperature ductility of Mg alloys

Jong-Kwan Lee[1,2], Hyo-Sun Jang[1], Antonio João Seco Ferreira Tapia[1,2], Nack Joon Kim[2]
and Byeong-Joo Lee[1]

[1] Department of Material Science and Engineering,
Pohang University of Science and Technology (POSTECH), Republic of Korea
[2] Graduate Institute of Ferrous Technology,
Pohang University of Science and Technology (POSTECH), Republic of Korea

Non-basal slips play an important role in overcoming the poor ductility and formability of magnesium. We have proposed that alloying elements can activate non-basal slips by reducing critical resolved shear stress anisotropy among slip systems and that the optimum content of alloying elements in binary Mg alloys can be estimated, using atomistic simulations [1,2]. However, the detailed criterion for the activation of <c+a> slips in multicomponent Mg alloys, which can be utilized in commercial Mg alloys, requires further understanding. We found that the critical resolved shear stress anisotropy of a multicomponent Mg alloy can be minimized, resulting in an activation of the <c+a> slips, if the alloy has a dislocation binding intensity equivalent to associated binary Mg alloys optimized to minimize the critical resolved shear stress anisotropy. We also found that the activation in multicomponent Mg alloys can be robust when the element with relatively weak dislocation binding is the main alloying element. It was confirmed through an experiment that the multicomponent Mg alloys satisfying the above criterion show higher room-temperature tensile elongation and formability than other alloys.

Further, as a structural material, a reasonable strength is required from Mg alloys and a precipitation hardening can be an effective way to improve the strength. Important here is that the additional alloying for precipitation hardening should not have a harmful effect on the optimized dislocation binding. A thermodynamic calculation can be utilized to estimate the amount of solute in matrix and precipitates. It will be demonstrated how the thermodynamic calculation can be combined with the atomistic simulation as a new alloy design technique to improve the strength without disturbing the well-optimized ductility and formability, together with an experimental verification.

[1] K.-H. Kim, J.B. Jeon, N.J. Kim, B.-J. Lee, Scripta Mater. **108**, 104 (2015).
[2] K.-H. Kim, J.H. Hwang, H.-S. Jang, J.B. Jeon, N.J. Kim, B.-J. Lee, Mater. Sci. Eng. A **715**, 266 (2018).

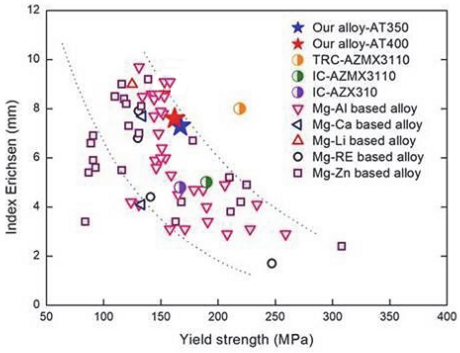

Fig. 1. Formability vs. Strength of various Mg alloys.

Electron Theory Calculation of Thermodynamic Properties of Alloys and Its Application to Theoretical Phase Diagrams

Hiroshi Ohtani [1*] and Masanori Enoki [1]

[1] Institute of Multidisciplinary Research for Advanced Materials,
Tohoku University, Sendai 980-8577, Japan

In controlling to maximize the functions of various materials, the role which the CALPHAD (Calculation of Phase Diagrams) method has played is very large. However, it is very difficult to apply this technique to the system which has not been clarified in experiments, metastable regions, and non-equilibrium phases. Then in this study, new approach to constitute phase diagrams will be proposed for incorporating with such problems.

In order to make a phase diagram of a certain system, the identification of the ordered structure which constitutes the phase region is most important. Then the ground structures of the system were estimated by first-principles calculations based on genetic algorithm, and the free energies of their structures are evaluated by electronic calculations and statistical thermodynamic techniques. In addition, the phase diagrams at finite temperature were theoretically constructed using the calculated free energies, and the result was compared with the experimental knowledge.

As an example of the calculation results, the theoretical phase diagram for Fe-Mo-B ternary system at T = 1323 K is shown in Fig. 1(a). For comparisons, calculated phase diagrams by the authors group using CALPHAD method is shown in Fig. 1(b), together with experimental values. The space groups and compositions of many ground structures obtained by the calculations correspond well with the experimental findings, but the agreement is not perfect. However, by including metastable structures by only a few kJ/mol than the ground state, it becomes clear that the appearance of almost all structures can be predicted based on this technique. The new calculation technique of such theoretical phase diagrams suggested in the present study is expected to open up the possibility of estimation of unknown phase diagram, reexamination of experimental phase diagrams and discovery of new phases. On the other hand, examining the calculation conditions for improving the accuracy of energy calculation, consideration of the anharmonicity of atomic vibration, magnetic entropy effect, handling of solid solution, etc. are mentioned as problems requiring further consideration.

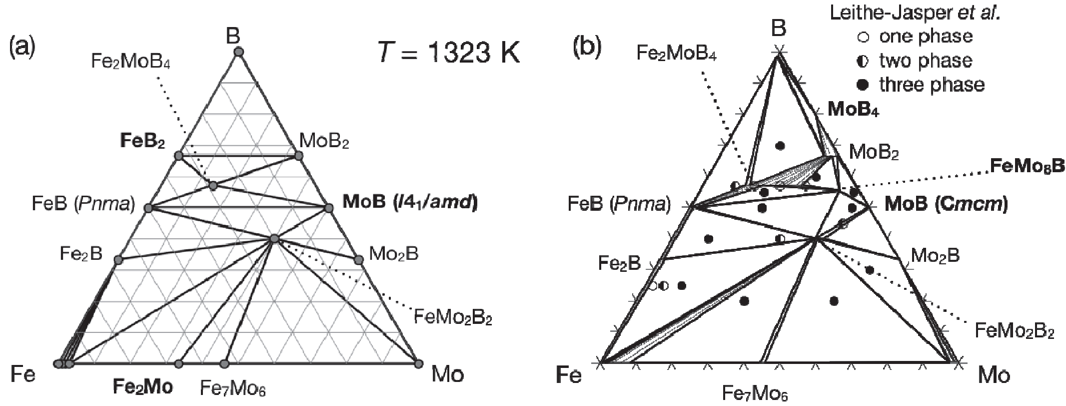

Fig. 1. (a) Theoretical phase diagram for Fe-Mo-B ternary system at T = 1323 K and (b) Calculated phase diagram by thermodynamic analysis with experimental data.

Resource logistics approach on critical resources for future society

Kazuyo Matsubae[1*] Kenichi Nakajima[2] Tetsuya Nagasaka[3]

[1]Graduate School of Environmental Studies, Tohoku University, Japan
[2] National Institute of Environmental Studies, Japan
[3]Graduate School of Engineering, Tohoku University, Japan

There is no doubt that the large-scale development and diffusion of climate change mitigation technologies is urgently required in our society. On the other hand, the acquisition of the additional mineral resources required by these technologies is expected to result in various negative impacts on the global environment. These include the depletion of limited mineral resources, damage to water bodies, stress on land surface areas, and the creation of toxic waste products.

Globally, the extraction of metal ores increased by more than 250% from 1970 to 2010. Copper is second only to iron ore in terms of the volume of metal ore extracted [1]. The recent increase in the global demand for copper [2] is certain to continue due to infrastructure maintenance in emerging countries and the increased production of electric vehicles [3]. However, since only a limited number of countries and regions are rich in copper and engaging in domestic copper extraction [4], many countries and regions procure copper through international trade-based supply chains.

The flow of resources in complex supply chains and the impact of green innovations on the life cycle of those resources needs to be understood. The importance of "resource logistics" has been growing in tandem with global concerns about resource and environmental constraints. Likewise, responsible mining, as a constituent of social responsibility associated with resource extraction and usage, is becoming increasingly important.

In this study, the focus was on copper as an indispensable material for climate change mitigation technologies. We estimated the amount of water used during the procurement of copper resources to support economic activities in different countries and regions (Fig.1)[5]. We also investigated the water supply risk for the water needed for these activities. The amount of water used in domestic copper mine production and that generated by copper ore imports was clarified.

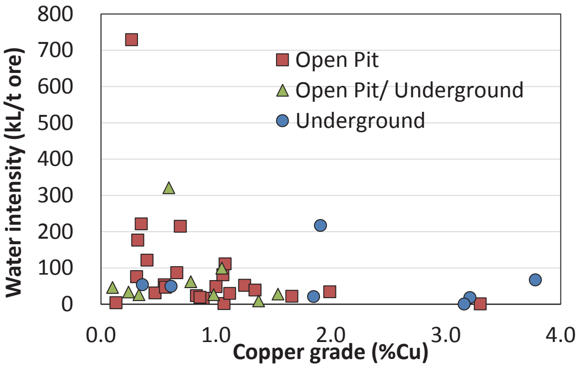

Fig.1 Water intensity against copper ore grade

[1] United Nations Environmental Programme, International Resource Panel (UNEP IRP), (2016) http://www.resourcepanel.org/file/423/download?token=Av9xJsGS

[2] K. Nakajima, I. Daigo, K. Nansai, K Matsubae, W. Takayanagi, M. Tomita, Y. Mastuno, Resour. Conserv. Recycl. **133**, 369–374. (2018)

[3] F. Un-Noor, S. Padmanaban, L. Mihet-Popa, M.N. Mollah, E.A. Hossain, Energies, **10**, 1217 (2017)

[4] United States Geological Survey (USGS), Minerals Yearbook, copper, (2015), https://minerals.usgs.gov/minerals/pubs/commodity/copper/myb1-2015-coppe.pdf

[5] A. Oashi, K, Matsubae, K. Nakajima, T. Nagasaka, Proceedings of Institute of Life Cycle Assessment, B2-03 (2018)

Kink Strengthening of Mille-feuille Structures in Mg Alloys

Eiji Abe

Department of Materials Science and Engineering, University of Tokyo,
7-3-1, Hongo, Bunkyo-ku, Tokyo, 113-8656, JAPAN

Dilute Mg alloys containing a few atomic percent of transition-metal and rare-earth element have attracted increasing attentions because of their excellent mechanical properties [1]. The remarkable microstructural feature common for all of these Mg alloys is formation of a novel type of long-period stacking/order (LPSO) structures [2,3], which reveal a remarkable strength through the warm-extrusion process. During the process the LPSO crystals are deformed not by simple dislocation migrations but kink formations (Fig. 1) that are the direct relevance to realize excellent properties of the alloys. From the extensive studies of the LPSO-structured Mg alloys for more than the past two decades, it has become apparent that the kink regions indeed provide an extra strengthening effect [4] for the alloys, but its detailed mechanism is not fully understood yet.

In order to deepen our understanding of the veiled work-hardening mechanism related to kink, we have launched the new project aiming the establishment of the “Kink strengthening phenomenon” as a universal strengthen principle [5]. In the meantime, the LPSO structure can be generally viewed as “Mille-feuille structure (MFS)”, in the sense that they are constructed by alternate stacking of microscopic hard- and soft-layer. That is, regarding LPSO-forming Mg alloys, the isolated structural unit is found to be highly stable even when distributed sparsely/randomly to form MFS [6]. Our recent studies have confirmed that the MFS-Mg alloys indeed reveal the kink strengthening, whose effect seems to be more prominent than LPSO Mg alloys. Therefore, solving the critical condition and universality on the kink-strengthening phenomenon will certainly lead to a further development of lightweight structural materials, including novel Al and Ti alloys, and even polymer materials in the future.

[1] Y. Kawamura, K. Hayashi, A. Inoue, and T. Masumoto, *Mater. Trans.* **42** (2001) 1172.
[2] E. Abe, Y. Kawamura, K. Hayashi, and A. Inoue, *Acta Mater.* **50** (2002) 3845.
[3] D. Egusa, and E. Abe, *Acta Mater.* **60** (2012) 166.
[4] K. Hagihara, M. Yamasaki, Y. Kawamura, and T. Nakano, *Acta Mater.* **163** (2019) 226.
[5] https://www.mfs-materials.jp/en/
[6] M. Egami, I. Ohnuma, M. Enoki, H. Ohtani, and E. Abe, *Materials and Design* **188** (2020)

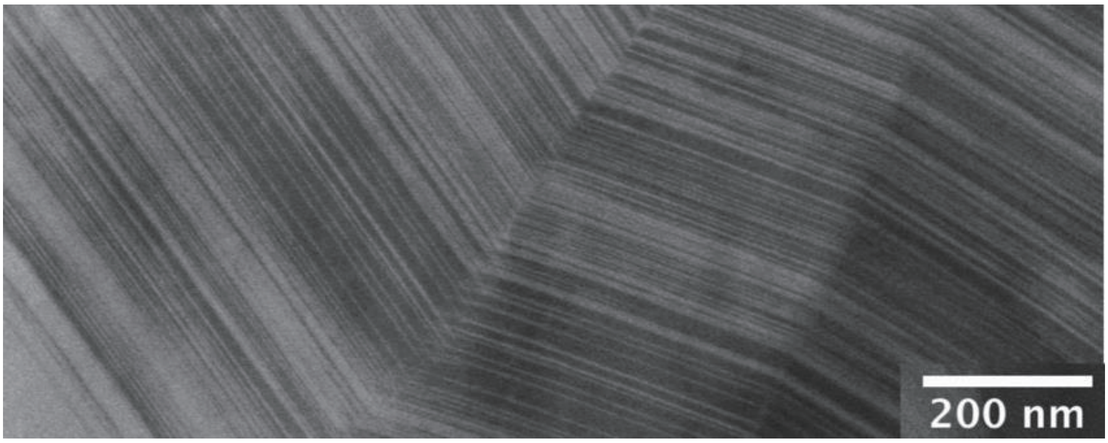

Fig. 1. HAADF-STEM image of kink-deformed MFS regions in a $MgZn_1Y_2$ alloy

Development of γ′-strengthened Co-base superalloys with improved comprehensive performances

Qiang Feng [1], Longfei Li [1], Wendao Li [1], Zou Min [1], Xiaoli Zhuang [1]
[1] Beijing Advanced Innovation Center for Materials Genome Engineering,
State Key Laboratory for Advanced Metals and Materials,
University of Science and Technology Beijing, Beijing 100083, China

In 2006, Sato and Ishida et al. in Tohuku University discovered the novel γ′-strengthened Co-Al-W-base alloys, which show potential for improved mechanical properties at high temperature than conventional Co-base alloys, opening up a new path for the development of Co-base superalloys. Since then, worldwide efforts have been made to improve the comprehensive performance of this new type of materials.

In the last decade, our group have done a plenty of investigations on the alloying effects of Ta, Ti, Nb, Mo and V on the γ′ solvus temperature, γ/γ′ two-phase stability and precipitation of secondary phases of Co-Al-W-base alloys, through the traditional "trial and error" method. A Co-Al-W-Ta-Ti quinary single crystal alloy was designed which demonstrates good high temperature γ/γ′ microstructural stability and excellent creep property, owning to the interaction effect of Ta and Ti. However, such quinary single crystal alloy is not suitable for engineering application, due to the narrow γ/γ′ two-phase region, higher alloy density and the absence of alloying elements for environmental resistance.

In recent years, an accelerated methodology integrating CALPHAD, diffusion-multiple approach and machine learning method is developed in our group to systematically understand the alloying effects of different elements, i.e. Ni, Al, W, Ti, Ta, Ni, Mo, on the multicomponent γ′-strengthened Co-base alloys, by which the Co-based superalloys with well balance of long-term microstructural stability, strength and oxidation resistance could be developed for different service purposes, such as turbine blades and disks. This work will be very helpful for the future alloy design efficiently.

[1] J. Sato, T. Omori, K. Oikawa, I. Ohnuma, R. Karinuma, K. Ishida, Cobalt-base high-temperature alloys, Science **312**, 90-91 (2006).
[2] J.-C. Zhao, Combinatorial approaches as effective tools in the study of phase diagrams and composition–structure–property relationships, Prog. Mater. Sci. **51**, 557-631 (2006).

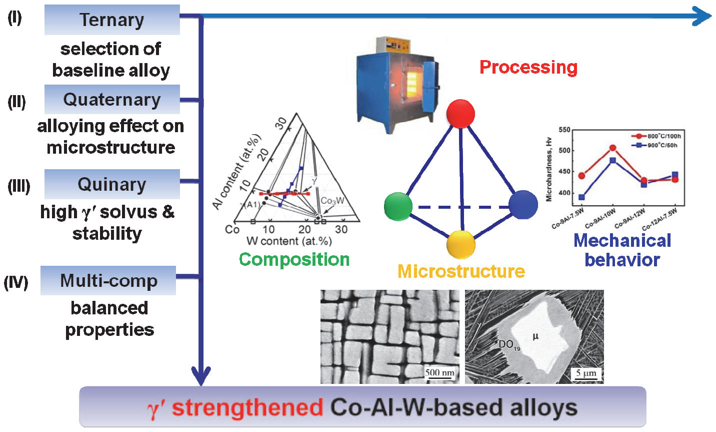

Fig. 1. Research Road Map of novel γ′ strengthened Co-base alloys.

Characterization of Dislocation Motions in Metallic Materials by TEM In-situ Straining and Nanoindentation

Takahito Ohmura[1, 2, 3*], Seiichiro. Ii[1] and Hongxing. Li[1]

[1] National Institute for Materials Science, Tsukuba
[2] Course of Advanced Nanomaterials Science and Engineering, Kyushu University, Fukuoka
[3] Elements Strategy Initiative for Structural Materials, Kyoto University, Kyoto

Local deformation behavior in metallic materials governs macroscopic properties and involves dislocation motion deeply. One can elucidate the fundamental mechanisms of the microstructure-properties relation through great potential approaches including dynamic observation of the dislocation glide by TEM in-situ straining and probing the local mechanical response through nanoindentation under an applied stress.

Load-displacement curves by nanoindentation clearly show the plasticity initiation and the subsequent deformation in “pop-in” behavior on the loading segment. Fig. 1 shows probability distributions of magnitudes in the first pop-in and the subsequent one as a function of the stress drop $\Delta\sigma$ for a single crystal Fe with (001) surface orientation [1]. The first event, which is a transition from pure elastic strain to an elastoplastic deformation, shows Gaussian like distribution, indicating a thermally-activated process of dislocation nucleation at defect-free region in the material. On the other hand, the second and subsequent events follow a power-law function like Gutenberg-Richter model in seismology, suggesting a dislocation avalanche as a catastrophe phenomenon.

Dynamic interactions between lattice dislocation and grain boundaries can be captured by TEM in-situ straining. In the case of $\Sigma 3$ coincidence site lattice grain boundary in pure Al bicrystal, the slip transfer goes through the boundary with a dislocation reaction there [2]. The <110> lattice dislocation dissociates into a grain boundary dislocation and another <110> lattice dislocation in the adjacent grain. Since the dislocation self energy is proportional to a square of a magnitude of the Burgers vector and is exactly the same for the <110> lattice dislocations in the original and the adjacent grains, the energy barrier for the slip transfer corresponds to the formation of the grain boundary dislocation. In the early stage of deformation below the yield stress in an ultra-fine-grained (UFG) steel, dislocations in grain interior move forward to a grain boundary and then are absorbed there with no pilling up. Dislocation density in the grain interior decreases with increasing strain, which is consistent with a case in a macroscopic tensile specimen, therefore the extra hardening in Hall-Petch plot in the UFG steel can be attributed to a starvation of the mobile dislocation based on a combination of Orowan model and Johnston-Gilman theory.

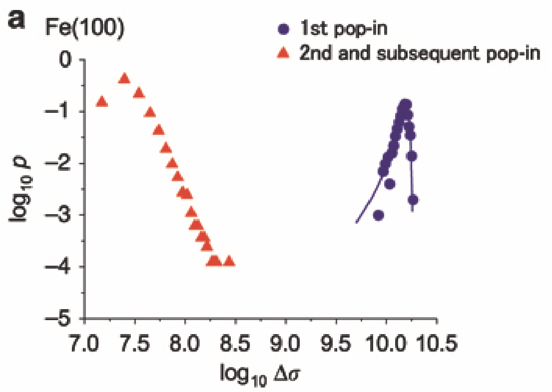

Fig. 1. Probability distributions of first pop-in and subsequent one magnitudes as a function of the stress drop for Fe [1].

[1] Y. Sato, S. Shinzato, T. Ohmura, T. Hatano, S. Ogata, Nature Comm., **11**, 4177 (2020).
[2] S. Ii, T. Enami, T. Ohmura, S. Tsurekawa, submitted.
[3] H. Li, S. Gao, Y. Tomota, S. Ii, N. Tsuji, T. Ohmura, submitted.

Challenges of composite powder fabrication for additive manufacturing

NOMURA Naoyuki* and ZHOU Weiwei

Department of Materials Processing, Graduate School of Engineering, Tohoku University,
6-6-02, Aramaki Aza Aoba, Aoba-ku, Sendai, Miyagi 980-8579, Japan

Additive manufacturing (AM) has attracted much attention as a new method for creating parts with complicated shape. The consumer side sometimes calls the method 3-D printing, and the technical innovation is rapidly going forward during the last decades especially for high -power heat source, large build fabrication, process monitoring, and so on. In this process, the 3-D CAD data is sliced to provide the AM machine and the laser or electron beam are scanned on the powder according to the data. The irradiated powder is melted and consolidated with the cross-section shape. The powder is recoated depending on the required resolution thickness and is scanned again according to the next layer data. This process is performed repeatedly until the parts are obtained. This method can from complicated shapes with internal structure impossible by traditional fabrication method. Thus, AM can realize the parts with innovative design. Steels, Ni, Ti, and Al alloys powders are already provided for AM, and the variety of metal powders applicable to AM is increasing as the application fields are expanding such as medical implants, molds for plastics, and aerospace.

In our research group, we are now focusing on the fabrication of composite powders (Fig. 1) to develop additively manufactured composites having superior properties to the AM metallic builds. In this presentation, several composite powders developed by our group and the AM builds showing characteristic microstructures will be introduced [1-3].

[1] W. Zhou, X. Sun, K. Kikuchi, N. Nomura, K. Yoshimi, and A. Kawasaki, Mater. Des., **137**, 276-285 (2018).

[2] W. Zhou, K. Kikuchi, N. Nomura, K. Yoshimi, and A. Kawasaki, J. Alloy Comp., **819**, 152981 (2020).

[3] N. Nomura, W. Zhou, Z. Zhou, and K. Yoshimi, Ceramics Japan, **55**, 90-92 (2020).

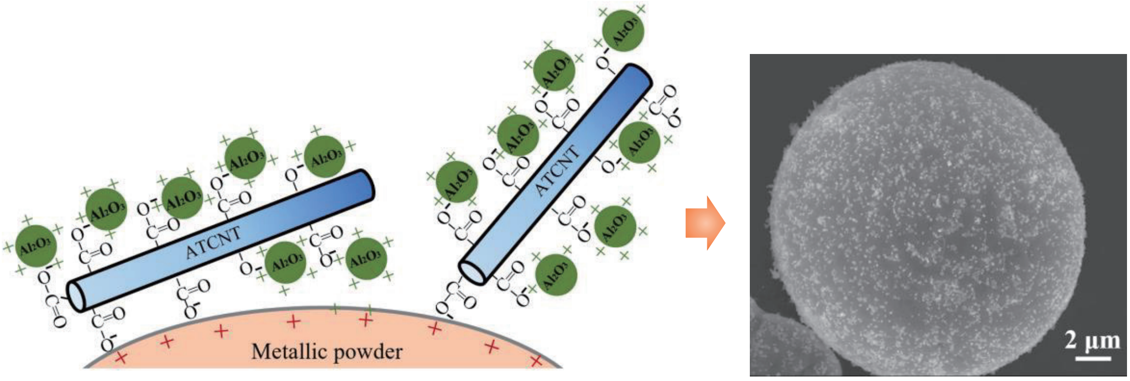

Fig. 1. Schematics and SEM image of a NiAlCrMo/ATCNT/Al_2O_3 composite powder [1] (reuse with the permission of Elsevier).

High-throughput Characterization Methods for Corrosion Research

Ying JIN, Zhaogui LAI, Yang ZOU, Chaoyang ZHAO

National Center for Materials Service Safety, University of Science and Technology Beijing,
Beijing 100083, China

Corrosion assessment is a pivotal step in the development of new inhibitors, coatings, and anti-corrosion alloys. In order to improve the low-efficiency of traditional techniques for electrochemical characterization, the high-throughput theory and methodology have been proposed to address this issue in the past two decades. This lecture is to present examples to illustrate this possibility, in which two material libraries were selected to demonstrate the application of high throughput multi-analytical techniques in material comprehensive evaluation, one is an artificial Fe-Cr-Ni thin film specimen, the other is a natural 308L-309L/SA508 weld joint specimen.

The demonstrated high throughput study involved multi-analytical techniques. Electron probe X-ray microanalysis (EPMA) and X-ray diffraction (XRD) of synchrotron radiation source were used to characterize composition and microstructure, respectively. Metallographic observations were conducted by scanning electronic microscope (SEM) and automatic photographing optical microscope (OM). Scanning Kelvin probe (SKP) or scanning Kelvin force microscopy (SKPFM) was utilized to evaluate the nobility of the specimens with different compositions. In addition, the electrochemical properties were characterized by a self-assembled high-throughput local electrochemical test apparatus.

Moreover, high-throughput data analysis techniques were also developed and utilized to accomplish data processing more effectively and intelligently. For instance, hierarchy clustering was implemented to categorize the thousands of X-ray diffraction patterns. Multiple machine learning (ML) classification algorithms were adopted to predict the corresponding equvilent circuit model (ECM) of a bunch of electrochemical impedance spectroscopy (EIS), and employed various meta-heuristic global optimization algorithms to automatically fit the parameters of ECM. As a result, the relationship between composition-structure-property could be extracted through data mining.

Calcium Phosphate Coating of Mg/Mg alloys for Biomedical Use

Sachiko Hiromoto[1]*

[1]National Institute for Materials Science, 1-2-1 Sengen, Tsukuba 305-0047

Magnesium/Mg alloys are starting to be practically used for biodegradable medical devices such as bone screws and stents. The initial rapid corrosion of Mg/Mg alloys reduces the strength and the generated H_2 gas forms cavities which can prevent the surrounding tissue to adhere to the material surface. The corrosion control of Mg/Mg alloys is thus a crucial issue. We developed hydroxyapatite (HAp) and octacalcium phosphate (OCP) coatings [1] and the coatings retarded the corrosion speed of Mg/Mg alloy in a cell culture medium and in mouse subcutaneous tissue [2,3]. The HAp coating retarded the initial corrosion of Mg/Mg alloys in rat femurs and enhanced the bone formation [4]. In this presentation, the formation of the HAp coatings and the corrosion behavior of HAp-coated Mg/Mg alloys in various environments will be introduced.

As a substrate, Mg-3mass% Al-1mass% Zn (AZ31) discs were used for the immersion test in a cell culture medium and the implantation test in mouse subcutaneous tissue. Pure Mg rods were used for the implantation test in rat femurs. HAp coatings were formed on the substrates by immersing in a previously reported solution [2] at 90℃ for 1~2 hours.

Figure 1 shows SEM images of HAp-coated and uncoated Mg/Mg alloy immersed/implanted in various environments. The corrosion layer of the HAp-coated Mg/Mg alloy was thinner than that of the uncoated specimens in medium and soft and hard tissues. It was demonstrated that the HAp coating is effective to retard Mg corrosion in vitro and in vivo.

In medium, corrosion progressed homogeneously under the HAp layer (Fig. 1(b)); whereas in soft and hard tissues, localized corrosion was observed under the HAp layers (Fig. 1(c, e)). In gelatin-added medium, in which mass transfer was restricted, HAp-AZ31 showed localized corrosion under the HAp layer (Fig. 1(d)). Corrosion product in medium partly dissolved while that in soft tissue mostly undissolved (Fig. 1(f, g)). The localized corrosion under the HAp layers in soft and hard tissues indicates that the low diffusivity and relatively small liquid content of tissues allowed body fluid to permeate preferentially through the defects of HAp layers. It is suggested that the mass diffusivity and liquid content in the surrounding tissues influences the corrosion behavior of HAp-coated Mg/Mg alloys.

[1] S. Hiromoto et al., Electrochim. Acta. **54**, 7085-7093 (2009). [2] S. Hiromoto, M. Inoue, T. Taguchi, M. Yamane, N. Ohtsu, Acta Biomater. **11**, 520-530 (2015). [3] S. Hiromoto, Corros. Sci. **100**, 284-294 (2015).[4] S. Hiromoto, E. Nozoe, K. Hanada, T. Yoshimura, K. Shima, T. Kibe, N. Nakamura, K. Doi (submitted).

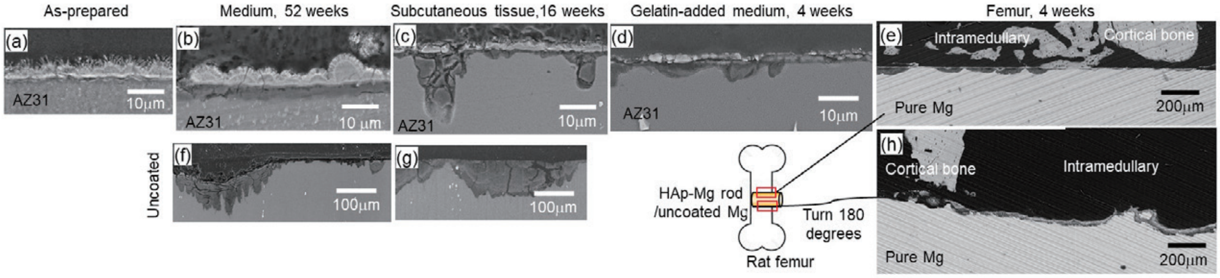

Fig. 1 Cross-section SEM images of (a-d) HAp-AZ31 and (f,g) uncoated AZ31 (a) as-prepared, (b, f) immersed in medium for 52 weeks, (c,g) implanted in mouse subcutaneous tissue for 16 weeks and (d) immersed in gelatin-added medium for 4 weeks and (e) HAp-Mg and (h) uncoated Mg implanted in rat femur for 4 weeks.

Effect of Anodizing on Galvanic Corrosion Prevention of Pure aluminum Coupled to Pure iron and stainless steel

Takumi Kosaba[1*], Izumi Muto[1] and Yu Sugawara[1]

[1]Department of Materials Science, Tohoku University

Due to the prevention of global warming, the demand for weight reduction of automobiles is increasing these days: then the multimaterial structures, which is one of the methods to achieve the weight reduction, attract great interest. Because of low cost and high stiffness, aluminum alloys and steels joints are anticipated to utilize in the structures. However, galvanic corrosion is expected to occur on less noble potential metals such as aluminum alloys.

The evaluation of galvanic corrosion has been generally performed by corrosion potential difference; therefore, the active dissolution of aluminum alloys is accelerated because the electrode potential of aluminum alloys increased by the coupling. In the case of the galvanic corrosion in chloride solutions at near-neutral pH, the anodic reaction on aluminum alloys are oxide film formation and/or localized corrosion generation like pitting. For pure aluminum and aluminum alloys, the generation of localized corrosion is generally evaluated by the critical potential for localized corrosion, such as pitting potential. Consequently, in chloride solutions at near-neutral pH, galvanic corrosion should be evaluated by comparison between electrode potential of aluminum alloys under coupling and the critical potential for localized corrosion.

To prevent the galvanic corrosion, inhibitor and surface modification have been adapted to these joints. Among these techniques, anodizing is expected to be effective as the surface modification techniques because thicker anodic oxide film contributed to improvement on corrosion resistance of aluminum alloys; however, there is little research related to the improvement on galvanic corrosion resistance of aluminum alloys under coupling with steels by anodizing.

In this research, we investigated the galvanic corrosion behavior of pure aluminum coupled to pure iron in diluted synthetic seawater. This electrolyte simulated the chloride solutions at near-neutral pH relevant to atmospheric environments. The galvanic corrosion tests were carried out by zero resistance ammeter techniques. Moreover, the galvanic corrosion behavior of anodized aluminum coupled to pure iron or Type 430 stainless steel was studied. Pure aluminum surface was modified by anodizing in sulfuric acid at various anodizing voltage and time conditions. we performed the galvanic corrosion tests between anodized aluminum and pure iron or Type 430 stainless steel in diluted synthetic seawater, and the thickness of anodic oxide film to prevent galvanic corrosion damage on anodized aluminum was determined.

Future of High Value Manufacturing (Introduction of Bio-Medical Applications for the Super Aging Society)

Tsunemoto Kuriyagawa

Tohoku University, 6-6-01 Aramaki Aoba, Aoba-ku, Sendai 980-8579

We aim to promote innovations of pico- & nano-precision Micro/Meso Mechanical Manufacturing (M4 process) at the frontier of manufacturing technology, including ultra-precision mechanical manufacturing technologies for various shapes, nano-precision fabrication for 3D microstructures, atom/molecule manipulation for nanostructures and so on. Our goal is not only to create high-precision shapes, but also to generate functional structures on the shape by controlling the micro textures. Today, I will introduce an unique technology, which is powder jet deposition (PJD). The deposition mechanism of PJD was studied with smoothed particle hydrodynamics (SPH) and molecule dynamics (MD) simulations. The deformation of a particle and a substrate by impact was successfully simulated. From the result, a thick film is generated due to the repetition of the deposition of the stagnation areas. The blasting experiments were also conducted to study the machining mechanism at transition condition. The machining surface was analyzed with SEM and TEM. It was that found from these results, the removal process of the substrate material and deposition process of particles onto the substrate occur concurrently under the transition conditions. Utilizing the PJD, a hydroxyapatite film has been successfully deposited on a human tooth as a new dental treatment.

[1] M. Mizutani, C. Kuji, H. Ohisa, S. Nishimura, K. Mizutani, R. Akatsuka, K. Sasaki, S. Xu, K. Shimada, and T. Kuriyagawa, Particle fracture behavior and deposition mechanism in powder jet deposition (PJD), J. of JSAT, 61 (1), 28-33 (2017).

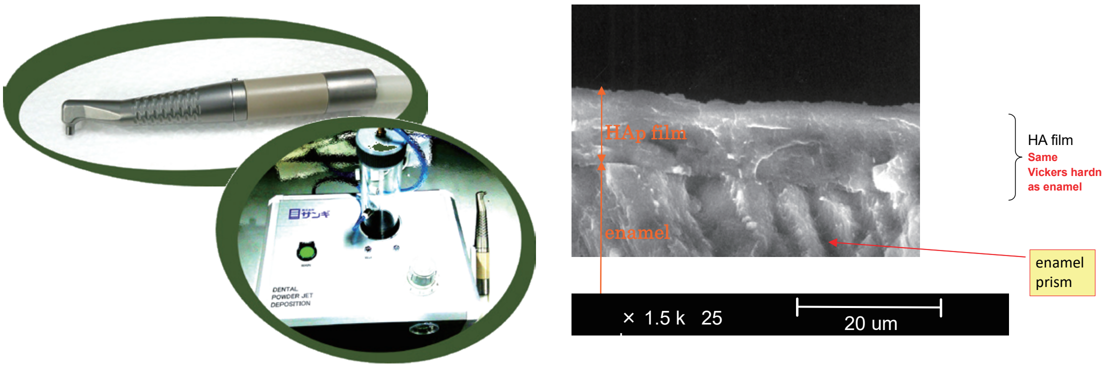

Fig. 1. Developed dental PJD unit and deposited HA film on human enamel.

Protein-based molecular evolution for nano-bioengineering

Mitsuo Umetsu[1,2]

[1] Department of Biomolecular Engineering, Graduate School of Engineering,
Tohoku University
[2] Center of Advanced Intelligence Project, RIKEN, Japan

Protein is a biopolymer where the amino acids with various side chain are dehydrated, and the sequence of amino acids are coded by DNA. The variety of the amino acid sequences, called sequence space, is so huge that a diversity of function can be expressed. The design of amino acid sequence lead directly to a creation of functional protein, but no reliable rational sequence design has been established. Molecular evolution is widely used in protein engineering, where a library of protein variants by means of mutagenesis on a scaffold protein and the variants with a specific function are survived in the selection process. However, the massive scale of sequence space makes it tough to explore a goal variant, because preparing the library with the goal variants and screening the variants from the library are low probability. In this background, we study the “library design cycle”, where a local area with a goal variants in sequence space is identified at first step by mean of wet techniques, bioinformatics, and AI , and we explore the goal variants in the designed local library. With this methodology, we are creating various available recombinant proteins in the therapeutic, diagnostic, environmental, and material fields. Here, I show several attractive proteins for nanobiotechnology and therapeutic fields, by means of our powerful approach for accelerated discovery of functional proteins.

[1] T. Niide, N. Manabe, H. Nakazawa, K. Akagi, T. Hattori, I. Kumagai, and M. Umetsu, *Langmuir*, **35**, 3067−3076 (2019).
[2] Y. Saito, M. Oikawa, H. Nakazawa, T. Niide, T. Kameda, K. Tsuda, and M. Umetsu, *ACS Synthetic Biology*, **7**, 2014–2022 (2018).
[2] H. Fujii, Y. Tanaka, H. Nakazawa, A. Sugiyama, N. Manabe, A. Shinoda, N. Shimizu, T. Hattori, K. Hosokawa, T. Sujino, T. Ito, T. Niide, R. Asano, I. Kumagai, and M. Umetsu, *Advanced Therapeutics*, 1700031 (2018).
[3] H. Nakazawa, D.-M. Kim, T. Matsuyama, N. Ishida, A. Ikeuchi, Y. Ishigaki, I. Kumagai, and M. Umetsu, *ACS Catalysis*, **3**, 1342-1348 (2013).

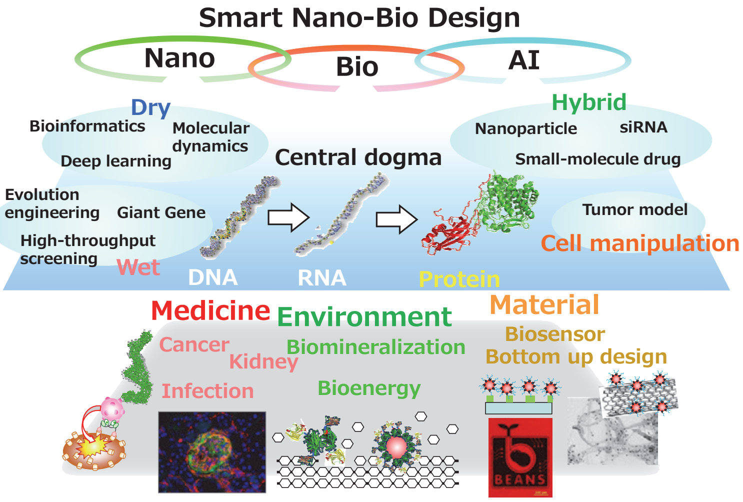

Fig. 1. Smart nano-bio design for the medical, environmental, and material fields

Electrochemistry Confined Nanopore: Design and Application in Single Molecule Sensing

Yi-Tao Long
School of Chemistry and Chemical Engineering, Nanjing University, Nanjing, 210023, P. R. China, E-mail: yitaolong@nju.edu.cn

The single molecule measurement has enhanced the precision and depth of our knowledge about living system. Learning from nature, the million years of evolution have produced the membrane proteins which acts as a single biomolecule interface for capturing and identifying a single molecule of interests, and makes biological process occurring. Here, we focus on the biological nanopore-based single biomolecule interface for single molecule measurements.[1-3] We outline the design of nanopore-based single biomolecule interface which provides rich heterogeneities and stochastics information about each molecule. Then, we focus on the future areas beyond DNA sequencing including detecting rare species, resolving the hidden intermediates, depicting the spectra for the covalent/non-covalent interactions, tracing the dynamic pathways of single molecule behaviors.[4-6] A concept “single-molecule ionic spectrum”, which is considered as “a special music of molecule”, may potentially map the non-covalent interaction at atomic level in future. Since the characteristic interaction determines the sensitivity of nanopore, ideally the frequency analysis of nanopore data could be used not only for DNA sequencing, RNA sequencing, protein sequencing but also all kinds of single molecule detection. As ideally transferring the frequency-energy spectrum from the ionic current into the voice frequency, we illustrate that a nanopore-based single-biomolecule interface likes a tuba. When a single analyte flows into the ‘tuba’, its dynamic interaction with the pore could be modulated by the residue of the pore (‘button’) and the resonance space at the single-molecule interface (‘tuba’). As a result, the incredible music of a single molecule will be played with a typical rhythm and melody.

1. Y. L. Ying, C. Chao, Y. X. Hu. Y. T. Long, Natl. Sci. Rev., **5**, 450-520 (2018).
2. Y. Q. Wang, C. Cao, Y.-L. Ying, S. Li, M. B. Wang, J. Huang, Y. T. Long, ACS Sens., **3**, 779-783 (2018).
3. Y. Q. Wang, M.-Y. Li, H. Qiu, C. Cao, M.-B. Wang, X. Y. Wu, J. Huang, Y. L. Ying, Y. T. Long, Anal. Chem., **90**, 7790-7794, (2018).
4. C. Cao, Y. L. Ying, Z. L. Hu, D. F. Liao, H. Tian, Y. T. Long, Nat. Nanotechnol., **11**, 713-716 (2016).
5. C. Cao, Y T Long, Acc. Chem. Res. **51**, 331-341 (2018).
6. Y. L. Ying, Y. T. Long. J. Am. Chem. Soc., **141**, 15720-15729 (2019).

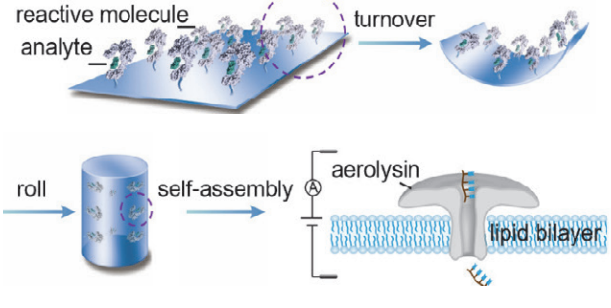

Figure. A self-assembled aerolysin membrane protein exampled as single biomolecule interface. The oligonucleotide is taken as an example for illustrating the analyte.

Interplay of Chemistry and Structure at Lattice Defects studied at the Atomic Scale

Dierk Raabe

Max-Planck-Institut für Eisenforschung,
Max-Planck-Str. 1, 40237 Düsseldorf, Germany

Lattice defects like interfaces, stacking faults and dislocations determine many mechanical, functional and kinetic properties of materials. Lattice defects do not merely constitute structural imperfections but they are often chemically decorated by solutes as described by the Gibbs isotherm 100 years ago. The interplay of structure and chemistry at lattice defects can lead to a wide range of phenomena and manipulation opportunities including Suzuki and Cottrell effects, confined elemental partitioning, linear and planar phase-like states, decomposition and low-dimensional transformations. All these effects alter the defects' energy, mobility, structure, cohesion and transport properties.

The lecture presents and discusses several aspects in that context:

First, recent progress is presented which allows imaging of both structure and composition features at lattice defects by using correlative imaging through field ion microscopy, atom probe tomography and electron microscopy [1,2]. Some of these observation methods are enhanced by using quantum mechanical simulations and machine learning.

Second, atomic-scale experiments on several material classes ranging from metals to thermoelectrics are presented which reveal that the interplay between defect structure and chemistry can lead to a much larger variety in compositional – structural states than commonly assumed. Examples are confined phase formation, athermal transformations, spinodal decomposition or inter-defect partitioning at lattice defects to name but a few phenomena, Fig. 1.

Third, some thermodynamic considerations are discussed which may guide better understanding and utilization of these phenomena.

[1] M. Kuzmina, M. Herbig, D. Ponge, S. Sandlöbes, D. Raabe, Linear Complexions: Confined Chemical and Structural States at Dislocations. Science **349**, 6252 (2015).

[2] D. Raabe, M. Herbig, S. Sandlöbes, Y. Li, D. Tytko, M. Kuzmina, D. Ponge, P. Choi, Grain Boundary Segregation Engineering in Metallic Alloys: A Pathway to the Design of Interfaces. Current Opinion in Solid State and Materials Science **18**, 253 (2014).

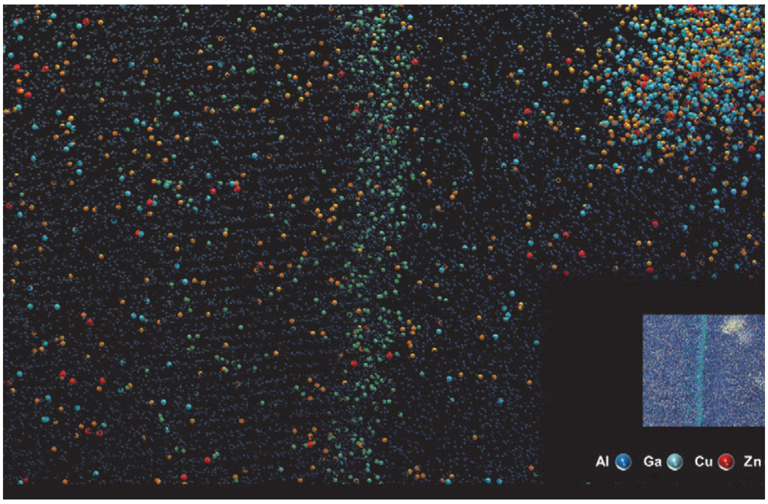

Fig. 1. Interface decoration in AlCuZn

Model Systems for Heterogeneous Catalysts at the Atomic Scale

Hans-Joachim Freund

Fritz-Haber-Institut der Max-Planck-Gesellschaft, Faradayweg 4-6, 14195 Berlin, Germany

We have created model systems for heterogeneous catalysts on the basis of thin oxide films. This permits us to apply the toolbox of surface science for characterization and reaction studies at the atomic scale. Two case studies to demonstrate how those systems may be studied at the atomic scale are reported.

The first one discusses a novel characterization technique, namely surface action spectroscopy, using concepts developed in gas phase studies to record vibrational spectra of extremely dilute specimen based on messenger desorption[1-3]. We demonstrate the extreme surface sensitivity of this technique by applying it to surface states of oxide surfaces, i.e. vanadia as well as iron oxides.

The second case study deals with a reaction in confined space using a model system based on a thin silica film, which is only bound to a metal substrate by dispersive forces, leaving a space between the oxide film and the metal substrate[4,5]. Here we study water formation from intercalated oxygen, adsorbed on the metal surface and hydrogen provided from the gas phase in operando, and deduce the details of the kinetics of the reaction in confined space in direct comparison to the equivalent open space reaction. To this end we use a spectro-microscope, operated at BESSYII and developed in the group, which allows to observe tempo-spatial distribution of reactants and deduce apparent activation energies. Those experimental observations are interpreted on the basis of DFT calculations and kinetic models.

References:

[1] Z. Wu, A. Płucienik, F.E. Feiten, M. Naschitzki, W. Wachsmann, S. Gewinner, W. Schöllkopf, V. Staemmler, H. Kuhlenbeck, and H.-J. Freund, Phys. Rev. Lett. **119**, 136101 (2017).

[2] Z. Wu, A. Plucienik, Y. Liu, M. Naschitzki, W. Wachsmann, S. Gewinner, W. Schöllkopf, H. Kuhlenbeck, and H.-J. Freund, Rev. Sci. Instrum. **89**, 083107 (2018).

[3] Y. Liu, Z. Wu, M. Naschitzki, S. Gewinner, W. Schöllkopf, X. Li, J. Paier, J. Sauer, H. Kuhlenbeck, and H.-J. Freund, J. Am. Chem. Soc. **142**, 2665 (2020).

[4] M.J. Prieto, H.W. Klemm, F. Xiong, D.M. Gottlob, D. Menzel, T. Schmidt, and H.J. Freund, Angew. Chem. Int. Ed. **57**, 8749 (2018).

[5] H.W. Klemm, M.J. Prieto, F. Xiong, G.B. Hassine, M. Heyde, D. Menzel, M. Sierka, T. Schmidt, and H.-J. Freund, Angew. Chem. Int. Ed. **59**, 10587 (2020).

Nanostructured magnetic materials for thermoelectric generation

Masaki Mizuguchi

Graduate School of Engineering, Nagoya University

The correlation between spin and charge in electronic transports has been energetically studied in a scheme of spintronics research. Recently, the coupling between heat current, spin current and charge current is also attracting much attention, and this newly established filed is called "spin caloritronics". The recent discovery of the spin Seebeck effect has explosively expanded this field, and various thermomagnetic effects related to spin current have been investigated. The Nernst effect is a common thermomagnetic effect, which has been known for a long time. When a temperature gradient is applied on a material with spontaneous magnetization, an electric field is induced in the perpendicular direction to both the temperature gradient and the magnetization, which is called the anomalous Nernst effect (ANE). We have reported ANE measurements of an $L1_0$-ordered epitaxial FePt thin film, which is a well-known material with a large spin-orbit coupling, for studying thermomagnetic effects in ordered alloys [1, 2]. We also studied the material dependence of ANE regarding the spin-orbit interaction in several perpendicularly magnetized ordered-alloy thin films [3]. Obtaining materials with a large ANE is indispensable to realize a practical application of ANE-based energy conversion. From this point of view, this talk describes our study on the ANE in various nanostructured materials. A novel material with the strong anisotropy in ANE, the enhancement of ANE for granular thin films, and spin caloritronic devices with magnetic nanostructures for ANE-based thermoelectric generation will be discussed [4-7].

The author thanks Mr. Hasegawa, Dr. Takanashi, Dr. Isogami, Dr. Sheng, Dr. Sharma, Dr. Ohe for their supports in experimental and theoretical studies. This research was partly supported by JST-CREST (JPMJCR1524), a Grant-in-Aid for Scientific Research (A) (17H01052) from Japan Society for the Promotion of Science, the Center for Spintronics Research Network (CSRN), and Collaborative Research Center on Energy Materials (E-IMR).

[1] **M. Mizuguchi**, S. Ohata, K. Hasegawa, K. Uchida, E. Saitoh, and K. Takanashi, Appl. Phys. Express **5**, 093002 (2012).
[2] Y. Sakuraba, K. Hasegawa, **M. Mizuguchi**, T. Kubota, S. Mizukami, T. Miyazaki, and K. Takanashi, Appl. Phys. Express **6**, 033003 (2013).
[3] K. Hasegawa, **M. Mizuguchi**, Y. Sakuraba, T. Kamada, T. Kojima, T. Kubota, S. Mizukami, T. Miyazaki, and K. Takanashi, Appl. Phys. Lett. **106**, 252405 (2015).
[4] S. Isogami, K. Takanashi, and **M. Mizuguchi**, Appl. Phys. Express **10**, 073005 (2017).
[5] **M. Mizuguchi** and S. Nakatsuji, Sci. Tech. Adv. Mater **20**, 262 (2019).
[6] H. Sharma, Z. Wen, K. Takanashi, and **M. Mizuguchi**, Jpn. J. Appl. Phys. **58**, SBBI03 (2019).
[7] P. Sheng, T. Fujita, and **M. Mizuguchi**, Appl. Phys. Lett. **116**, 142403 (2020).

Search for Superconductivity of Super-hydrides Synthesized under Extreme Condition

EINAGA Mari[1*], SAKATA Masafumi[2] NAKAO Harushige[1] and SHIMIZU Katsuya[1]

[1]KYOKUGEN, Osaka University, Machikaneyamacho 1-3, Toyonaka, Osaka 560-8531, Japan
[2] Faculty of Engineering, Gifu University, 1-1 Yanagido, Gifu city, Gifu, 501-1193, Japan
[3]JASRI, 1-1-1, Sayo-cho, Sayo-gun, Hyogo 679-5198.

At the end of 2014, a joint theoretical and experimental investigation broke the record for the superconducting critical temperature T_c by more than 30 K, reaching 203 K for hydrogen sulfide H_2S under a high pressure of 150 GPa which was the first increase in 20 years [1, 2]. After this discovery, several theoretical groups proposed the crystal structures and the value of T_c in a lot of binary and some ternary hydrides. However, only a few experimental works on the investigation of the way of synthesis and the transport properties of the predicted hydrides have been reported so far.

Most recently, direct synthesis of several hydrides, for instance, H_3S, LaH_{10}, PrH_9, ThH_7 made from the mixture of the elements (sulfur, lanthanum, praseodymium and thorium), and H_2 or hydrogen source has been reported from several groups [3-6]. Especially, lanthanum hydride shows the highest-$T_c \sim 250$ K with zero electrical resistance at 170 GPa [3].

Here we report our recent results of synchrotron x-ray diffraction with electrical resistance measurements to search for superconductivity of sulfur and lanthanum super-hydrides synthesized under high pressure and high temperature from sulfur and lanthanum super-hydride synthesized from H_2S or sulfur and hydrogen, or lanthanum and aluminium trihydride as the hydrogen source [7-9].

[1] A. P. Drozdov, M. I. Eremets, I. A. Troyan, V. Ksenofontov and S. I. Shylin, Nature **525**, 73-76 (2015).
[2] Y. Li, J. Hao, H. Liu, Y. Li, and Y. Ma, J. Chem. Phys., **140**, 174712 (2014).
[3] A. P. Drozdov, P. P. Kong, V. S. Minkov, S. P. Besedin, M. A. Kuzovnikov, S. Mozaffari, L. Balicas, F. F. Balakirev, D. E. Graf, V. B. Prakapenka, E. Greenberg, D. A. Knyazev, M. Tkacz and M. I. Eremets, Nature, **569**, 528–531 (2019).
[4] M. Somayazulu, M. Ahart, A. K. Mishra, Z. M. Geballe, M. Baldini, Y. Meng, V. V. Struzhkin, and R. J. Hemley, Phys. Rev. Lett. **122**, 027001(2019).
[5] D. V. Semenok, A. G. Kvashnin, A. G. Ivanova, V. Svitlyk, V. Y. Fominski, A. V. Sadakov, O. A. Sobolevskiy, V. M. Pudalov, I. A.Troyan and A. R.Ogano: Materials today **33**, 36 (2020).
[6] D. Zhou, D. V. Semenok, D. Duan, H. Xie, W. Chen, X. Huang, X. Li: Sci. Adv. **6**, eaax6849 (2020).
[7] M. Einaga, M. Sakata, T. Ishikawa, K. Shimizu, M. I. Eremets, A. P. Drozdov, I. A. Troyan, N. Hirao and Y. Ohishi, Nature Phys. **12**, 835 (2016).
[8] H. Nakao M. Einaga, M. Sakata, M. Kitagaki, K. Shimizu, S. Kawaguchi, N. Hirao and Y. Ohishi: J. Phys. Soc. Jpn. **88**, 123701 (2019).
[9] M. Sakata, M. Einaga, M. Dezhong, T. Sato, S. Orimo and K. Shimizu, Supercond. Sci. Technol. **33** 114004, (2020).

Collaboration among Computation, Experiments and Mathematics toward Next Generation Battery

Kazuto Akagi[*]

WPI-Advanced Institute for Materials Research (WPI-AIMR), Tohoku University

Exploration and design of new materials for energy devices is one of the important issues of modern materials science. The data driven approach known as "Materials Informatics" has brought us drastic change in various ways, but it is not a magic. We may find better materials by interpolation of a dataset based on machine learning techniques. But if we want to find novel materials by extrapolation, appropriate modeling based on scientific understandings of target systems is indispensable.

In this talk, we will focus on some recent activities in the field of development of high-performance next generation batteries, which is strongly expected from the viewpoint of environmental problem. First, we will briefly introduce "Advanced Target Project" in AIMR and "Fugaku Battery & Fuel Cell Project [1]" using the supercomputer Fugaku to see what are the latest interests and challenges there.

Next, two key components in my own approach to achieve reliable classical molecular dynamics simulations and enable quantitative characterization of large complex structural data will be shown (Fig.1). The former one is a framework optimizing force field parameters based on multi-objective genetic algorithm, and the latter one is topological data analysis based on persistent homology [2], respectively. We will see how these methods are applied to obtain the scientific understandings of thermodynamic behavior of solid electrolyte systems with hydride materials and polymer electrolyte systems for proton transport. Not only the on-going collaborations but possible collaborations necessary to solve the problems will also be mentioned.

[1] https://www.nims.go.jp/fugaku-denchi/en/index.html
[2] Y. Hiraoka et al., PNAS 113, 7035-7040 (2016).

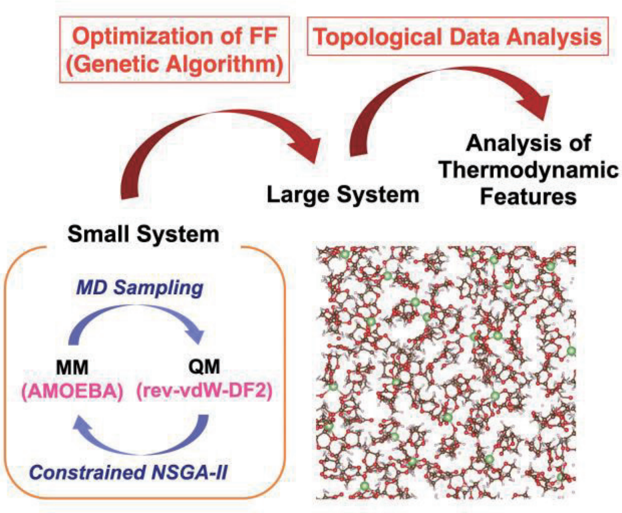

Fig. 1. Approach to battery materials by combination of reliable large-scale MD simulation and topological data analysis.

XPS Analysis of Functional Oxides

Andreas Klein*

Technical University of Darmstadt, Department of Materials and Earth Sciences, Electronic Structure of Materials Group, Otto-Berndt-Str. 3, 64287 Darmstadt, Germany

X-ray photoelectron spectroscopy (XPS) is widely used for the analysis of the chemical composition and oxidation states of surfaces. Apart from chemical and composition analysis, XPS can provide insights into the defect properties of the materials. This is provided by the possibility to determine the Fermi energy and its variation with doping and preparation conditions and its evolution during interface formation. Even highly insulating samples can be analyzed either via measuring thin films on conducting substrates or by using thin conducting top electrodes. As an example, Fig. 1 shows the Fermi energies of differently doped CeO_2 thin films. These data can be directly compared with defect chemistry calculations. Large data sets for a single material provide limits of the Fermi energy, which are directly related to the dominant compensation mechanism of doping.

Interface studies can reveal chemical interactions and help to understand the factors influencing Schottky barrier heights and heterojunction band alignment. By comparing with the Fermi energy limits, a fundamental understanding of compensation mechanisms is possible (see Fig. 1). A description of XPS basics and its application to functional oxides can be found in [1-3].

[1] A. Klein, T. Mayer, A. Thissen, and W. Jaegermann, *Photoelectron Spectroscopy in Materials Science and Physical Chemistry: Analysis of Composition, Chemical Bonding and Electronic Structure of Surfaces and Interfaces*, Bunsenmagazin 10 (2008), 124.

[2] A. Klein, *Energy band alignment at interfaces of semiconducting oxides: A review of experimental determination using photoelectron spectroscopy and comparison with theoretical predictions by the electron affinity rule, charge neutrality levels, and the common anion rule*, Thin Solid Films 520 (2012), 3721.

[3] A. Klein, *Interface Properties of Dielectric Oxides*, J. Am. Ceram. Soc. 99 (2016), 369.

[4] R. Schafranek, S. Li, F. Chen, W. Wu, and A. Klein, *$PbTiO_3$/$SrTiO_3$ interface: Energy band alignment and its relation to the limits of Fermi level variation*, Phys. Rev. B 84 (2011), 045317.

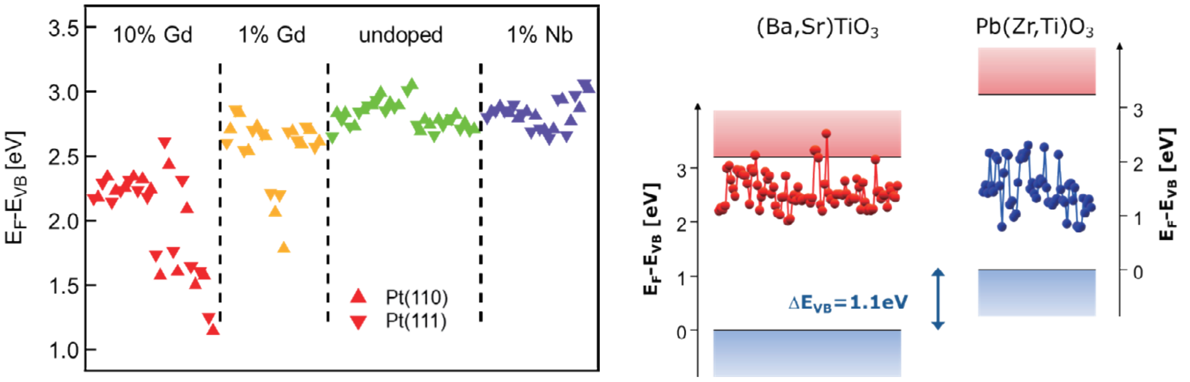

Fig. 1: (left) Fermi energies of differently doped and treated CeO_2 thin film samples deposited onto Pt coated MgO(110) and c-cut sapphire substrates; (right) Variation of the Fermi energy in BST and PZT films with aligned energy bands [4].

High-Temperature Acoustic Loss in Piezoelectric CTGS crystals

Y. Suhak, M. Schulz, H. Fritze

Institute of Energy Research and Physical Technologies,
Clausthal University of Technology

High-temperature stable piezoelectric crystals of the langasite family show a broad application potential in a wide temperature range. For example, the development of high-quality crystals supports the development of frequency filters [1]. Further, the mass sensitivity of resonant sensors at high temperatures offers advantages in the sensor technology of gases or soot particles and thus supports the development and the increase in efficiency and environmental compatibility of energy conversion processes [2,3].

Piezoelectric $Ca_3TaGa_3Si_2O_{14}$ (CTGS) crystals combine properties required for high-temperature transducers like excellent thermal and chemical stability, high phase transformation temperatures and low electromechanical losses. The fundamental resonance properties of high-temperature piezoelectric crystals such as maximum operation temperature and losses are reviewed. Atomistic transport properties of langasite-type crystals are then discussed and correlated with electromechanical losses. Here, the focus is put on dominating charge carriers, conductivity related losses and anelastic point defect relaxations. For example, oxygen transport is found to play a minor role. The analysis is applied to nominally identical CTGS crystals from several manufacturers which show different impurity levels. The electromechanical losses are analyzed as a function of temperature from room temperature up to 900 °C and compared with langasite. The overall loss and its contributions in CTGS crystals are shown in Fig. 1. Further, fundamental material properties including electrical conductivity and resonance frequency are monitored over a period of one year at 1000 °C and found to decrease by only 0.1 % and 0.4 %, respectively.

Finally, application relevant information about uncertainty in frequency determination and mass sensitivity is presented. For the given experimental conditions, a mass resolution of 50 ng is found for a CTGS resonator operated in thickness-shear mode at about 5 MHz and 700 °C.

[1] H. Kawanaka, H. Takeda, K. Shimamura, T. Fukuda, J. Crystal Growth 183, 274 (1998).
[2] X. Jiang, K. Kim, S. Zhang, J. Johnson, G. Salazar, Sensors 14, 144 (2014).
[3] Y. Suhak, W. L. Johnson, A. Sotnikov, H. Schmidt, H. Fritze, MRS Advances 4, 515 (2019).

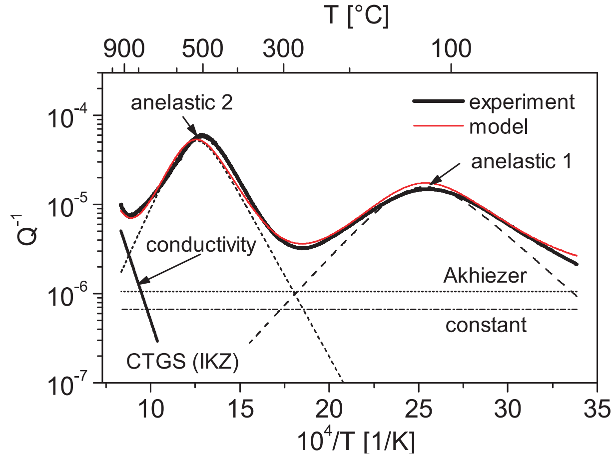

Fig. 1. Overall loss in CTGS and different temperature dependent loss contributions.

Impact of the Surface Space Charge Region on the Charge Transport in Oxides for Energy Applications

Matthias T. Elm[1*]

[1]Center for Materials research, Justus-Liebig University Giessen, Heinrich-Buff-Ring 16,
35392 Giessen
*Matthias.elm@phys.chemie.uni-giessen.de

Ion-conducting ceramic oxides are widely used for various applications in the field of electrochemical energy storage. While ceria and zirconia-based materials are used as electrolyte or electrode material for oxygen storage devices or solid oxide fuel cells, $LiCoO_2$-based ceramics are still the state-of-the art electrode material for lithium-ion batteries. In both cases, the electrode material exhibits a complex, porous architecture with a high surface area to ensure on the one hand the transport of the electronic and ionic charge carriers within the porous framework and on the other hand the exchange of oxygen with the surrounding atmosphere or the exchange of lithium ions with the electrolyte, respectively. However, due to the high grain boundary density and surface area, the material may exhibit different electronic an ionic transport properties compared to the bulk. The reason is that at interfaces the local symmetry is broken, resulting in the formation of a space charge region with different defect-chemical properties compared to the bulk. Especially in nanostructured materials, where interface effects can dominate the overall behavior, the space charge region may significantly alter the electrical properties. As the working principle of all electrochemical devices is based on the transport of charged carriers, a fundamental understanding of the defect-chemistry at the interfaces is needed to further optimize the device performance for applications.

The talk will give an overview on recent results on the electrochemical investigation of the transport properties of (meso)porous oxide thin films. Due to their high surface-to-volume ratio, these films present an ideal model system to study the influence of the surface properties on the electronic and ionic transport processes. The results reveal an increased electronic conductivity in porous oxygen-ion conductors due to the formation of a space charge region, not only in the case of mixed-conducting ceria but also for YSZ, whose bulk pendant is a purely ionic conductor. Furthermore, in these oxides protonic surface conductivity arises, which can be altered by modifications of the surface [1]. Finally, the talk will discuss the influence of the space charge region on the lithium storage capacity in mesoporous Nb-doped TiO_2 [2], which represents a promising anode material for lithium ion batteries.

[1] E. Celik, R.S. Negi, M. Bastianello, A. Maziklin, T. Brezesinski, M.T. Elm, Phys. Chem. Chem. Phys. **22**, 11519 (2020).

[2] J. Yue, C. Suchomski, P. Voepel, R. Ellinghaus, M. Rohnke, T. Leichtweiss, M.T. Elm, B.M. Smarsly, J. Mater. Chem. A **5**, 1978 (2017).

Catalytic Activity of Cobalt-Based Oxides for the Cathodic Reaction of IT-SOFC

Yuto Tomura, Toma Tazawa, Itaru Oikawa and Hitoshi Takamura

Department of Materials Science, Graduate School of Engineering, Tohoku University,
Sendai 980-8579, Japan

Cobalt-containing oxides such as LSC and BSCF are well-known to exhibit a superior oxygen reduction reaction (ORR) activity at intermediate temperatures for IT-SOFC. Even though their perovskite-type structure having a large amount of highly mobile oxygen vacancies is definitely responsible for their cathode performance, the catalytic activity of cobalt element itself is not well understood. The focus of this study is then to clarify its catalytic activity at intermediate temperatures apart from the perovskite-type structure. In this investigation, a modified pulse isotopic exchange technique was used to quantitatively evaluate the dissociative adsorption rate of Co–Fe-based spinel-type and Co–Mg-based rock salt-type oxides. The catalytic activity increased with increasing concentrations of the Co ion regardless of crystal structure. The non-linear relationship between the catalytic activity and the Co concentration indicated that the improvement in the catalytic activity of the Co-rich samples by the formation of Co clusters is greater than that resulting from a simple increase in the number of Co ions (Fig. 1). That effect was likely more remarkable in the Co-rich system because of the outstanding catalytic activity of Co_3O_4, which is comparable to the overall surface exchange rate of MIECs, and its relatively low activation energy compared to Fe-containing spinel-type oxides. The importance of the Co element in catalytic activity at high temperatures was confirmed [1].

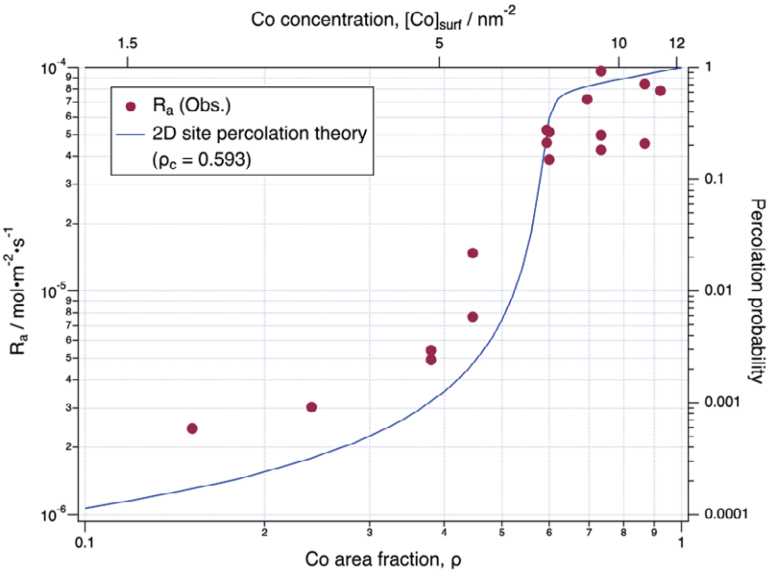

Fig. 1: Dissociative oxygen adsorption rate (R_a) as a function of Co area fraction for Co-Mg and Co-Fe-based oxides.

[1] Y. Tomura, T. Tazawa, I. Oikawa and H. Takamura, *J. Mater. Chem. A*, in press.

Flat Visible-Light Absorption Properties of Inorganic Thin Films Prepared by Pulsed Laser Deposition

Mina Yamaguchi[1], Akihiro Ishii[1], Itaru Oikawa[1], Yusuke Yamazaki[2], Masaaki Imura[2],
Toshimasa Kanai[2] and Hitoshi Takamura[1]

[1] Department of Materials Science, Graduate School of Engineering, Tohoku University,
Sendai, Japan
[2] Nippon Electric Glass Co., Ltd.

Preference for a classy black turn-off appearance and for distinct dark colors on flat-panel displays has led to a high demand for optically black materials. For use in flat-panel displays, the black materials must have three non-negotiable properties. They are required to have a large optical density (i.e. high magnitude of absorbance), have absorption which is less wavelength-dependent in the visible range (λ=400–700 nm), and also be homogeneous at the micro scale to avoid light scattering. It is difficult to satisfy these three requirements simultaneously. Our groups developed a newly concept that is coexistence of semiconducting absorption and metallic absorption mechanisms and controlling the composition.

$Nb_xTi_{1-x}O_2$, a solid solution combining the reduced titanium and niobium oxide phases were prepared by pulsed laser deposition (PLD), and their optical absorption properties were shown to be large in magnitude at an almost constant value of $\approx 17\ \mu m^{-1}$. Localized Nb-Nb dimers in the metallic $Nb_xTi_{1-x}O_2$ phase open an optical band gap which gives rise to semiconducting behavior [1]. Ti-O-N and tungsten-doped Ti-O-N prepared using nitrogen plasma assisted PLD also show the large and flat absorption coefficient of approximately 40 μm^{-1} in the visible range. The 4.1 mol%W-doped $Ti(O,N)_x$, which had a rock-salt-type structure, was optically jet-black. The origin of the flat wavelength dispersion in the W-doped $Ti(O,N)_x$ was attributed to the coexistence of semiconducting absorption and metallic absorption mechanisms. DFT calculations suggest that the 5d states achieved when using doped tungsten provide high absorption in the mid-wavelength range, whereas undoped-$Ti(O,N)_x$ was characterized by weak absorption [2].

In addition to a flat and large absorption coefficient in the visible range, an electrically insulative property is required for the application of the touch-panel displays; however, it is difficult to achieve these properties simultaneously in single phase because they are basically trade-off relation. Nano-sized metal particles dispersed into an insulator matrix are focused on in this study, in which the coexistence of free-carrier absorption of metal and inter-band absorption of insulator is expected. Cu-Bi_2O_3 and Ag-Fe_2O_3 thin films were prepared by PLD. The 30mol%Cu-Bi-O films and the 45mol%Ag-Fe-O thin films showed the large and the flat absorption in visible range. These sample have large sheet resistance ($R_{\mathrm{sheet}}>10^8$ ohm/sq.) even though the Cu and Ag peaks were observed in the XRD patterns, respectively. The ADF-STEM image of the Ag-Fe-O thin film shows three phases mixed in nanometer scale. These phases were identified as metallic Ag, spinel iron oxide and amorphous Ag-Fe-O phase from the element mapping and the electron diffraction pattern. In this thin film, Ag was separated partially by the insulator matrix, which have Ag and large resistance. This microstructure seems to be responsible for the electrically insulative property even for high Ag content.

[1] A. Shimabukuro, A. Ishii, I. Oikawa, Y. Yamazaki, M. Imura, T. Kanai and H. Takamura, *Appl. Surf. Sci.* **464**, 61 (2019).
[2] M. Yamaguchi, A. Ishii, I. Oikawa and H. Takamura, *Appl. Surf. Sci.* **534** 147616 (2020).
[3] A. Ishii, M. Yamaguchi, I. Oikawa, Y. Yamazaki, M. Imura, T. Kanai and H. Takamura, *phys, status solidi RRL*, **14**, 2000160 (2020)

Basic Properties of Vesicles as Biomaterials

Peter Walde

Laboratory for Multifunctional Materials, Department of Materials, ETH Zürich,
Vladimir-Prelog-Weg 5, 8093 Zürich, Switzerland

Amphiphilic molecules − with their hydrophilic and hydrophobic parts − are fascinating molecules since they assemble in aqueous solution into various types of polymolecular aggregates. SDS (sodium dodecylsulfate), for example, is a simple *micelle-forming* surfactant. Highly dynamic, thermodynamically stable, spherical SDS micelles form in water above the critical micellization concentration (CMC) and above the critical micellization temperature (CMT). Other types of aggregates may also form from amphiphiles in aqueous solution. It depends on (i) the chemical structure of the amphiphile, (ii) the concentration, (iii) the temperature, (iv) the composition of the aqueous solution, and - in many case - (v) the way the amphiphiles are brought in contact with the aqueous solution. In the latter case, the aggregates obtained are only kinetically stable and not thermodynamically). The phospholipid POPC (1-palmitoyl-2-oleoyl-*sn*-glycero-3-phosphocholine) belongs to this category. It is a typical *bilayer-forming* amphiphile, and is present in the lipid matrix of eukarytic membranes. POPC does not form micelles since the hydrophobic part is too large. Instead, POPC assembles into bilayers which self-close into vesicles in dilute aqueous solution, usually micrometer-sized *multilamellar* vesicles (MLVs), whereby several self-closed bilayers are arranged concentrically. Upon storage, MLVs sediment and form a separate phase, in equilibrium with the aqueous solution. For obtaining submicrometer-sized dispersed *unilamellar* POPC lipid vesicles (also called liposomes), the POPC molecules have to be "guided" during the assembly process or the MLVs obtained have to be sized-down mechanically. Unilamellar vesicles of a certain size and lamellarity are obtained by "guided assembly" and not by true self-assembly. Such vesicles can be stable for days or months if the energy barrier for vesicle fusion to MLVs is high. Similarly to lipid vesicles, vesicles can also be obtained from synthetic bilayer-forming amphiphilic block copolymers. They are called polymer vesicles or polymersomes.

Liposomes and polymersomes with their trapped aqueous volume and soft membrane are versatile compartment systems. They are investigated or already commercially applied as biomaterials in the field of drug delivery, even with considerations for possible future applications as artificial organelles.

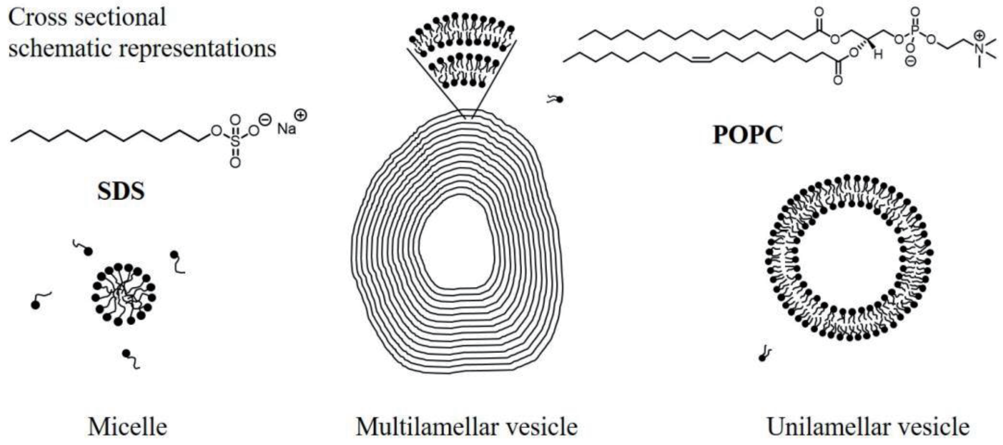

Bottom up approaches to synthetic cellularity

T-Y Dora Tang
Max Planck Institute for Cellular Molecular Biology and Genetics
Pfotenhauer Strasse 108, 01307 Dresden, Deutschland

Biology is well equipped in exploiting a large number of out of equilibrium processes to support life. A complete understanding of these mechanisms is still in its infancy due to the complexity and number of the individual components involved in the reactions. However, a bottom up approach allows us to replicate key biological processes using a small number of basic building blocks. Moreover, this methodology has the added advantage that properties and characteristics of the artificial cell can be readily tuned and adapted.

Here, I will present strategies for the design and synthesis of artificial cells based on hydrophobic effects such as lipid vesicles and proteinosomes and liquid-liquid phase separation of oppositely charged components (coacervates) and describe how these compartments may be used as platforms for implementing dynamic biological behaviours including: intercellular communication or autocatalysis.

Sustainable Reproduction of Vesicles coupled with Surface Confined Template Polymerization

Minoru Kurisu[1*], Peter Walde[2] and Masayuki Imai[1]

[1]Laboratory for Soft Matter and Biophysics, Department of Physics, Tohoku University
[2]Laboratory for Multifunctional Materials, Department of Materials, ETH Zürich

Construction of autonomously reproducing molecular assembly system from simple soft matter is one of the key approaches to understand what bridges non-living and living forms of matter. Here we show a sustainable growth and division (i.e. reproduction) of cell-size vesicles coupled with mutual catalytic relationship between vesicle membrane and membrane surface-confined polymerization [1]. Mutual catalytic relationship has been considered as an important clue to construct self-reproducing molecular system [2]. Concerning to the mutual catalysis, template polymerization reaction is a promising system in which monomers are arranged by a preformed macromolecule (template), and then they are polymerized interacting with the template. In order to construct reproduction system with vesicle and polymer, we focused on template polymerization of aniline on the surface of vesicle composed of AOT (i.e. sodium bis-(2-ethylhexyl) sulfosuccinate) [3]. In this system, polymerization reaction is localized on the vesicle surface, and specific form of polyaniline (polyaniline emeraldine salt form) is obtained due to interactions between AOT and polyaniline. In addition, polyaniline synthesized on the AOT vesicle surface promote selective incorporation of membrane molecules from bulk solution. As a result, synthesis of specific form of polyaniline and growth of membrane that works as template for the polyaniline is coupled: mutual catalytic relationship between polymer and membrane. To the vesicle growth system, we then introduced spontaneous vesicle division mechanism. Coupling between geometry of membrane molecules and local membrane curvature is known to be an important molecular mechanism which enables spontaneous vesicle division without the help of sophisticated biological mechanism such as using cytoskeleton protein [4, 5]. In our case, we introduced cholesterol as the second membrane molecules to the vesicle growth system composed of AOT and polyaniline, and we succeeded in realizing sustainable growth and division cycles of vesicle. This vesicle reproduction system is constructed not from complicated biological molecular system such as using nucleic acid and protein, but from simpler chemical reactions and components. We expect that the development of this work will give a contribution for discussing what is the minimal form of life, how it can emerge from non-living system and how it is stabilized.

[1]Kurisu, M. et al., *Communications Chemistry*, **2**:117(2019)
[2]Eigen, M. and Schuster, P. "*The Hypercycle*", Springer, Germany (1979)
[3]Junker, K. et al., *RSC Advances*, **2**, 6478–6495 (2012)
[4]Sakuma, Y. et al., *Physical Review Letters*, **107**, 198101 (2011)
[5]Jimbo, T. et al., *Biophysical Journal*, **110**, 1551-1562 (2016)

Theoretical approaches to topological materials

Shuichi Murakami[1,2*]

[1]Department of Physics, Tokyo Institute of Technology, 2-12-1 Ookayama, Meguro-ku,
Tokyo 152-8551, Japan.
[2]Materials Research Center for Element Strategy,
Tokyo Institute of Technology, 4259 Nagatsuta-cho, Midori-ku, Yokohama 226-8503, Japan

Topological materials have been attracting much interest in condensed matter physics. To date, thousands of materials have been identified to be topological by combining theories on topological materials with materials databases in an automatic way. Meanwhile, apart from automated searches, we need deeper understanding on topological nature of topological materials, from the materials science perspective. In my presentation, we explain a series of our works to understand their origins from various theoretical viewpoints. For example, studies on topological-nontopological phase transitions have shown us a new class of topological materials called topological semimetals, which have been established among the family of topological materials [1,2]. Remarkably, the notion of topological materials also brings about renewed interest on the known materials, such as bismuth bilayer film as a two-dimensional topological insulator [3], and alkaline earth metal calcium at high pressure as a topological nodal line semimetal [4]. Furthermore, we propose that electrides, in which electrons serve as anions in ionic crystals, are good candidates for topological materials [5,6,7]. Recently we also study higher-order topological insulators, in which boundary gapless states appear at corners and hinges of the crystals [7]. We show that in higher-order topological insulators, the dependence of the hinge states/corner states on crystal shapes show new features unique to higher-order topological insulators.

[1] S. Murakami, New J. Phys. **9**, 356 (2007).
[2] S. Murakami, M. Hirayama, R. Okugawa, and T. Miyake, Sci. Adv. **3**, e1602680 (2017).
[3] S. Murakami, Phys. Rev. Lett. **97**, 236805 (2006).
[4] M. Hirayama, R. Okugawa, T. Miyake, and S. Murakami, Topological Dirac Nodal Lines and Surface Charges in fcc Alkaline Earth Metals, Nat. Commun. **8**, 14022 (2017).
[5] M. Hirayama, S. Matsuishi, H. Hosono, and S. Murakami, Phys. Rev. X **8**, 031067 (2018).
[6] M. Hirayama, R. Okugawa, and S. Murakami, J. Phys. Soc. Jpn. **87**, 041002 (2018).
[7] M. Hirayama, R. Takahashi, S. Matsuishi, H. Hosono, S. Murakami, arXiv:2004.03785 (to appear in Phys. Rev. Research).

Morphology of Crystals in Melt Growth Processes

Kozo Fujiwara[1*]

[1]Institute for Materials Research, Tohoku University, Katahira 2-1-1, Aoba-ku, Sendai,
980-9577 Japan

A lot of crystalline materials are produced by solidification/crystal growth from melts. The morphologies of crystal and crystal-melt interface during crystallization processes affect microstructure of crystalline materials. Therefore, it is important to understand how the morphologies of crystal and crystal-melt interface are formed during crystallization processes. Usually, it is difficult to observe the crystal-melt interface directly in the melt growth processes since the melting point of inorganic materials is high. Therefore, we have developed an in-situ observation system which consists of a crystal growth furnace and a digital microscope [1]. That system enables us to observe crystal growth processes at an elevate temperature more than 1000℃. In this presentation, we will show the crystal growth shapes upon a normal growth and a dendritic growth from Si melt. The morphological transformation of crystal-melt interfaces of some crystalline materials will also be shown.

Figs. 1 (a) and (b) show Si crystals growing upon a normal growth mode and a dendritic growth mode from Si melts. It is found that the shape of Si dendrite is different from that of well known dendrites of metallic alloys. We will show that when a crystal contains two parallel twin boundaries, the growth kinetics at the crystal/melt interface changes and the crystal initiates dendritic growth [2]. The growth mechanism of this dendrite is different from the dendrites of metallic materials. We could observe such the dendrite growth caused by twin boundaries also in GaSb compound semiconductor [3].

Fig. 2 shows a morphological transformation of planar crystal-melt interface to zigzag-faceted interface during unidirectional solidification of Si [4]. This phenomenon is known as the interface instability. We will show that the interface instability is promoted when a growing crystal contains grain boundaries [5].

[1] K. Fujiwara, Y. Obinata, T. Ujihara, N. Usami, G. Sazaki, K. Nakajima, J. Crystal Growth **262**, 124-129 (2004).
[2] K. Fujiwara**,** K. Maeda, N. Usami, K. Nakajima, Phys. Rev. Lett. **101**, 055503 (2008).
[3] K. Shiga, M. Kawano, K. Maeda, H. Morito, K. Fujiwara, Scr. Mater. **168**, 56-60 (2019).
[4] M. Tokairin, K. Fujiwara, K. Kutsukake, N. Usami, K. Nakajima, Phys. Rev. **B 80**, 174108 (2009).
[5] K. K. Hu, K. Maeda, K. Shiga, H. Morito, and K. Fujiwara, Materialia **7**, 100386 (2019).

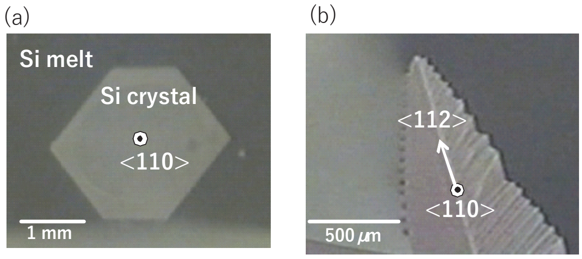

Fig. 1 Si crystals growing in the (a) normal growth and (b) dendritic growth mode.

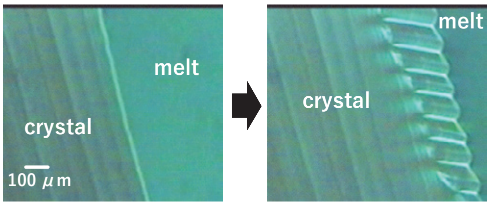

Fig. 2 Instability of crystal-melt interface of Si.

Nanometer-scale local crystal structure analysis using convergent-beam electron diffraction

Kenji Tsuda*

Frontier Research Institute for Interdisciplinary Sciences (FRIS),
Tohoku University, Sendai 980-8578, Japan
*email: k_tsuda@tohoku.ac.jp

Novel physical properties caused by local crystal structures such as relaxors have been reported increasingly. Convergent-beam electron diffraction (CBED) is an analysis method suitable for examining such nano-scale local crystal structures with the use of a nanometer-sized electron probe. It was established as the most powerful technique to determine crystal point- and space-groups [1]. We have been developing a quantitative analysis method to determine structural parameters based on fitting between experimental CBED intensities and dynamical diffraction (multiple scattering) simulations [2-4]. Electrostatic potential and electron density distributions of a local specimen area can be reconstructed from the determined structural parameters.

An important issue of the CBED is to develop a method for examining specimens with local structural variations. For this purpose, combined use of scanning the transmission electron microscopy (STEM) and the CBED was proposed (STEM-CBED) [5], where CBED patterns are acquired pixel-by-pixel by scanning the electron probe with a sub-nanometer scan step. Using the STEM-CBED method, we investigated local structures of perovskite-type ferroelectric oxides. Nano-scale spatial fluctuations of the rhombohedral polarization clusters were successfully visualized in both of the ferroelectric and paraelectric phases of $BaTiO_3$ and $KNbO_3$ [5-8]. These results provide crucial information on the mechanism of the structural phase transformations of these ferroelectrics. The STEM-CBED was recently applied for visualizing ferroaxial domains in $NiTiO_3$ [9], where rotational structural distortions of ferroaxial domains were observed with the aid of higher-order Laue zone reflection disks.

Another important issue of the CBED is to improve the sensitivity and accuracy of the quantitative structure analysis using CBED patterns. A promising way for this is the use of the large-angle CBED (LACBED) method [1], which is a technique to obtain intensity distributions of CBED reflection disks in a larger angular range beyond the Bragg angle. In a Fe 3*d* orbital-ordered phase of $FeCr_2O_4$, it was demonstrated that electron density distributions of the Fe 3d orbitals can be successfully reconstructed using LACBED data through excitation of characteristic Bloch waves [10]. Application of machine learning will be discussed for reducing computing time needed for LACBED simulations.

References:
[1] *e.g.* Tanaka and Tsuda, *J. Electron Microsc.*, **60**, S245 (2011).
[2] Tsuda and M. Tanaka, *Acta Cryst.*, **A55**, 939 (1999).
[3] Ogata, Tsuda and Tanaka, *Acta. Cryst.*, **A64**, 587 (2008).
[4] Tsuda *et al.*, *Phys. Rev. B*, **81**, 180102 (2010).
[5] Tsuda, Yasuhara and Tanaka, *Appl. Phys. Lett.*, **102**, 051913 (2013).
[6] Tsuda and Tanaka, *Appl. Phys. Express*, **8**, 081501 (2015).
[7] Tsuda and Tanaka, *Appl. Phys. Express*, **9**, 071501 (2016).
[8] Tsuda and Tanaka, *Jpn. J. Appl. Phys.*, **56**, 10PB09 (2017).
[9] Hayashida *et al.*, *Nat. Commun.*, **11**, doi:10.1038/s41467-020-18408-6 (2020).
[10] Morikawa and Tsuda, *Microsc.*, doi:10.1093/jmicro/dfaa041 (2020).

Abnormal Raman Modes in Janus Monolayers and Weyl Semimetals

Shengxi Huang[1]

[1]Department of Electrical Engineering, The Pennsylvania State University, University Park, Pennsylvania 16802 United States

In this talk, I will discuss the abnormal Raman modes that we have discovered recently for two material systems: Janus monolayer and Weyl semimetal. Janus transition metal dicalcogenide (TMD) is a newborn of the two-dimensional (2D) materials family [1]. Its structure is similar to TMDs such as MoS_2, but one layer of chalcogen is different from the other layer, one example being MoSSe. Due to the unique crystal structure of Janus TMD and the induced out-of-plane dipole moment, we found that Janus monolayer enhances the interlayer coupling when forming van der Waals heterostructures, observed in the low-frequency Raman spectroscopy [2]. On the other hand, Weyl semimetals are a recently-discovered class of topological materials with numerous peculiar properties including chiral anomaly, surface Fermi arc, giant optical nonlinearity, etc. [3] We have observed the broken Raman symmetry and the polarization dependent Fano line shape [4]. The unconventional phenomena can be attributed to the unique electronic band structures and phonon dispersions. Both works demonstrated that Raman spectroscopy is an effective tool to probe the material structure and interface coupling, and can be correlated with electronic properties.

[1] Lu, A.Y., Zhu, H., Xiao, J., Chuu, C.P., Han, Y., Chiu, M.H., Cheng, C.C., Yang, C.W., Wei, K.H., Yang, Y. and Wang, Y., 2017. Janus monolayers of transition metal dichalcogenides. Nature Nanotechnology, 12(8), pp.744-749.

[2] Zhang, K., Guo, Y., Ji, Q., Lu, A.Y., Su, C., Wang, H., Puretzky, A.A., Geohegan, D.B., Qian, X., Fang, S. and Kaxiras, E., 2020. Enhancement of van der Waals interlayer coupling through polar Janus MoSSe. Journal of the American Chemical Society. In press.

[3] Xu, S.Y., Belopolski, I., Alidoust, N., Neupane, M., Bian, G., Zhang, C., Sankar, R., Chang, G., Yuan, Z., Lee, C.C. and Huang, S.M., 2015. Discovery of a Weyl fermion semimetal and topological Fermi arcs. Science, 349(6248), pp.613-617.

[4] Zhang, K., Pang, X., Wang, T., Han, F., Shang, S.L., Hung, N.T., Nugraha, A.R., Liu, Z.K., Li, M., Saito, R. and Huang, S., 2020. Anomalous phonon-mode dependence in polarized Raman spectroscopy of the topological Weyl semimetal TaP. Physical Review B, 101(1), p.014308.

Circularly Polarized Raman Scattering of Two-Dimensional Materials

Lianming Tong*

Center for Nanochemistry, College of Chemistry and Molecular Engineering, Peking
University, Beijing 100871, P.R. China
*Email: tonglm@pku.edu.cn

Raman spectroscopy is a powerful tool for the characterization of materials. The peak positions correspond to the energies of specific phonons, which give information on the composition and the lattice structures of materials. The intensity is determined by the optical transitions and the coupling between electrons and phonons. Generally, a linearly polarized laser is used for excitation. However, circularly polarized Raman scattering can provide more information that is not accessible by linear polarization.

In this talk, I will introduce our recent work on circularly polarized Raman scattering of two-dimensional (2D) materials. 2D materials are layered crystals of atomic thickness with intralayer chemical bonding but interlayer van der Waals interaction, which possess superior optical, electrical, mechanical and thermal properties. Raman scattering has been widely used to characterize the fine structures of 2D materials, such as layer number, defects and type of edges. In our work, we use circularly polarized laser for the excitation of Raman scattering in layered MoS_2 and ReS_2. MoS_2 belongs to a hexagonal crystal family, and the point group of the unit cell for bulk MoS_2 is D_{6h}. ReS_2 is anisotropic and belongs to triclinic crystal family.

The schematic of helicity-resolved Raman scattering and the corresponding Raman spectra of MoS_2 are shown in Figure 1. By helicity-resolved, the helicity of Raman scattered light is also resolved and compared to that of the incident light.[1] Using this technique, we characterized the excitonic nature and evaluated the relative contribution of the two kinds of electron/exciton−phonon interactions, that is, deformation potential (DP) or the Fröhlich interaction (FI).[2-3] On the other hand, for ReS_2, we observed distinct difference in Raman spectra excited by left- and right-handed circularly polarizations (LCP and RCP) even without the selection of helicity. This phenomenon is attributed to the different phase factors of electron-photon matrix elements excited by LCP and RCP. The difference is then amplified by the electron-phonon coupling.[4]

[1] Y. Tatsumi, T. Kaneko, and R. Saito, Phys. Rev. B **97**, 195444(2018).
[2] Y. Zhao, S. Zhang, Y. Shi, Y. Zhang, R. Saito, J. Zhang, and L. Tong, ACS Nano **14**, 10527 (2020).
[3] Y. Zhao, S. Han, J. Zhang, and L. Tong, J. Raman Spectrosc. 2020, DOI: 10.1002/jrs.5996.
[4] S. Zhang, J. Huang, Y. Yu, S. Wang, T. Yang,* Z. Zhang, J. Zhang, and L. Tong*, *in prepration.*

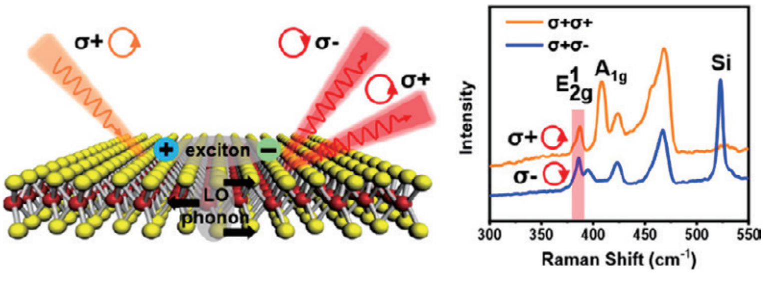

Fig. 1. Schematic of helicity-resolved Raman scattering and corresponding Raman spectra of MoS_2.

Double Resonant Raman Scattering in TMDCS

Teng Yang[1*], Jianqi Huang[1*], Huaihong Guo[2] and Riichiro Saito[3]

[1] Shenyang National Laboratory for Materials Science, IMR, CAS, Shenyang, China
[2]College of Sciences, Liaoning Shihua University, Fushun, China
[3] Department of Physics, Tohoku University, Sendai, Japan

Raman spectra of TMDCs have been reported for several decades. The first-order Raman process in TMDCs has been widely investigated and is now well understood. However, the study of second-order Raman spectra has not yet given consistent assignments for different TMDCs. We study the second-order Raman process of monolayer TMDCs, by combining *ab initio* density functional perturbation calculations with experimental Raman spectroscopy and electron-phonon Wannier (EPW) method [1-4]. The calculated electronic band structure and the density of states show that the resonance Raman process occurs at the M point in the Brillouin zone (**Figure 1**), where a strong optical absorption occurs due to a logarithmic Van Hove singularity of the electronic density of states. The double resonance Raman process with intervalley electron-phonon coupling connects two of the three inequivalent M points in the Brillouin zone, giving rise to second-order Raman peaks due to the M-point phonons. The calculated vibrational frequencies and laser-energy dependent Raman spectra of the second-order Raman spectra agree with the observed laser-energy-dependent Raman shifts in experiment. We also predicted the polarization dependence of the double resonant Raman modes.

[1] H. Guo, T. Yang, M. Yamamoto, L. Zhou, et al., Phys. Rev. B 91, 205415 (2015).
[2] Hsiang-Lin Liu, Huaihong Guo, et al., Phys. Chem. Chem. Phys. 17 (22), 14561 (2015).
[3] R. Saito, A. R. Nugraha, E. H. Hasdeo, S. Siregar, Huaihong Guo, Teng Yang, Physica Status Solidi B 252 (11), 2363–2374 (2015).
[4] Hsiang-Lin Liu, Teng Yang, Yuki Tatsumi, Ye Zhang, Baojuan Dong, Huaihong Guo, et al., Scientific Reports 8, 11398 (2018).

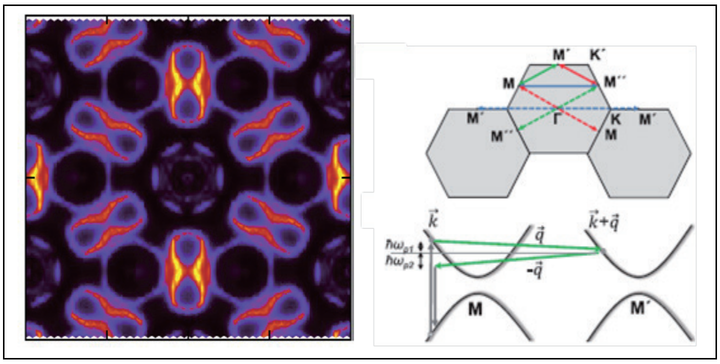

Figure 1. (left) Raman intensity of one mode in the Brillouin zone at a certain laser energy. (right) The schematics of the double resonance process (electron-photon and electron-phonon

POSTER ABSTRACTS:
Materials Science

P-1

Innovative Strategies for High-Performance Cross-linked Polymer Electrolytes for Rechargeable Lithium Ion Batteries

Manjit Singh Grewal[1], Kazuaki Kisu[1], Shin-ichiro Orimo[1,2], Hiroshi Yabu[1]

[1]WPI-Advanced Institute of Materials Research (WPI-AIMR), Tohoku University, 2-1-1, Katahira, Aoba-Ku, Sendai 980-8577, Miyagi Japan,
[2]Institute of Materials Research (IMR), Tohoku University, 2-1-1, Katahira, Aoba-Ku, Sendai 980-8577, Miyagi Japan)
[1]TEL/FAX: ＋81-22-217-6341/6342, E-mail: grewal.manjit.singh.d3@tohoku.ac.jp, hiroshi.yabu.d5@tohoku.ac.jp

Present work aims for an attempt to simultaneously improve the functions and properties in an electrolyte based on cross-linked network polymer comprising solvate ionic liquids that represent an emergent class of innovative polymer electrolytes. Such electrolytes are promising as they possess not only sufficient mechanical properties to separate the electrodes, but also provide as high ionic conductivity as possible, as high a transference number of the active cation as possible, and form a good, electrochemically stable interface with both of the electrode materials (1-3).

This presentation will highlight work on a series of free-standing cross linked network polymer electrolytes prepared from poly(ethylene glycol) diacrylate (PEGDA) prepolymer host in low molar ratios plasticized by different concentrations of solvate ionic liquids (equimolar tetraglyme and bis(trifluoromethane) sulfonamide lithium (LiTFSI) salt) *via* solvent-free photo-induced cross-linking. In this manner of concurrent exploitation of photo-induced cross-linking and *in situ* functionalization procedures, kinetically driven inhibition of the PEG-chains crystallization is readily achievable at ambient conditions, leading to polymer electrolytes that possess high mechanical stiffness as well as liquid-like ion motions. The as-prepared polymer networks exhibited excellent comprehensive performance in terms of high ionic conductivity (1.0 × 10-4 S cm-1 at 45 °C), a wide electrochemical window (4.5 V), high lithium ion transference number (0.45), good uniform lithium stripping and plating profiles under long hours of cell operation.

We envisage that the proposed approach for innovative soft polymer electrolytes would lead to a rational designing to address the existing challenges of lithium ion polymer batteries.

References:

1. M. S. Grewal, K. Kisu, S. Orimo, H. Yabu, *Chem. Lett.*, **2020**, 49 | doi:10.1246/cl.20057**22020**.
2. L. Porcarelli *et al.*, *Sci. Rep.* 6, **2016**, 19892.
3. M. S. Grewal, M. Tanaka, H. Kawakami, *Electrochim. Acta*, 15, **2019**, 307, 148.

Unveiling the lithium-oxygen electrochemistry by in situ liquid cell transmission electron microscopy

Jiuhui Han[1,2], Chen Hou[1], Chuchu Yang[1], and Mingwei Chen[1,3]

[1] WPI-Advanced Institute for Materials Research (WPI-AIMR), Tohoku University
[2] Frontier Research Institute for Interdisciplinary Sciences (FRIS), Tohoku University
[3] Department of Materials Science and Engineering, Johns Hopkins University

In situ transmission electron microscopy (TEM) is emerging as a powerful tool for studying micro- and nanoscale dynamic phenomena in real-time and real-space. In particular, the recently developed liquid-cell TEM has opened up new opportunities to investigate chemical and electrochemical reactions in liquid media. Here we present the utilization of *in situ* liquid-cell TEM for investigating the fundamental electrochemistry of non-aqueous lithium-oxygen ($Li\text{-}O_2$) battery, the emerging energy storage system that can theoretically deliver ten times more energy than today's lithium-ion batteries. By directly visualizing the dynamic processes of the $Li\text{-}O_2$ reactions during synchronized electrochemical measurements, *in situ* TEM has identified where/when/how the discharge products accumulate and evolve, as well as their correspondence to the electrochemical responses with spatially and time-resolved capabilities. These studies provide important insight into the fundamental mechanisms, such as the reaction pathways and kinetics, of $Li\text{-}O_2$ batteries and the working principles of solid and liquid catalysts.

[1] C. Hou[†], J. H. Han[†], P. Liu, G. Huang, and M. W. Chen, *Nano Lett.* **20**, 2183-2190 (2020).
[2] C. Hou, J. H. Han, P. Liu, C. C. Yang, G. Huang, T. Fujita, A. Hirata, and M. W. Chen, *Nano Energy* **47**, 427-433 (2018).
[3] C. C. Yang[†], J. H. Han[†], P. Liu[†], C. Hou, G. Huang, T. Fujita, A. Hirata, and M. W. Chen. *Adv.Mater.* **29**, 1702752 (2017).
[4] J. H. Han, K. Watanabe, and M. W. Chen, *Operando observations of $Li\text{-}O_2$ reaction dynamics*, in *Analysis and Evaluation Technology of Lithium-Ion Batteries*, Technical Information Association Inc., pp. 453-464 (2019).

P-3

The Large Magnetoresistance in $BaMn_2Bi_2$ Antiferromagnet and its Possible Origins

K.-K. Huynh[A], T. Ogasawara[B], S. Y. Matsushita[A], M. Kimata[C],
T. Tahara[D], T. Kida[D], M. Hagiwara[D], K. Tanigaki[A]

[A]WPI-AIMR, Tohoku University,
[B]Dept.Phys, Grad. Sch. Science, Tohoku University,
[C]Inst. Mat. Res. (IMR), Tohoku University,
[D]Advanced High Magnetic Field Science, Grad. Sch. Science, Osaka University

$BaMn_2Pn_2$ compounds, in which Pn denotes a pnictogen element, are intriguing antiferromagnets with a (122) tetragonal layered structure and a G-type antiferromagnetic ordering (AFM) of Mn^{2+} sublattice. Whereas the crystal structure resembles that of the (122) iron pnictide superconductors, the G-type AFM along the *c*-axis results in the magnetic point group 4'/*m'mm'*. This point group is odd under both time reversal (TR) and space inversion (SI) but even under the combination symmetry PT = TR×SI. Theoretical studies of $BaMn_2Pn_2$ predicted novel physical phenomena, such as a magnetic hexadecapole order and a current induced nematicity, as the consequences of this symmetry [1]. On the other hand, the orbital degree of freedom of the half-filled 3*d*-shell of the Mn^{2+} provides another interesting aspect and some studies suggested that these materials show an orbital-selective magnetism being near to a Mott transition [2].

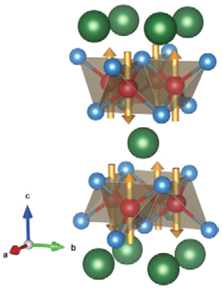

***Fig 1**: $BaMn_2Pn_2$*

In its temperature-resistivity curve, a $BaMn_2Pn_2$ exhibits a metal-to-insulators transition from a bad metallic behavior to an insulating-like as the temperature decreases. In our previous study, we reported a very large positive magnetoconductivity (MC) appearing in the insulating regime of all $BaMn_2Pn_2$ compounds [3]. As shown in Fig. 2, the MC appears large only under magnetic fields perpendicular to the Neel vector and its magnitude is sufficient to re-introduce the metallic state in the case of $BaMn_2Bi_2$. The origin of the MC and how it connects to the AFM as well as to the hexadecapole order have remained unclear. In this report, we approach this question by studying the insulating regime under zero magnetic fields of $BaMn_2Bi_2$. Our study suggests that the insulating behavior of $BaMn_2Bi_2$ does not originate from a band gap but rather from a localization of charge carriers at the Fermi level. Based on this observation, we will propose relevant mechanisms for the MC in $BaMn_2Pn_2$'s and discuss the mechanisms from the viewpoint of the symmetry and the orbital degree of freedom.

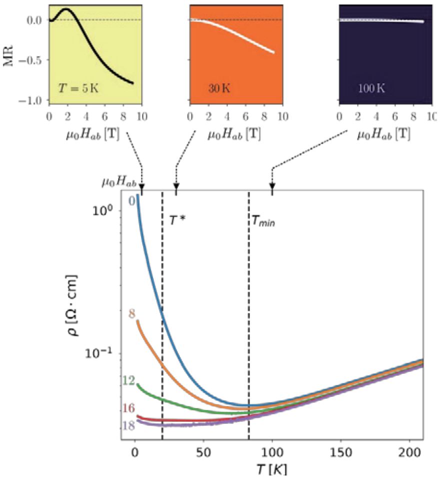

***Fig 2:** Large MC in $BaMn_2Bi_2$*

[1] Watanabe, H., Youichi Y., PRB 96, 064432 (2017)

[2] Craco L., Carara S. S., PRB 97, 205114 (2018)

[3] Huynh. K.K et al, PRB 99, 195111 (2019)

Increased Curie Temperature and Enhanced Perpendicular Magneto Anisotropy of $Cr_2Ge_2Te_6$/NiO Heterstructures

H. Idzuchi[1-3*], A. E. Llacsahuanga Allcca[3], X. C. Pan[1], K. Tanigaki[1], and Y. P. Chen[1-4]

[1]WPI Advanced Institute for Materials Research (AIMR), Tohoku University, Sendai 980-8577, Japan
Astronomy, Purdue University, West Lafayette, Indiana 47907, USA
[2]Center for Science and Innovation in Spintronics, Tohoku University, Sendai 980-8577, Japan
[3]Purdue Quantum Science and Engineering Institute and Department of Physics and
[4]School of Electrical and Computer Engineering and Birck Nanotechnology Center, Purdue University, West Lafayette, Indiana 47907, USA

Magnetism in two-dimensional van der Waals materials has received significant attention recently. The Curie temperature reported for those materials, however, has been so far remained relatively low. Here, we measure magneto-optical Kerr effects (MOKE) under perpendicular magnetic field for van der Waals ferromagnet $Cr_2Ge_2Te_6$ as well as its heterostructure with antiferromagnetic insulator NiO. We observe a notable increase in both Curie temperature and magnetic perpendicular anisotropy in $Cr_2Ge_2Te_6$/NiO heterostructures compared to those in $Cr_2Ge_2Te_6$. Measurements on the same exfoliated $Cr_2Ge_2Te_6$ flake (on a SiO_2/Si substrate) before and after depositing NiO show that the hysteresis loop can change into a square shape with larger coercive field for $Cr_2Ge_2Te_6$/NiO (Fig.1). The maximum Curie temperature (T_C) observed for $Cr_2Ge_2Te_6$/NiO reaches ~120 K, is nearly twice the maximum T_C ~ 60 K reported for $Cr_2Ge_2Te_6$ alone. Both enhanced perpendicular anisotropy and increased Curie temperature are observed for $Cr_2Ge_2Te_6$ flakes with a variety of thicknesses ranging from ~5 nm to ~200 nm. The results indicate that magnetic properties of two-dimensional van der Waals magnets can be engineered and controlled by using the heterostructure interface with other materials.

[1] H. Idzuchi, A. E. Llacsahuanga Allcca, X. C. Pan, K. Tanigaki and Y. P. Chen, Appl. Phys. Lett. **115**, 232403 (2019).

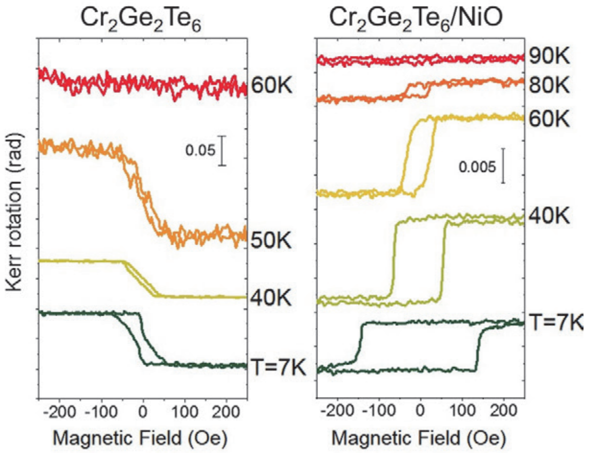

Fig. 1. MOKE curves for $Cr_2Ge_2Te_6$ flake with and without NiO at various temperature.

Space-filling open microfluidics for droplet collection by hierarchical transport: generative design of fractal hyperbranched channels

Hiroyuki Kai[1*]

[1]WPI-Advanced Institute for Materials Research (WPI-AIMR), Tohoku University

Open microfluidics enables controlled transport of liquid droplets on the solid surface. Wettability patterning on the surface has been utilized to trap droplets and guide their transport. Megaridis' group developed an open microfluidic channel for the fast transport of aqueous droplets using a narrow superhydrophilic strip with width gradient surrounded by superhydrophobic surface [1]. Their open microfluidic channel takes advantage of a coating of a mixture of titanium oxide nanoparticles and Capstone® ST-100 fluoroacrylate copolymer, which is originally superhydrophobic and turns superhydrophilic when irradiated with ultraviolet (UV) light. This superhydrophilic microfluidic channel can be readily fabricated by photolithography. We developed open microfluidic channels that collect aqueous liquid from the solid surface by directional transport and hierarchical fusion of droplets in hyperbranched channels [2]. Triangular regions that are filled with hyperbranched patterns of fractal geometry, called space-filling trees [3], were automatically generated by software with recursive algorithm. Following the fabrication of photomasks with the generated patterns, the space-filling open microfluidic channels were fabricated on a plastic film by photolithography. When fine water droplets were sprayed on the surface of the film, fast (< 1 s) and highly efficient (74% ± 9%) accumulation of water to a focal point at the center (a circle of 2mm radius) by repeated transport and merging of the droplets in a hierarchical manner was observed. the algorithms were developed to generate patterns of space-filling open microfluidic channels that fill an arbitrary convex polygon, where the structural variation can be readily prepared by varying a small number of parameters for the pattern-generating functions [4].

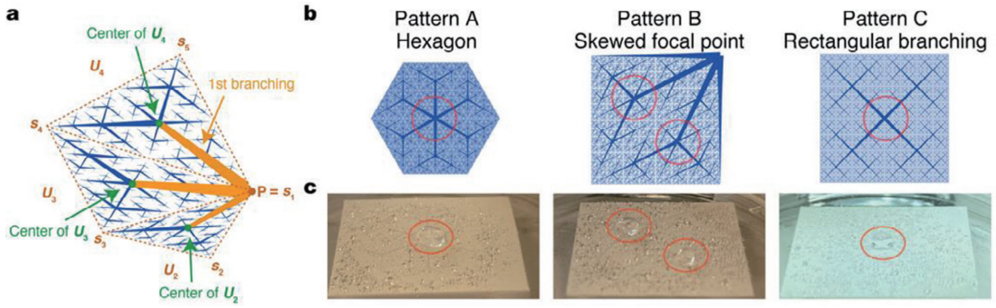

Figure 1: (a) Patterning algorithm of space-filling open microfluidics for an arbitrary polygon and focal point in the case that the focal point is one of the vertices of the polygon (b) Representative patterns, A (left), B (middle), and C (right). (c) Accumulated water blobs after spraying water droplets for the patterns A, B, and C.

[1] A. Ghosh et al., *Lab on a Chip* **14**, 1538 (2014).
[2] H. Kai*, R. Toyosato, and M. Nishizawa*, *RSC Adv*. **8,** 15985 (2018).
[3] J.J. Kuffner and S.M. LaValle, *2011 IEEE/RSJ International Conference on Intelligent Robots and Systems (IROS)*, 2199–2206, 2011.
[4] H. Kai*, *MicroTAS 2020.*

Interface-Engineered Magnetic Gilbert Damping: An Experimental and Theoretical Study in Perpendicularly Magnetized Fe/MgAl$_2$O$_4$ Heterostructures

R. Mandal[1]*, Q. Xiang[1], K. Masuda[1], Y. Miura[1], H. Sukegawa[1], S. Mitani[1] and Y. K. Takahashi[1]

[1] Research Center for Magnetic and Spintronic Materials, National Institute for Materials Science (NIMS), Tsukuba 305-0047, Japan

Gilbert damping is one of the most unexplored issues in magnetic materials, particularly in interface-engineered heterostructures. A recent critical issue of high-speed [1-3] and energy-efficient spintronic devices is coexistence of low magnetic Gilbert damping constant (α) and large perpendicular magnetic anisotropy (PMA). To investigate both in a model system experimentally and theoretically, a flat, lattice-matched interface has been developed in an Fe (0.7 nm)/MgAl$_2$O$_4$ (3 nm) epitaxial bi-layer film by varying the *ex-situ* annealing temperature, which is main catalyst to vary the interface oxidation degree and PMA energy densities. Here, the optimized procedure for interface engineering allows to achieve the lowest α (0.013) ever reported and a strong interfacial PMA energy (0.8 MJ m^{-3}). By employing different interfacial atomic configurations in a first-principles calculation, the origin of the PMA energy and α has been explained. The d(yz) and d(zx) orbitals of the interfacial Fe atoms in the minority-spin states are responsible for orbital moment and its anisotropy. Furthermore, the matrix elements between these two orbitals in the non-spin-flip term predominately contribute to damping. These detailed findings provide a clear insight into the development of materials with strong PMA energies and low damping characteristics, thereby facilitating promising future spintronic applications.

[1] S. S. P. Parkin, C. Kaiser, A. Panchula, P. M. Rice, B. Hughes, M. Samant, S.-H. Yang, Nat. Mater. **3**, 862 (2004).

[2] S. Ikeda, K. Miura, H. Yamamoto, K. Mizunuma, H. D. Gan, M. Endo, S. Kanai, J. Hayakawa, F. Matsukura, H. Ohno, Nat. Mater. **9**, 721 (2010).

[3] L. Berger, Phys. Rev. B **54**, 9353 (1996).

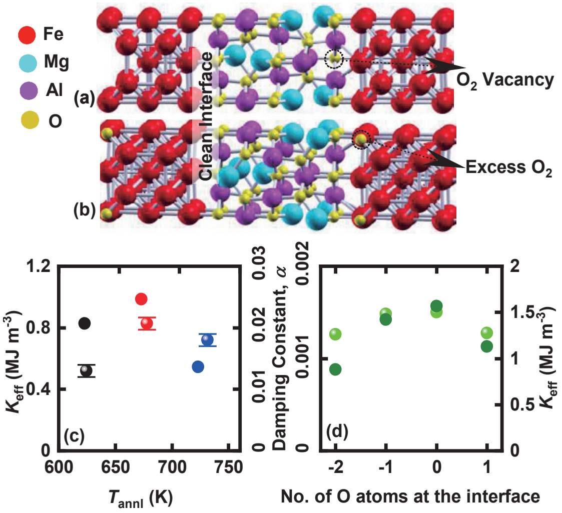

Fig. 1. Schematic of the Fe/MgAl$_2$O$_4$ (MAO) [001] interfaces with (a) oxygen-poor and (b) oxygen-rich (b) interfaces. The experimental and calculated magnetic Gilbert damping constant α and the perpendicular magnetic anisotropy (PMA) energy is plotted as a function of the annealing temperature T_{annl} (c) and number of oxygen atoms, n_{O} at the interface (d).

P-7

Atomic-layered antiferromagnet with perpendicular magnetic anisotropy

K. Z. Suzuki[1,2], and S. Mizukami[1,2,3]

[1] WPI Advanced Institute for Materials Research, Tohoku University, Sendai, Japan
[2] Center for Spintronics Research Network (CSRN), Tohoku University, Sendai, Japan
[3]CSIS (CRC), Tohoku University, Sendai, Japan
e-mail: kazuya.suzuki.d8@tohoku.ac.jp

Recently, an antiferromagnet has attracted much attention in spintronics [1]. Because their zero net magnetization and strong exchange coupling are distinct from conventional ferromagnet, thus, it is expected to be promising material for future spin-torque devices. Recently, we found that an atomic-layered antiferromagnetic Mn grown on a CoGa seed layer exhibits perpendicular anisotropy. In addition, a magnetic tunnel junctions utilizing atomic-layered Mn shows clear tunnel magnetoresistance (TMR) effect at room temperature [2]. In this poster presentation, we report structural (Fig.1) and magnetic properties (Fig.2) and TMR effect of MTJs using atomic-layered Mn electrode. Moreover, we demonstrate the electrical switching of their magnetization by spin-orbit torque.

Refference
[1] T. Jungwirth et al., Nat. Nanotechnology 11, 231 (2016)
[2] K. Z. Suzuki et al. ACS Appl. Mater. Interfaces 10, 43305 (2018)

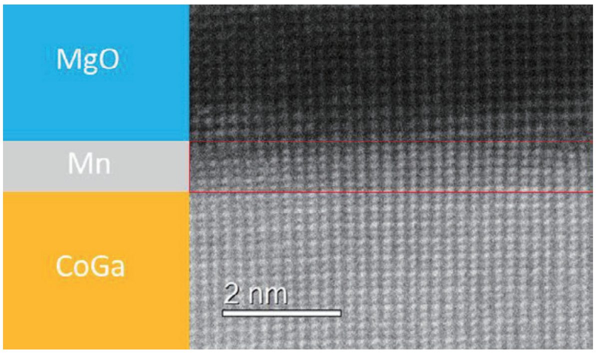

Fig.1 The cross-sectional HAADF-STEM image of the CoGa/Mn/MgO layers.

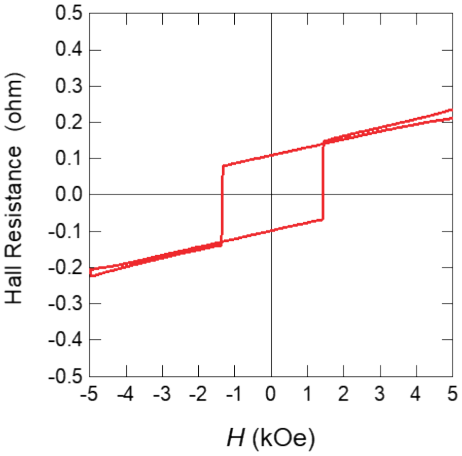

Fig.2 Anomalous Hall effect of the CoGa/Mn/MgO structure.

P-8

Turbulent Mixing Phenomenon and Solvent Effects on Kinetics of Supercritical Hydrothermal Synthesis: Reaction of Nickel Nitrate to Nickel Oxide

Akira Yoko[1], Gimyeong Seong[2], Takaaki Tomai[3], Tadafumi Adschiri*[1,2,3]

[1] WPI-Advanced Institute for Materials Research (WPI-AIMR), Tohoku University
[2] New Industry Creation Hatchery Center, Tohoku University, Sendai 980-8579, Japan
[3] Institute of Multidisciplinary Research for Advanced Materials, Sendai 980-8577, Japan,
*Email: akira.yoko.c7@tohoku.ac.jp

Reaction kinetics of hydrothermal synthesis for the nickel nitrate to nickel oxide that occurs in a wide range of temperatures and pressures around the critical point of water was evaluated. The effects of mass transfer on the reaction rate were evaluated using a two-flow mixing system. The mixing rate, which affects reaction kinetics was successfully described using *Re* number and temperature. The kinetics under reaction control conditions was obtained based on the mixing study. The hydroxyl ion concentration, which varies greatly around the critical point, strongly affects the reaction kinetics. Results suggest that the hydroxyl ion is a reactant of the hydrothermal reaction. With consideration of that fact, the intrinsic reaction constant was evaluated to understand the solvent effects. Near the critical point, the properties of water change greatly with even slight changes of temperature and pressure. Strong solvent effects on the intrinsic kinetic constant were observed. An acceleration of intrinsic kinetics above the critical temperature or with reduced pressure in a supercritical condition is attributable to a decrease in the dielectric constant. This dielectric constant effect on the intrinsic rate constant from gas-like to liquid-like atmospheres can be explained well using the Kirkwood equation, which suggests a missing link between Eyring's gas-phase absolute kinetics theory and the Kirkwood liquid phase solvent effect theory.

[1] A. Yoko, Y. Tanaka, G. Seong, D. Hojo, T. Tomai, T. Adschiri, J. Phys. Chem. C **124 (8)**, 4772–4780 (2020).

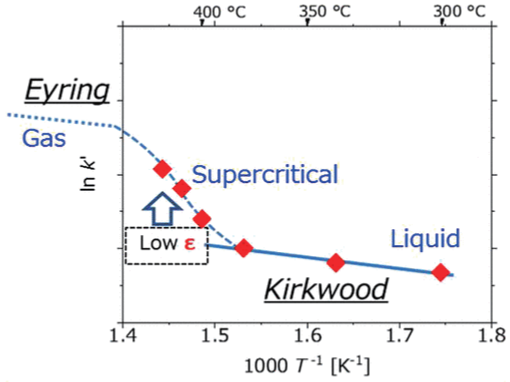

Fig. 1. Solvent effects around critical point [1].

P-9

Nonreciprocal Electronic Transport in an Itinerant Antiferromagnet $PdCrO_2$ with 120-degree Spin Structure

M. Akaike*, Y. Nii, H. Masuda and Y. Onose

Institute for Materials Research, Tohoku University

Non-collinear magnets have attracted much attention due to its non-trivial magnetic transport. It can be caused by an emergent field owing to the complex spin arrangements. In order to elucidate the mechanism, the precise understanding of the magnetic structure is essential. While the neutron diffraction measurements should play a significant role, some probes sensitive to symmetry breakings can also provide valuable information and help identify accurate spin structures. We study the magnetic structure in an itinerant antiferromagnet $PdCrO_2$ utilizing nonreciprocal electronic transport, a symmetry-sensitive probe.

Generally speaking, in the spatial inversion and time-reversal symmetries simultaneously broken systems, the responses for rightward and leftward stimuli are different from each other. The nonreciprocal electronic transport is electrical resistivity depending on the sign of electric current [1].

In $PdCrO_2$, the magnetic moments show the 120-degree structure below $T_N = 37$ K. The unconventional anomalous Hall effect proposed to be induced by the spin-chirality is observed at low temperatures [2]. To examine the interesting spin-chirality scenario, precise information of 120-degree structures such as interlayer couplings is indispensable. A recent neutron scattering analysis proposed the staggered chirality structure [3]. It means that the chiralities of each even and odd layers are opposite to each other.

Here, we fabricate a microscopic device (Fig. 1(a)) and observe the nonreciprocal electronic transport. As shown in Fig. 1(b), we have found the finite nonreciprocity below the Neel temperature. It indicates the breaking of the spatial inversion symmetry in the antiferromagnetic state. In the poster, we will discuss possible spin structures based on the detailed magnetic field dependence of nonreciprocal electronic transport.

[1] Y. Tokura, and N. Nagaosa, Nature Communications **9**, 3740 (2018).

[2] H. Takatsu, S. Yonezawa, S. Fujimoto, and Y. Maeno, Phys. Rev. Lett. **105**, 137201 (2010).

[3] H. Takatsu, G. Nénert, H. Kadowaki, H. Yoshizawa, M. Enderle, S. Yonezawa, Y. Maeno, J. Kim, N. Tsuji, M. Takata, Y. Zhao, M. Green, and C. Broholm, Phys. Rev. **B89**, 104408 (2014).

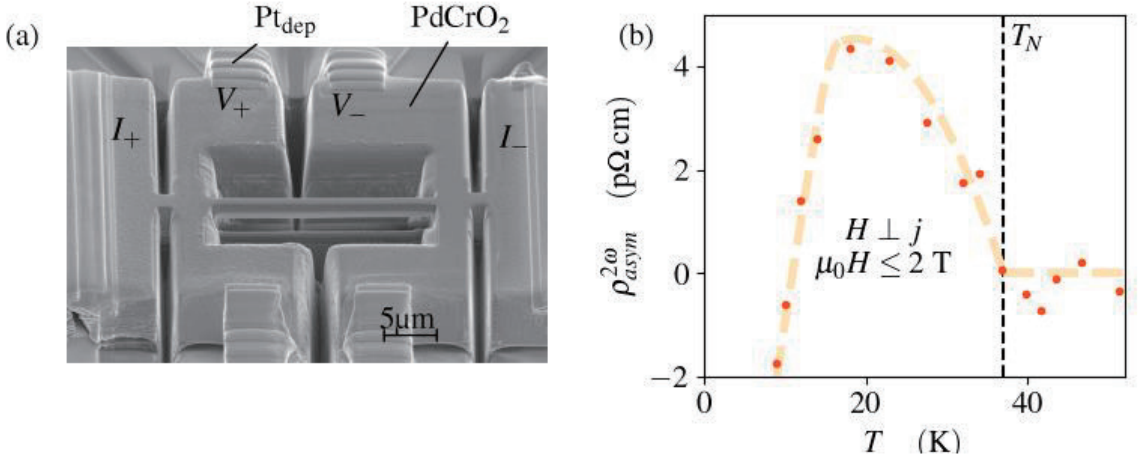

Fig. 1. (a) SEM image of the sample device.
(b) Temperature dependence of averaged nonreciprocal electronic transport in $H \perp j$.

Epitaxial $L1_0$-FeNi Films with a High Degree of Order and Uniaxial Magnetic Anisotropy Fabricated by a Denitriding Method

Keita Ito[1,2], Masahiro Hayashida[1], Takumi, Ichimura[1], Takahiro Nishio[3], Sho Goto[3],
Hiroaki Kura[3], Tomoyuki Koganezawa[4], Masaki Mizuguchi[5], Yusuke Shimada[1],
Toyohiko J. Konno[1], Hideto Yanagihara[6], and Koki Takanashi[1,2,7]

[1] Institute for Materials Research, Tohoku University, Japan
[2] Center for Spintronics Research Network, Tohoku University, Japan
[3] Advanced Research and Innovation Center, DENSO CORPORATION, Japan
[4] Japan Synchrotron Radiation Research Institute, SPring-8, Japan
[5] Department of Materials Process Engineering, Nagoya University, Japan
[6] Department of Applied Physics, University of Tsukuba, Japan
[7] Center for Science and Innovation in Spintronics, Core Research Cluster,
Tohoku University, Japan

Ferromagnetic materials possessing large uniaxial magnetic anisotropy energy (K_u) and composed of earth abundant elements are required in order to realize the next-generation permanent magnets. We have focused on the $L1_0$-ordered FeNi alloy as a rare-earth free high K_u ferromagnetic material [1]. Recently, the synthesis of polycrystalline $L1_0$-FeNi powder by denitriding FeNiN powder was reported, and a degree of order (S) of 0.71 was achieved [2]. However, the exact K_u value of $L1_0$-FeNi formed by the denitriding method is still unclear, and the evaluation of K_u using a single-crystal $L1_0$-FeNi is required. In this study, we grew epitaxial FeNiN films by molecular beam epitaxy and fabricated $L1_0$-FeNi films by nitrogen topotactic extraction, and characterized their S and K_u values.

20 nm-thick FeNiN films were grown on $SrTiO_3(001)$ substrates at 200, 250, and 350 °C by supplying Fe, Ni, and radio-frequency N_2 plasma, simultaneously [3]. Denitriding was performed by *ex-situ* furnace annealing at 300 °C for 4 h under an H_2 gas flow rate of 1 L/min at ambient pressure. Structure of the samples was characterized by x-ray diffraction measurements using Cu-$K\alpha$ radiation and synchrotron radiation ($h\nu$ = 7.11 keV), and cross-sectional scanning transmission electron microscope (STEM) measurements. Magnetization curves were measured by vibrating sample magnetometer at room temperature, and the K_u value was estimated by magnetic torque measurements.

The epitaxial $L1_0$-FeNi films oriented with the *a*-axis perpendicular to the film plane having two variants with the orthogonal in-plane *c*-axes are fabricated. For the sample grown at 350 °C, the S and K_u values are evaluated to be 0.87 and 5.9×10^5 J/m^3, respectively. In spite of the large S value exceeding those reported previously [1,2], the K_u value is modestly high. The exchange length of $L1_0$-FeNi (3.2 nm) is comparable to the variant sizes of our samples estimated by the STEM measurements. This strongly suggests that the obtained macroscopic K_u value is smaller than the actual K_u of each variant [4].

This work was supported by the Future Pioneering Program “Development of magnetic material technology for high-efficiency motors” (Proposal No. JPNP14015) commissioned by the New Energy and Industrial Technology Development Organization, Japan. The synchrotron radiation XRD was conducted at the BL46XU of SPring-8 with the approval of JASRI (Proposal No. 2019A1802).

[1] K. Takanashi *et al*., J. Phys. D: Appl. Phys. **50**, 483002 (2017).
[2] S. Goto *et al*., Sci. Rep. **7**, 13216 (2017).
[3] K. Ito *et al*., J. Magn. Soc. Jpn. **43**, 79 (2019).
[4] K. Ito *et al*., Appl. Phys. Lett. **116**, 242404 (2020).

P-11

Chirality memory stored in magnetic domain walls in the ferromagnetic state of MnP

N. Jiang[1], Y. Nii[2,3], H. Arisawa[2], E. Saitoh[2,4,5,6], and Y. Onose[2]

Department of Basic Science, The University of Tokyo[1],
Institute for Materials Research, Tohoku University[2],
PRESTO, Japan Science and Technology Agency [3],
Department of Applied Physics, The University of Tokyo[4]
Advanced Science Research Center, Japan Atomic Energy Agency[5]
Advanced Institute for Materials Research, Tohoku University[6]

Chirality is a lack of mirror symmetry in matter. In the human body, some molecules, such as amino acids, are homo-chiral, meaning that they show only one certain chiral state. In biology, it is important to elucidate how chiral information is transferred and memorized.

Chirality also appears in magnetic structures. One example is a helical magnetic structure, in which the ordered direction of the magnetic moment spatially rotates in a plane perpendicular to the propagation vector. The sense of rotation is reversed by any mirror operation and therefore determines the chiral state. Similar magnetic chirality shows up in a Bloch-type domain wall (DW) in ferromagnets. The magnetic moment rotates on the domain wall, and the sense of rotation is responsible for the chirality, similarly to helimagnets. We report the transfer of chiral information from a helical magnetic structure to a ferromagnetic DW during a helimagnetic to ferromagnetic phase transition in an itinerant helimagnet MnP. The 2nd harmonic resistivity $\rho^{2\mathrm{f}}_{\mathrm{asym}}$, which reflects the breaking down of mirror symmetry, was found to be almost unchanged after heating the sample above the ferromagnetic transition temperature and cooling it back to the helimagnetic state. The application of a magnetic field along the easy axis in the ferromagnetic state quenched the chirality-induced 2nd harmonic resistivity. This indicates that the chirality memory effect originated from the ferromagnetic domain walls[1].

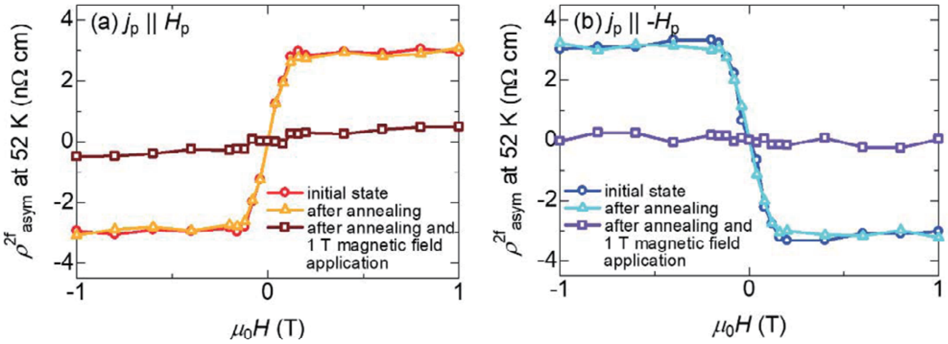

Fig. 1. Magnetic field dependence of $\rho^{2\mathrm{f}}_{\mathrm{asym}}$ at 52 K at the initial state (circles), that after annealing at 80 K (triangles), and that after annealing at 80 K and application of 1 T magnetic field along the c-axis (squares). The initial $\rho^{2\mathrm{f}}_{\mathrm{asym}}$ was positive ($j_{\mathrm{p}} \parallel H_{\mathrm{p}}$) and negative ($j_{\mathrm{p}} \parallel -H_{\mathrm{p}}$) in (a) and (b), respectively.

[1] N. Jiang, Y. Nii, H. Arisawa, E. Saitoh, and Y. Onose, arXiv:2010.02491 (2020).

Transparent $CaHfO_3$ crystals synthesized by the Core Heating method

Yutaro Kurashima[1], Shunsuke Kurosawa[1,2], Rikito Murakami[1,3], Akihiro Yamaji[1,2], Kei Kamada[1,2,3], Masao Yoshino[1], Satoshi Toyoda[1,2], Hiroki Sato[1,2], Yuui Yokota[1], Yuji Ohashi[1,2], Takashi Hanada[1], Akira Yoshikawa[1,2,3]

[1] Tohoku Univ. IMR, 2-1-1 Katahira, Aoba-ku, Sendai, Miyagi 980-8577, Japan
[2] Tohoku Univ. NICHe, 6-6-10 Aramaki-aza-Aoba, Aoba-ku, Sendai, Miyagi 980-8579, Japan
[3] C&A corp., 1-15-9 Ichibancho, Aoba-ku, Sendai, Miyagi 980-0811, Japan

Scintillators are used in medical imaging such as positron emission tomography. The gamma-ray stopping power is one of the most important properties of scintillators, and the power is proportional to the effective atomic number to the 4-5. Hf compounds like Ce doped $CaHfO_3$, $SrHfO_3$ and $BaHfO_3$[1] are attractive scintillator materials with high effective atomic numbers. However, the crystal growth of Hf compounds by the conventional crystal growth method has been not suitable and material search is not advanced. This is because Hf compounds typically have a much high melting point (melting point of $SrHfO_3$: ~2730°C). For material search of Hf compounds with a high melting point, we have developed a novel crystal growth method using electric arc, “Core Heating (CH) method”. The CH method can be applied for the material search of high melting point materials due to fast growth time, less raw materials (a few g) and no crucibles. As a first demonstration of crystal growth of Hf based scintillation materials by the CH method, we grew transparent Ce-doped $CaHfO_3$ crystals. Ce-doped $CaHfO_3$ has a relatively high effective atomic number and lower melting point than other Hf compounds like $SrHfO_3$.

Ce-doped $CaHfO_3$ samples were synthesized by the CH method in the first time. We placed raw material powder and an iridium tablet on Cu hearth. The iridium tablet was melted by the electric arc and raw material powder was melted by melted iridium. After that, we gradually weakened the output of the electric arc and we got transparent Ce-doped $CaHfO_3$ crystals. Synthesized crystals were cut and mirror polished, and samples were prepared.

We succeeded in the growth of the transparent Ce-doped $CaHfO_3$ crystals synthesized by the CH method first time. Figure 1 shows a photograph of transparent Ce-doped $CaHfO_3$ crystal synthesized by the CH method. The crystals were confirmed as a single phase ($CaHfO_3$) using X-ray diffraction. Some optical and scintillation properties were measured such as transmittance, photo-luminescence spectra, light output, and scintillation decay time. For instance, the transmittance was approximately 54% and the scintillation decay time component was approximately 22 ns. This sample was found to have fast decay time than conventional scintillators.

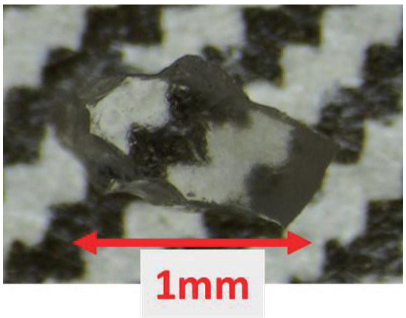

Fig. 1. Photograph of transparent Ce-doped $CaHfO_3$ crystal synthesized by the CH method

[1] S. Kurosawa, J. Pejchal, S. Wakahara, et al., Radiat. Meas. **56** (2013) 155–158.

Study on the bandgap structure for Ce:(La, Gd)$_2$Si$_2$O$_7$ scintillators

S. Kurosawa, Y. Shoji, R. Murakami, T. Horiai, A. Yamaji, A. Yoshikawa
Institute for Materials Research (IMR) & New Industry Creation Hatchery Center (NICHe),
Tohoku University

Recently, the pyrochlore crystals described with an $A_2Si_2O_7$ formula, have been studied as scintillation materials, where the A is(are) rare-earths. The $Gd_2Si_2O_7$ (GPS), $Lu_2Si_2O_7$ (LPS) Ce:(Gd, La)$_2$Si$_2$O$_7$ (Ce:La-GPS) have been investigated with good light outputs or energy resolutions [1-4]; The light outputs were estimated to be over 30,000 photons/MeV [5]. Also, good scintillation properties were found to be stable up to 450 K, as has been reported earlier for Ce:LPS and Ce:La-GPS crystals. Although Ce:LPS cannot be applied to oil well logging due to its intrinsic background, Ce:La-GPS can be.

The temperature dependence was found to be related to the bandgap energy and defect level; generally, a sample with large energy-deference between the bottom of conduction band and 5d level of Ce^{3+} (hereafter, we describe "5d-conduction band") can maintain the light output at even high temperature. In this paper, we evaluated scintillation properties and their bandgap structure including the 5d-conduction band for Ce:La-GPS materials.

Ce:(Gd$_{1-x}$ La$_x$)$_2$Si$_2$O$_7$ crystals were grown by the micro-pulling down method and Czochralski (Cz) process Moreover, Ce:Gd$_2$SiO$_5$ which is one of the conventional materials for oil well logging was prepared. The bandgap energies were estimated from transmittance spectra at 5 K using synchrotron faculty named Ultraviolet Synchrotron Orbital Radiation Facility (UVSOR) in Japan. 5d-conduction band was evaluated with photon- stimulated luminescence. Some traps were estimated by the thermo-luminescence technique.

The bandgap energies for Ce:(Gd, La)$_2$Si$_2$O$_7$ were large values (~ 7.1 eV) than that of conventional scintillation materials such as Ce:Gd$_2$SiO$_5$ The results showed that the energy gap between the Ce^{3+} 4f- level ($^2F_{5/2}$) to bottom of the conduction band is estimated ~4.2 eV, and the gap of 4f – 5d was evaluated to be 3.2 eV from emission spectrum data. Thus, the 5d-conduction band was calculated to be 1.0 eV. Moreover, we confirm the energy using other methods, vacuum referred binding energy.

The 5d-conduction band energy of Ce:La-GPS was similar to conventional scintillators (i.e. Ce:Lu$_3$Al$_5$O$_{12}$:1.07 eV, Ce:Y$_3$Al$_5$O$_{12}$: 1.05 eV). Thus, we found some defect(s)/traps can be rated to the temperature dependence. Thermo-luminescence glow curves of Ce:La-GPS and Ce:Gd2SiO5 (Ce:GSO), and Ce:La-GPS had small number of traps than Ce:GSO. In this paper, we show the band gap structures for these samples and the mechanism of thermal quenching for these samples.

[1] S. Kawamura, et al , in IEEE Nuclear Scie. Symp. Conf. Rec. 2006, pp.1160-1163 (2006).
[2]S. Kawamura, et al. NIM**A583**, 356 (2007).
[3]J. H. Kaneko, et al. , NIM**A529,** 307 (2004).
[4]L. Pidol,et al. IEEE TNS **51**, 1084 (2004).
[5] A. Suzuki, S. Kurosawa, and A. Yoshikawa et al., Appl. Phys. Express **5,** 102601 (2012).

Hydrogen-assisted Damage Evolution in Nitrogen-doped Duplex Stainless Steel

Milene Yumi Maeda[1,2*], Motomichi Koyama[1,3], Hayato Nishimura[1,4], Osvaldo Mitsuyuki Cintho[2] and Eiji Akiyama[1]

[1]Institute for Materials Research (IMR), Tohoku University, Katahira 2-1-1, Aoba-ku, Sendai 980-8577, Japan
[2]Materials Engineering Department, State University of Ponta Grossa, Av. Gen. Carlos Cavalcanti, 4748, Uvaranas, Ponta Grossa, Paraná, 84030-900, Brazil
[3]Elements Strategy Initiative for Structural Materials (ESISM), Kyoto University, Yoshida-honmachi, Sakyo-ku, Kyoto 606-8501, Japan
[4]Department of Quantum Science and Energy Engineering, Graduate School of Engineering, Tohoku University, Aramaki Aza Aoba, Aoba-ku, Sendai, Miyagi, Japan

Duplex stainless steels are multiphase steels, whose microstructure consists of ferrite and austenite. The use of duplex steels is increasing because they present corrosion resistance coupled with superior mechanical properties and weldability [1–3]. Additionally, they have lower Ni contents in their composition, which lowers their cost and turn them into attractive replacement options for austenitic stainless steels. Furthermore, high-strength duplex stainless steels have been developed through nitrogen doping and grain refinement [4–6]. As duplex stainless steels have been used as structural materials in chemical, petrochemical, marine and oil and gas industries [1,7], the effects of hydrogen on their mechanical properties are practically important.

In this work, the effects of hydrogen on ductility loss and fracture behavior of a nitrogen doped duplex stainless steels are investigated via tensile testing after electrochemical hydrogen pre-charging. Hydrogen pre-charging drastically decreased the steel ductility, but the strength was increased at some extent, attributed to the solid solution hardening. Post-mortem microstructure analyses were performed to characterize the microstructural damage evolution and fracture surface. Hydrogen charging of the steel resulted in quasi-cleavage and intergranular fractures, which were associated with transgranular austenite cracking and ferrite/austenite interface cracking, respectively. The hydrogen was observed to assist occurrence of deformation twinning in austenite. The crucial factors that resulted in brittle-like cracking were deformation twinning in austenite and nitrogen-related solution hardening.

[1] Gunn RN, Acmm, **45**, 2, 12845bae.001 (1998).
[2] Andersson J-O, Alfonsson E, Canderyd C, Groth HL, Proc Stainl. Steel World Conf, (2010).
[3] Canderyd C, Pettersson R. Int Corros Conf Ser, **5,** 4081–90 (2012).
[4] Chou SL, Tsai WT, Mater Sci Eng A, **99, 00174-4** (1999).
[5] Lo KH, Shek CH, Lai JKL, Mat Sci Eng R, **65**, 03.001 (2009).
[6] Knyazeva M, Pohl M, Structure. Metallogr Microstruct Anal, **2**, 00668 (2013).
[7] Azevedo CRF, Pereira BH, Wolynec S, Padilha AF, Eng Fail Anal, **97**, 12.009 (2019)

Effects of Residual Stress on Hydrogen Embrittlement of a Stretch-Formed Tempered Martensitic Steel Sheet

Hayato Nishimura[1, 2], Tomohiko Hojo[1], Hiroyuki Saito[3], and Eiji Akiyama[2]

[1] Institute for Materials Research, Tohoku University (IMR)
[2] Graduate School of Engineering, Tohoku University
[3] National Institutes for Quantum and Radiological Science and Technology

The strength of automotive frame parts has increased for improvements in impact safety and light-weighting. However, when the tensile strength of the high-strength steel exceeds more than 1 GPa, hydrogen embrittlement becomes a critical issue [1]. Besides, we have to consider the effects of residual stress and plastic strain, which are introduced by press-forming, on hydrogen embrittlement properties when high-strength steels are applied for automotive structural parts. In this study, the effects of residual stress and plastic strain on the hydrogen embrittlement of the stretch-formed tempered martensitic steel sheet were investigated.

In this study, we used a commercial steel rod with a chemical composition of 0.35C-0.18Si-0.74Mn-0.0011P -0.0017S-1.15Cr-0.15Mo (mass %). A sheet specimen of 40 × 40 × 1 mm^3 was taken from the rod annealed at 850 ^{o}C for 2 h and tempered at 530 ^{o}C for 3 h and polished. Stretch forming was conducted by using a hemispherical punch with a radius of 8.5 mm at a crosshead speed of 1 mm min^{-1} until a stroke of 4.2 mm. Hydrogen was introduced by using the cathodic hydrogen charging method in an aqueous solution of 3% NaCl + 20 g L^{-1} NH_4SCN. The initial potential was -1.1 V vs/AgCl and the potential was decreased 100 mV every 24 h. The residual stress distribution in the sample was analyzed by finite element method (FEM) using Abaqus cae and was measured by means of X-ray diffraction method at BL14B1 in SPring-8.

Figure 1 shows the crack growth behavior of the specimen. Cracking occurred at the foot of the impression where the sample was contacted near the jig and grew along the circumferential direction. Figure 2 shows the distributions of the radial and circumferential stresses and plastic strain in the stretch-formed specimen. Both measured and calculated profiles show similar tendency, which supports the reliability of the FEM analysis. Both the circumferential and radial stresses at the foot were high, and the circumferential stress became high at the edge of the region contacted to the punch. On the other hand, plastic strain was high around the top of the specimen. It is concluded that the presence of tensile stress has a large effect on the occurrence of hydrogen embrittlement of the stretch-formed steel sheet.

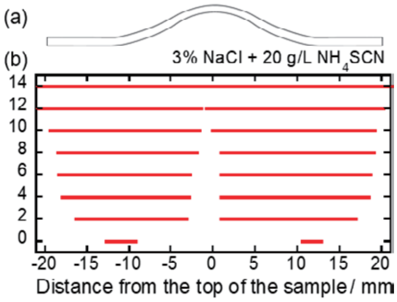

Fig. 1 (a) Schematic views of the cross section of the stretch-formed specimen and (b) the crack growth with time.

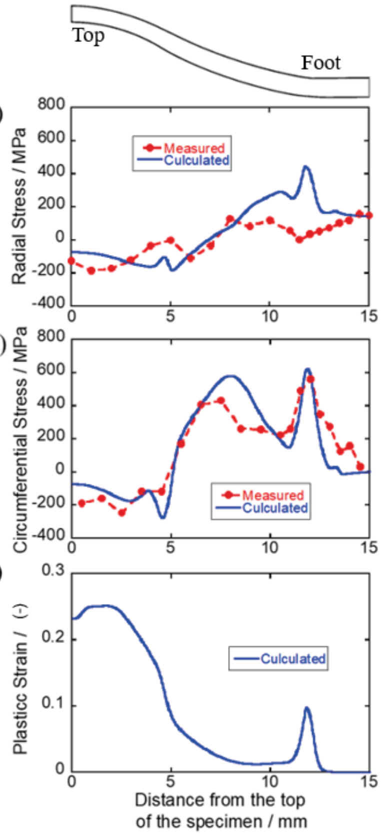

Fig. 2 (a) Radial stress, (b) circumferential stress, and (c) plastic strain of center of sample.

[1] T. Tarui, S. Yamazaki, Tetsu-to-Hagané, **88**, 612 (2002).

Effects of Mn addition on bainitic transformation in Fe-0.3N alloy

Mitsutaka Sato[1*], Kazuki Hara[2], Goro Miyamoto[1] and Tadashi Furuhara[1]

[1] Institute for Materials Research, Tohoku University
[2] Graduate School of Engineering, Tohoku University

1. Introduction

Nitrogen (N) is an interstitial element that thermodynamically stabilizes austenite (g) in a similar way to carbon (C). Since the eutectoid composition of the Fe-N alloy is on the higher concentration side than that of the Fe-C alloy, more amount of N can be enriched in γ, resulting in a larger amount of retained γ as compared to the Fe-C based alloy.

We have studied the effects of Mo, Cr and Si addition on the bainite transformation of Fe-N alloys to develop a new high strength TRIP steel using nitrogen and it was found that the large amount of retained γ was obtained due to the suppression of γ'-Fe_4N precipitation by Cr addition [1]. However, since the volume fraction of retained γ is still lower than that of conventional Fe-C based TRIP steels, the effect of Mn addition on the bainite transformation of Fe-N alloys was investigated in order to obtain more retained γ.

2. Experimental procedures

Fe-1mass% and -2mass% Mn alloys were used as starting materials. The samples were nitrided at 1000 °C for 1 h. to obtain 0.3mass%N in H_2/NH_3 mixture atmosphere. After the nitriding, sample was dropped into a salt bath heated up to 500 °C and isothermally annealed until 3600 s, followed by quenching into iced water. Microstructure observation was performed by OM and SEM. The volume fraction of phases was measured by XRD and point-counting methods. N content at the α/γ interface was measured by FE-EPMA.

3. Results

Fig.1 shows the microstructure of the samples after 3600 s holding. As shown by the white dotted lines, the MAs between the BFs in both 1Mn and 2Mn are divided, suggesting the possibility of decomposition of the MAs with the long time holding. In 2Mn, the width of MAs was thicker and the volume fraction of BF was lower. XRD measurement revealed that only diffraction peak of α was observed for 1Mn at 5 s, while α and γ peaks were observed after 10 s. In 2Mn, only α peaks were found in 5 s and 10 s holding, and α and γ peaks were found after 60 s. In 2Mn, only α peak was found after 5 s and 10 s holding. The diffraction peaks of the γ' phase were not observed at any holding time.

The transformation curves for 1Mn and 2Mn are shown in Fig. 2, which were obtained from point counting and XRD measurements. The amount of retained γ were 14.8% for 60s holding 1Mn alloy and 16.8% for 3600s holding 2Mn, respectively, which were higher than all samples investigated in a previous study [1]. From the comparison of the transformation curves, the bainitic transformation is retarded by Mn addition.

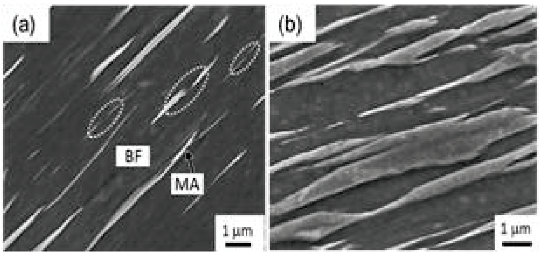

Fig.1 SEM images of (a) 1Mn and (b) 2Mn transformed at 500 °C for 3600 s

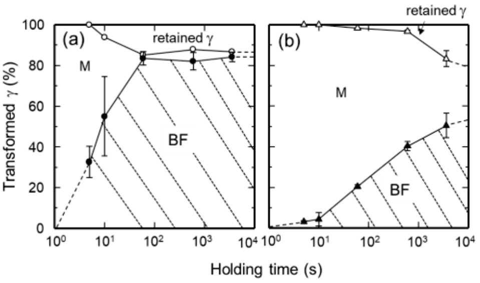

Fig.2 Transformation curves of (a)1Mn and (b)2Mn at 500 °C

[1] M. Sato, S. Shimaya, G. Miyamoto, and T. Furuhara, CAMP-ISIJ **31** 287 (2008).

P-17

Anomalous Behavior of Magnetization and Magnetic Resonance in the Chiral Helimagnet

Yuya Sawada[1] and Masayuki Hagiwara[2]

[1] Institute for Materials Research, Tohoku University
[2] Graduate School of Science, Osaka University

“Chirality”, which means left- or right-handedness, plays a crucial role in the symmetry properties of nano-scale phenomena in condensed matter physics. In materials science, chiral materials are frequently found in molecules or crystals with helical structures, and a chiral structure sometimes leads to the emergence of intriguing phenomena, such as chiral helicoidal order, skyrmion lattices, and topological Hall effect.

One of the monoaxial chiral magnets $CrNb_3S_6$ is known as the material that the helical magnetic order with a long period is realized along the c-axis below the long-range ordering temperature T_c = 127 K. In this material, it was theoretically predicted that the novel spin texture, which is described as an alternate helical magnetic and ferromagnetic (FM) order called the chiral soliton lattice (CSL) as shown in Fig. 1, emerges by applying a magnetic field perpendicular to the helical axis. In 2012, Togawa *et al.* has succeeded the direct observation of the CSL evolution of $CrNb_3S_6$ by using Lorenz microscopy techniques for the first time [1].

Based on the above, we have investigated the CSL natures and dynamics in magnetic fields by magnetization and electron spin resonance (ESR) measurements of $CrNb_3S_6$ under various conditions. In the presentation, we will introduce the peculiar behavior of hysteresis of magnetization and observed novel spiked signals superposed on and ESR signal due to the CSL dynamics [2].

This work has been collaborated with Mr. Yusuke Shimamoto, Dr. Yusuke Kousaka, Prof. Yoshihiko Togawa (Osaka Prefecture University), Dr. Takehito Nakano (Ibaraki University), Dr. Daichi Yoshizawa (Institute for Molecular Science), Dr. Jun-ichiro Ohe (Toho University), Dr. Yusuke Masaki (Tohoku University), Prof. Yusuke Kato (University of Tokyo), Prof. Yasuo Nozue (Osaka University), Prof. Jun-ichiro Kishine (Open University), and Prof. Katsuya Inoue (Hiroshima University), and supported by a Grant-in-Aid for Scientific Research (S) (No. 25220803) “Toward a New Class Magnetism by Chemically-controlled Chirality” and JSPS Core-to-Core Program, A. Advanced Research Networks.

[1] Y. Togawa, *et al.*, Phys. Rev. Lett **108**,107202 (2012).
[2] D. Yoshizawa, YS, *et al.*, Phys. Rev. B **100**, 104413 (2019).

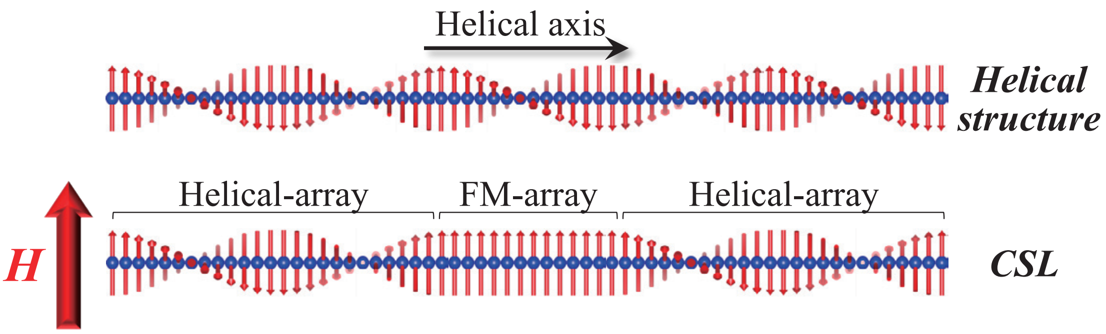

Fig. 1. Schematic of the helical magnetic structure and the chiral soliton lattice in a magnetic field applied perpendicular to the helical axis.

P-18

Detection of Complete Valley Polarization in Tellurium by Nonreciprocal Magnetoresistance

K. Sudo[1*], Y. Yanagi[1], T. Takahashi[2], K. Kobayashi[2,3], M. Suzuki[1] and M. Kimata[1]

[1] Institute for Materials Research (IMR), Tohoku University
[2] Dept. of Phys. Okayama University
[3] Research Institute for Interdisciplinary Science (RIIS), Okayama University

Elemental tellurium has a helical crystal structure and breaks mirror symmetry. Consequently, tellurium has a spin-splitting band due to the breaking inversion symmetry and spin-orbit interaction. Another important feature in tellurium is two local maximum in band structure in the momentum space. Therefore, tellurium has valley degrees of freedom with opposite spin polarization **[fig1 left]**. This spin-valley coupling allows us to manipulate valley polarization by applying magnetic field. When the magnetic field is applied along the c-axis (parallel to the spin-polarized axis), the energies of two valleys are lifted, and thus valley-polarized state is achieved.

In this study, we will report the valley-polarized state by measuring nonreciprocal magnetoresistance[1]. We observed anomalous suppression of nonreciprocal magnetoresistance in high magnetic fields **[fig2]**, whereas the nonreciprocal signal is usually proportional to magnetic field[1]. Based of our model, we have revealed that the maximum of nonreciprocal magnetoresistance correspond to the crossover field for the complete valley polarization.

This work is the first observation of valley polarization by nonreciprocal magnetoresistance although there are some observations of valley polarization by different transport probes so far. In this study, we have also demonstrated that tellurium has much smaller magnetic field to achieve complete valley polarization compared with conventional valleytronics materials[2,3], suggesting great advantage of this material for valleytronics.

[1] T. Ideue, K. Hamamoto, S. Koshikawa, M. Ezawa, S. Shimizu, Y. Kaneko, Y. Tokura, N. Nagaosa and Y. Iwasa Nat. Phys. 13, 578-583, 2017

[2] A. Arora, R. Schmidt, R. Schneider, M. R. Molas, I. Breslavetz, M. Potemski and R. Bratschitsch, Nano Lett. 2016, 16, 3624-3629

[3] Z. Zhu, J. Wang, H. Zuo, B. Fauque, R. D. McDonald, Y. Fuseya and K. Behnia, Nat. Commun. **8**, 15297 2017

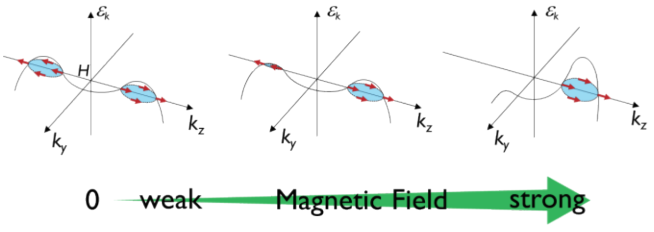

Figure 1 Valence band of Tellurium and valley-polarization by magnetic field.

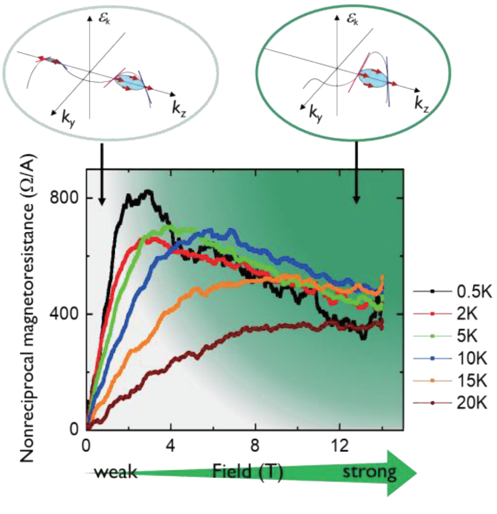

Figure 2 Magnetic field dependence of nonreciprocal magnetoresistance.

P-19

Fabrication of 3D micro-patterned metallic glass by imprinting process and application to Li-ion battery (LIB) electrode

Rise Takagi[1], Takeshi Wada[2] and Hidemi Kato[2]

[1]Department of Materials Science, Graduate school of Engineering, Tohoku University
[2] Institute for Materials Research, Tohoku University

Recently, a lot of efforts have intensively devoted to develop new electrode materials for improving the performance of LIB. Silicon (Si) has been proposed as a promising alternative anode active material to graphite that is used in LIB. The theoretical capacity of Si is about 10 times greater than graphite-based anode materials. However, the volume expansion of Si up to 280% upon lithiation causes self-destruction of Si active material and its delamination from the current collector, resulting in poor cycle properties [1].

In this study, we improve the battery performance of Si anode by using 3D microstructures on the metallic glass (MG) current collector. MG exhibits a supercooled liquid region upon heating, which allows viscous flow fabrication of nano to micro structures.

The 3D patterned MG current collector is expected to prevent the delamination of Si active material. In addition, enlargement of specific surface due to 3D patterns, sufficient vacant space to accommodate the volume expansion, and the excellent strength and elasticity of MG are expected to bring a better capacity, cycle life and rate performance. Therefore, we study fabrication 3D micro-patterns on MG by imprinting process and evaluated LIB performance of Si anode made of the patterned MG current collector.

Pd-based MG ($Pd42.5Ni7.5Cu30P20$, Pd-MG) ribbons were prepared by a single-roll liquid quenching method. Imprinting process was performed and using Si molds of slit-like patterns (9 µm width and 30 µm depth) fabricated by photolithography. Working electrodes were prepared by coating slurries Si as active material (60 wt.%), CB as a conducting agent (25 wt.%), and PI (15 wt.%) as binders dissolved in NMP on a Pd-MG current collector. In the half-cell setup, the electrode was tested in an R2032 coin-type cell, assembled with a lithium foil counter electrode, a separator (PVDF) and the electrolyte (1 M $LiPF6$ in EC/DMC, the use of FEC additive).

The image of imprinted Pd-MG is shown in Fig.1.. Pd-MG with a slit-like structure and 22 µm in depth was successfully fabricated by imprinting tests. The fabricated Pd-MG current collector with the active material in the structure is shown in Fig.2.. The charge-discharge measurements revealed that the capacity of the imprinted Pd-MG based electrode was greater than that of the conventional copper foil based one.

[1] M. N. Obrovac, L. Christensen, D. B. Le and J. R. Dahn: J. Electrochem. Soc., **154**(2007), A849-A855.

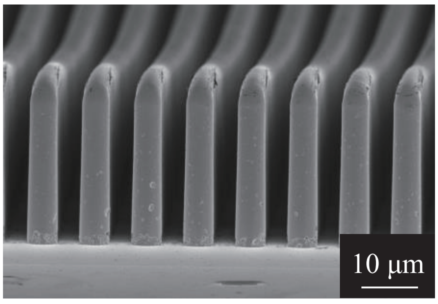

Fig. 1. SEM image of imprinted Pd-MG

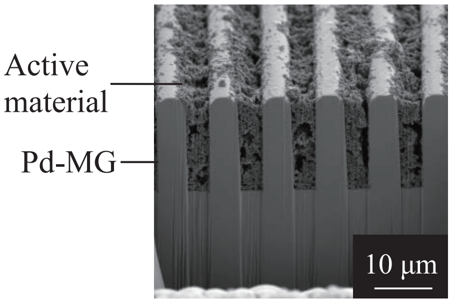

Fig. 2. SEM image of Pd-MG current collector pasted with slurry

P-20

Nano/Meso-scale Chemical State Visualization of Functional Materials Using Ptychography-XAFS

Nozomu Ishiguro* and Yukio Takahashi

International Center for Synchrotron Radiation Innovation Smart (SRIS)/
Institute of Multidisciplinary Research for Advanced Materials (IMRAM),
Tohoku University, 1-1-1 Katahira, Aoba-ku, Sendai 980-8577, Japan

Heterogeneity in structures and chemical states of practical function materials is often considered one of the critical factors of their unique properties. Ptychography-XAFS, a combination of X-ray ptychography imaging, which is the scanning-type coherent X-ray diffractive imaging that provides real-space images of sample with 10 nm scale resolution, and XAFS spectroscopy, provides high spatial-resolution images of not only the nano/mesoscopic structures of the non-uniform materials but also their chemical states (e.g., composition, valence, local structures, etc.). Herein, we present applications of ptychography-XAFS for chemical state visualization of functional materials such as heterogeneous catalysts and battery materials.

We first applied three-dimensional ptychography-XAFS to Pt-supported ceria-zirconia automobile exhaust catalyst single particles ($Pt/Ce_2Zr_2O_x$; $7 \leqq x \leqq 8$), which are known for typical oxygen storage/release materials by reproductive redox between $Ce_2Zr_2O_7$ (Ce^{3+}) and $Ce_2Zr_2O_8$ (Ce^{4+}). Three-dimensionally resolved Ce L_{III}-edge XAFS spectra of partially oxidized $Pt/Ce_2Zr_2O_x$ particles were successfully obtained with 40–48 nm resolution, visualizing the heterogeneous distribution of Ce valence in the bulk of the catalyst particles. Unsupervised data mining was then applied to visualize 3D nanoscale chemical maps, which revealed heterogeneous reaction modes inside the individual catalyst particles during the oxygen storage processes (Fig. 1) [1, 2]. We also investigated the chemical state of lithium-titanate (LTO) particles ($Li_xTi_5O_{12}$; $4 \leqq x \leqq 7$), which is known as an electrode-active material for Li ion batteries. LTO particles with different charge/discharge conditions were prepared, and spatially-resolved Ti *K*-edge XAFS spectra were successfully obtained (Fig. 2).

In summary, we successfully visualized chemical states of heterogeneous catalysts and battery materials by ptychography-XAFS. This high-resolution spectro-imaging will be a promising tool to visualize the hidden nature of materials functionalities.

[1] M. Hirose, N. Ishiguro, K. Shimomura, N. Burdet, H. Matsui, M. Tada, Y. Takahashi: Angew. Chem. Int. Ed. **57**, 1474 (2018).
[2] M. Hirose, N. Ishiguro, K. Shimomura, D.-N. Nguyen, H. Matsui, H. C. Dam, M. Tada, Y. Takahashi: Communs. Chem. **2**, 50 (2019).

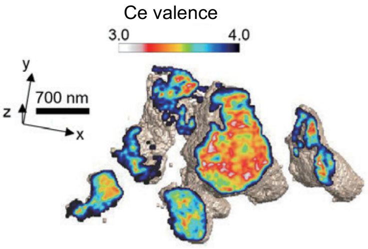

Fig. 1. 3D Ce valence image of partially oxidized $Pt/Ce_2Zr_2O_x$ particles.

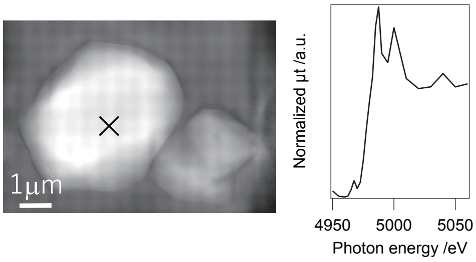

Fig. 2. Absorption image and spatially-resolved Ti *K*-edge XAFS of LTO particles.

P-21

Organic-Inorganic Hybrid Nanoimprint Replica Molds for Industrial Application

Shunya Ito*, Takahiro Nakamura, Masaru Nakagawa

Institute of Multidisciplinary Research for Advanced Materials (IMRAM),
Tohoku University, 2-1-1 Katahira, Aoba-ku, Sendai, Miyagi 980-8577

UV nanoimprint lithography (UV-NIL) is one of industrially acceptable on-demand micro/nano-fabrication technologies owing to its ease of use and high throughput. In UV nanoimprinting, micro/nano-structures on a mold surface are transferred onto UV cured resin films for subsequent lithography process. Fused silica master molds, often called synthetic quartz molds, are mainly used because of high transparence to UV light for curing, in addition to low thermal expansion coefficient and high mechanical strength. In addition, the use of replica molds is a way to reduce the mold cost especially in device fabrication (Fig. 1). Organic replica resin molds are widely used; however, the resins have lower mechanical strength than inorganic fused silica molds. In this study, we investigated the mold performances of hybrid materials composed of organic monomers and methacrylate-modified inorganic silica nanoparticles (NP_{MC}) in step-and-repeat UV nanoimprinting over 100 cycles.[1]

Hybrid liquids were prepared by adding NP_{MC} into 1,10-decanediol diacrylate (AC10) and 1,10-decanediol dimethacrylate (MC10). Heterogeneous combination of polymerizable groups, such as AC10 and NP_{MC}, maintained a fluidity suitable for molding in UV nanoimprinting, while homogeneous combination of MC10 and NP_{MC} lost fluidity at a smaller NP_{MC} content. The hybrid resin film and nanostructures comprising AC10 and NP_{MC} showed the increase in mechanical strength measured by nanoindentation. The hybrid mold with 100- and 45-nm-width convex lines enabled pattern transfer without line-collapse defects on UV cured films by step-and-repeat imprints in 128 cycles (Fig. 2). We concluded the hybrid mold showed pattern formability through step-and-repeat imprints, which was derived from the organic component, and durability of the mold in the imprints, which was derived from the inorganic component.

[1] S. Ito et al., *Bull. Chem. Soc. Jpn.* **93**, 862 (2020).

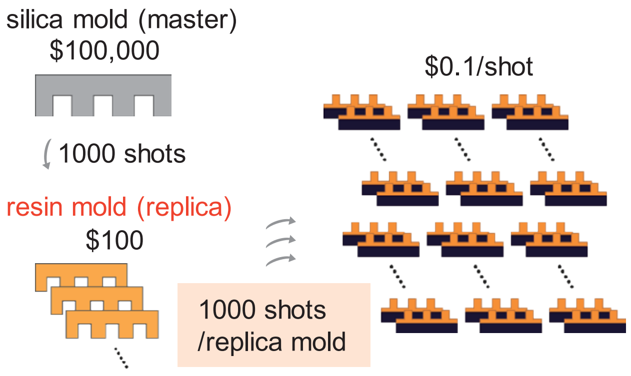

Fig. 1. Schematic illustration of the use of replica mold reducing mold cost for industrial application.

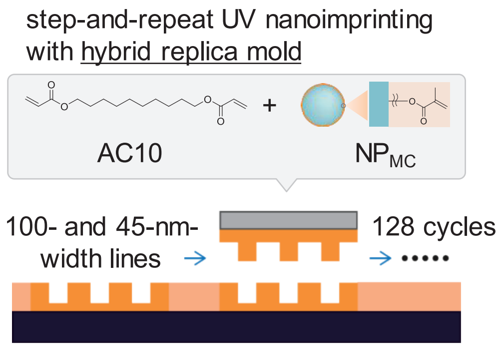

Fig. 2. Step-and-repeat imprints in 128 cycles with the hybrid replica mold.

Rational design of peptide targeting intrinsically disordered protein p53 and discovery of liquid-liquid phase separation of p53

Kiyoto Kamagata[1*] and Tomoshi Kameda[2]

[1] Institute of Multidisciplinary Research for Advanced Materials, Tohoku University,
Katahira 2-1-1, Aoba-ku, Sendai, 980-8577, Japan
[2] Artificial Intelligence Research Center, National Institute of Advanced Industrial Science
and Technology (AIST), Koto, Tokyo, 135-0064, Japan

Intrinsically disordered regions (IDRs) of proteins are involved in many diseases. However, the flexible IDRs hinder the use of 3D structure-based drug design methods. Here, we developed a rational design method to obtain a peptide that can bind an IDR using only protein sequence information [1]. We applied the method to the disordered C-terminal disordered domain of a tumor suppressor p53. The designed peptide showed the suppression of binding to DNA and sliding along DNA by p53 using NMR, molecular dynamics simulation, and single molecule measurements [2]. Also, we recently found that p53 itself induces liquid-liquid phase separation through multivalent electrostatic interactions between two IDRs [3]. We showed that the designed peptide suppressed the liquid-liquid phase separation of p53 by blocking the interaction of the IDRs. Sequence-based design may be useful in targeting IDRs for therapeutic purposes.

[1] K. Kamagata, E. Mano, Y. Itoh, T. Wakamoto, R. Kitahara, S. Kanbayashi, H. Takahashi, A. Murata and T. Kameda, Sci. Rep., **9**,8584 (2019)

[2] D. R. G. Subekti, A. Murata, Y. Itoh, S. Takahashi and K. Kamagata, Sci. Rep., **10**, 13697 (2020).

[3] K. Kamagata, S. Kanbayashi, M. Honda, Y. Itoh, H. Takahashi, T. Kameda, F. Nagatsugi, and S. Takahashi, Sci. Rep., **10**, 580 (2020)

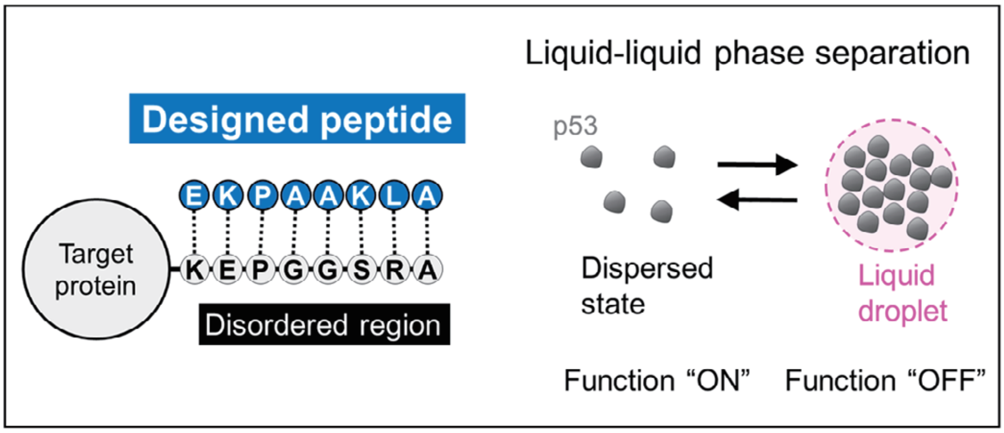

Fig. 1. Design of peptide targeting flexible intrinsically disordered protein and liquid-liquid phase separation of p53

P-23

Analysis of the Effect of Powder Heterogeneity in Compression Molding

Yuki Kondo[1*], Kizuku Kushimoto[2], Shingo Ishihara[2] and Junya Kano[2]

[1]Graduate School of Environmental Studies, Tohoku University
[2] Institute of Multidisciplinary Research for Advanced Materials, Tohoku University

Powder compression molding processes are used in various products such as ceramics, powder metallurgy and pharmaceuticals. In the processes, the microscopic structure of compression-molded body has an important role on the quality and productivity of the products. For instance, the heterogeneity of the microscopic structure would influence strength of the products. The heterogeneity is caused by differences of particle size, density and flowability. However, the effect of powder heterogeneity on compression molding is not understood well because it is difficult to observe deformation behavior of small particles directly. The purpose of this study is to investigate the effects of powder heterogeneity on compression molding by using numerical simulations that have advantages of visualizing the deformation behavior in detail. In this study, the effect of the yield point of elastic-plastic materials on the deformation behavior was investigated.

Numerical simulations were used Advanced Distinct Element Method Ductile Model (ADEM Ductile Model) [1] based on Distinct Element Method (DEM) [2]. The ADEM Ductile Model can express elastic deformation of elastic-plastic materials. In ADEM Ductile model, joint springs are set between DEM particles to represent elastic deformation. In addition, the plastic deformation is represented by updating the natural length of the joint springs when the length of joint springs exceeds the Plastic starting strain (Psl).

In this study, the particles filled in a rectangular frame were compressed to investigate the effect of the yield points on particle deformation behavior by changing the Psl. **Fig. 1** shows the pictures of simulation after compression. When Psl is small, the particles remain deformation after unloading and fill the gaps. While, when Psl is large, the particles are not so deformed and is similar to the original shape because the natural length of the joint spring is not updated on the compression.

From the above, it was found that the ADEM ductile model can analyze the deformation behavior in compression process and that the model could investigate the effects of powder heterogeneity on compression molding.

[1] K. Ono, K. Kushimoto, S. Ishihara, J. Kano, J. Soc. Powder Technol., Japan, **56**, 58-65, (2019)

[2] P. A. Cundall, O. D. L. Strack, Geotechnique, **29**, 47-65, (1979)

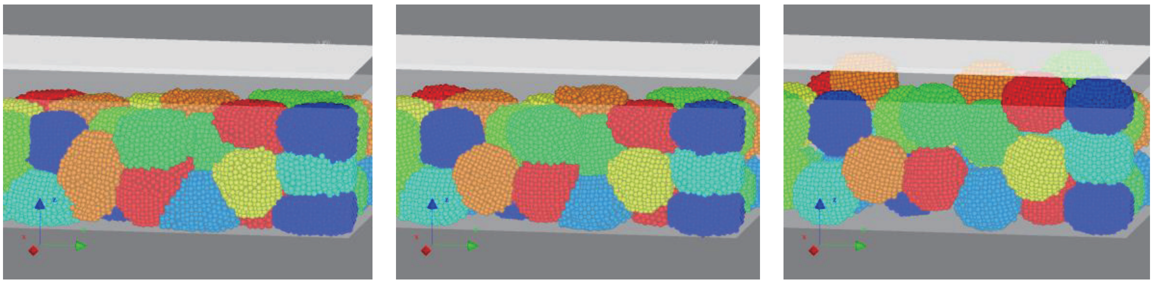

(a) Psl = 0.002 [-]   (b) Psl = 0.02 [-]   (c) Psl = 0.2 [-]

Fig. 1 Pictures of particles after compression when the Plastic starting length is varied

Stable and orthogonal DNA base pair with translocated recognition units

Hidenori Okamura[1,2*], Giang Hoang Trinh[1,2], Zhuoxin Dong[1,2], and Fumi Nagatsugi[1,2*]

[1]Institute of Multidisciplinary Research for Advanced Materials, Tohoku University, 2-1-1 Katahira, Aoba-ku, Sendai 980-8577, Japan, [2]Department of Chemistry, Graduate School of Science, Tohoku University, 6-3 Aramaki Aza-Aoba, Aoba-ku, Sendai 980-8578, Japan.

All living forms on Earth utilize four distinct nucleosides - A, G, C, T - to store their genetic information in DNA. This information is transcribed to RNA and subsequently translated into various proteins to maintain the biological activities. Such gene expression is based on the precise and exclusive formation of A-T and G-C canonical base pairs through hydrogen bonding (**Fig. 1a**). If one can expand these genetic letters beyond the canonical nucleobases, it would increase the functionality of gene expression system thus leading to the development of novel biotechnology and drug discovery. To this end, creation of unnatural base pair (UBP) is considered to be one of the most promising methods. Several research groups have reported sets of unnatural bases which form orthogonal pairing without interacting with canonical ones, yet active in replication, transcription, and translation[1-3]. These UBPs have been utilized for developing nucleic acid-based nanostructures, antibody-like structured DNA for therapeutic/diagnostic purposes as well as to expand the genetic code for biosynthesis of artificial proteins[4]. The previously reported UBPs, however, still have significant room for improvement with respect to achieving orthogonal and stable base pair formation as well as the multiple/consecutive incorporation into DNA.

In order to establish a robust unnatural base pair system, in this study, we propose a new design concept for the creation of unnatural base pairs. Our design involves the introduction of nucleobase-like hydrogen bonding units to the position isolated from the canonical bases, thereby achieving orthogonality to the canonical nucleobases (**Fig. 1b**). In order to verify our design concept, we chemically synthesized DNA strands containing the newly-designed nucleosides using solid-phase DNA synthesis method and evaluated the base pairing properties by UV melting temperature (T_m) measurement. We found that the newly designed UBPs exhibit comparable stability to the canonical A-T and G-C pair, while the significant destabilization was observed with the mismatched combinations. Furthermore, the CD spectroscopic study revealed that the duplex DNA containing our UBPs adopts a global structure similar to the fully-natural DNA. The details of molecular design, synthesis as well as base-pairing properties will be discussed in the presentation.

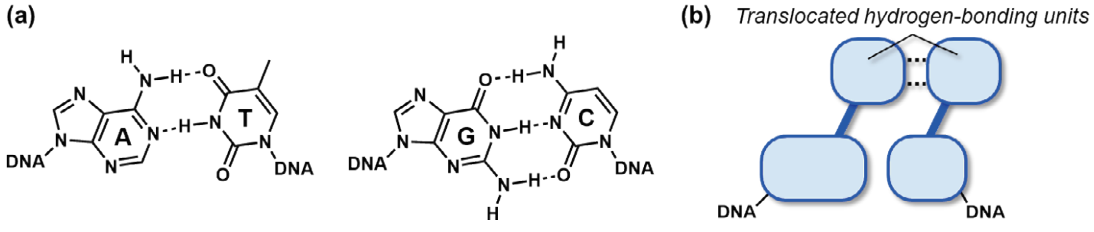

Fig. 1. (a) Structures of canonical A-T and G-C base pairs and (b) the design concept of UBP proposed in this study

[1] Y. Zhang, B. M. Lamb, A. W. Feldman, A. X. Zhou, T. Lavergne, L. Li, F. E. Romesberg, Proc. Natl. Acad. Sci. USA., **114**, 1317 (2017).
[2] M. Kimoto, R. Yamashige, K. Matsunaga, S. Yokoyama, I. Hirao, Nat. Biotech., **31**, 453 (2013).
[3] S. Hoshika, N. A. Leal, M. J. Kim, M. S. Kim, N. B. Karalkar, H. J. Kim, A. M. Bates, N. E. Watkins Jr., H. A. SantaLucia, A. J. Meyer, S. DasGupta, J. A. Piccirilli, A. D. Ellington, J. SantaLucia Jr., M. M. Georgiadis, S. A. Benner, Science, **363**, 884 (2019).
[4] K. Hamashima, M. Kimoto, I. Hirao, Curr. Opin. Chem. Biol., **46**, 108 (2018).

P-25

Development of a multi-turn time-of-flight electron analyzer toward molecular orbital imaging at ultra-high resolution

Yuuki Onitsuka, Isao Nakajima and Masahiko Takahashi

Institute of Multidisciplinary Research for Advanced Materials, Tohoku University

Molecular orbital (MO) is an important concept in molecular science and especially outer valence MOs of molecule play significant roles in chemical properties such as bonding, reactivity and molecular recognition. One of tools for probing MO is electron momentum spectroscopy (EMS) where an incident electron with an energy of the order of 1 keV or higher is used to eject a bound electron from molecule of interest and the resultant two outgoing electrons are detected in coincidence. The obtained EMS cross section is directly related to the electron momentum distribution of the ionized orbital, namely EMS enables one to look at individual MOs in momentum space. Contrary to the unique ability, EMS has been applied mainly to small and stable molecule due to instrumental sensitivity and energy resolution. In order to make good use of the unique ability toward various molecules involving large ones and low-density targets, such as radicals and transient species, both improvement of the sensitivity and resolution have been required. The sensitivity has been considerably improved by the development of a multichannel EMS apparatus [1]; however, the energy resolution has been insufficient.

In the present study, we propose a multi-turn time-of-flight (MT-TOF) electron analyzer with ultra-high energy resolution, which is shown in Fig. 1 [2]. The performance tests were carried out through electron trajectory simulations which showed dramatically improvement the energy resolution by a factor of about 27 with respect to the multichannel EMS apparatus while maintaining the high collection efficiency. In the poster session, we will present the current condition for the development and discuss our future EMS study after the development, such as its application into medicinal chemistry.

[1] M. Yamazaki, H. Satoh, M. Ueda, D. B. Jones, Y. Asano, N. Watanabe, A. Czasch, O. Jagutzki, and M. Takahashi, Meas. Sci. Techcol. **22**, 075602 (2011).
[2] I. Nakajima, Y. Onitsuka, M. Takahashi (in preparation)

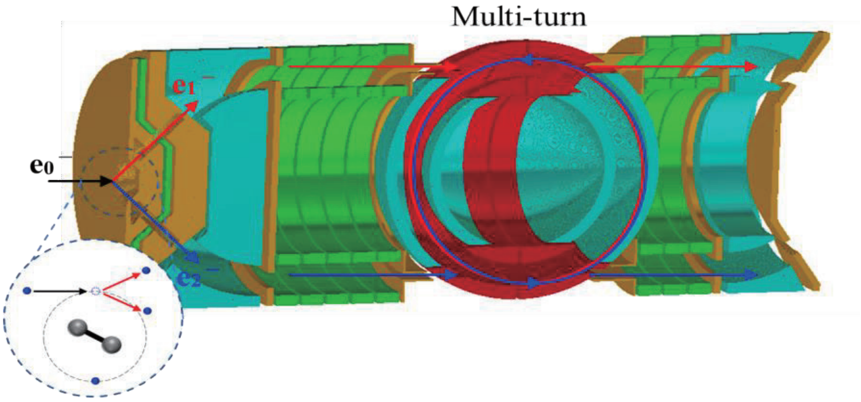

Fig. 1. Schematic cross section of the MT-TOF analyzer for EMS experiments.

Cryo-EM structures of SERCA2b reveal the mechanism of regulation by the luminal extension tail

Yuxia Zhang[1], Michio Inoue[1,5], Akihisa Tsutsumi[2], Satoshi Watanabe[1,5], Tomohiro Nishizawa[3], Kazuhiro Nagata[4,5], Masahide Kikkawa[2,5] and Kenji Inaba[1,5]*

[1] Institute of Multidisciplinary Research for Advanced Materials, Tohoku University
[2] Graduate School of Medicine, The University of Tokyo
[3] Graduate School of Science, The University of Tokyo
[4] Faculty of Life Sciences, Kyoto Sangyo University
[5] Core Research for Evolutional Science and Technology (CREST), Kawaguchi, Japan

Sarco/endoplasmic reticulum (ER) Ca^{2+}-ATPase 2b (SERCA2b) is a membrane protein that conducts Ca^{2+} uptake from the cytosol into the ER lumen and maintains the cellular calcium homeostasis in mammalian cells. Herein, we present cryo-EM structures of human SERCA2b in E1•AMP-PCP and E2•BeF_3^- states at 2.9 and 2.8 Å resolutions, respectively (Fig. 1). The structures revealed that the luminal extension tail (LE) characteristic of SERCA2b runs parallel to the lipid-water boundary near the luminal ends of transmembrane (TM) helices TM10 and TM7, and approaches the luminal loop flanked by TM7 and TM8. While the LE served to stabilize the cytosolic- and TM-domain arrangement of SERCA2b, deletion of the LE rendered the overall conformation resemble that of SERCA1a and SERCA2a, resulting in multiple classes of conformations. Thus, the LE appears to play a significant role in conformational regulation in SERCA2b, which is likely involved in the different kinetic properties of SERCA2b from those of other isoforms lacking the LE.

[1] Zhang, Y., Inoue, M., Tsutsumi, A., Watanabe, S., Nishizawa, T., Nagata, K., Kikkawa, M. and Inaba, K.* "Cryo-EM structures of SERCA2b reveal the mechanism of regulation by the luminal extension tail", ***Science Advances*** Vol. 6, no. 33, eabb0147. (2020)

[2] Inoue, M., Sakuta, N., Watanabe, S., Zhang, Y., Yoshikaie, K., Tanaka, Y., Ushioda, R., Kato, Y., Takagi, J., Tsukazaki, T., Nagata, K. and Inaba, K.* "Structural basis of sarco/endoplasmic reticulum Ca^{2+}-ATPase 2b regulation; ***Cell Reports*** 27, 1221-1230 (2019)

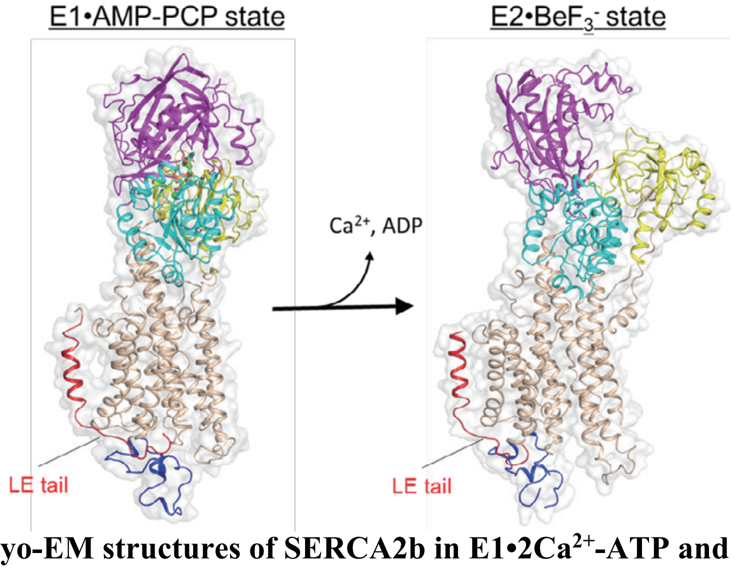

Fig. 1. cryo-EM structures of SERCA2b in E1•2Ca^{2+}-ATP and E2P states

P-27

Suppression of alkali elution from steelmaking slag for recycling

Graduate School of Engineering, Tohoku University Zuoqiao Zhu
IMRAM, Tohoku University Xu Gao, Shigeru Ueda, Shin-ya Kitamura

1. Introduction:

To suppress the alkali elution, when using steelmaking slag near sea and river, we have studied the dissolution behavior of each mineral phase in steelmaking slag with and without slag modification [1]. Then, the mineralogical phases, that cause the alkali elusion, were clarified [2,4]. Based on this result, several slags were synthesized and the suppression of the alkali elusion by the control of the mineralogical phases was shown [3,4]. To design the slag composition by the slag modification, in this study, a model to estimate alkali dissolution was established, by combining the dissolution behavior of each mineral phase.

2. Model construction

The dissolution rate of Ca from one crystal phase is defined as Eq. (1), assuming the rate controlling step is a non-steady-state diffusion through a film layer in liquid phase. Here, *A* is the interfacial area between the solid particle and leachate(m^2), *V* is the volume of the leachate (m^3); *D* is the diffusion coefficient in the liquid phase ($m^2 \cdot s^{-1}$); C_S^{Ca} is the concentration of Ca at the interface between the solid particle and leachate(mg/L), and the equilibrium value of each crystal phase is used; C_0^{Ca} is the initial concentration of Ca (mg/L); *t* is time (s). After integration, the apparent rate constant (*k'*) of each crystal phase is obtained as Eq. (2). Then, the Ca content from the synthetic slag can be estimated by summarizing the calculated Ca content from each phase using a factor *F*. The factor *F* is defined as Eq. (4), which expresses the difference of interfacial area between that for the leaching test of a single crystal phase and that for the leaching of the same phase from slag. After calculating the dissolution of Ca from slag, the pH of leachate is obtained by Eq. (5) which has been derived from previous study [4].

$$\frac{dC^{Ca}}{dt} = \frac{DA\left(C_S^{Ca} - C_0^{Ca}\right)}{V\sqrt{\pi D t}} \quad (1)$$

$$k' = \frac{2\sqrt{D}AC_S^{Ca}}{V\sqrt{\pi}} \quad (2)$$

$$C_{t^*}^{Ca,\,Slag} = F \times C_{t^*}^{Ca,Crys.} \quad (3)$$

$$F = \frac{A_{Crys.in\ slag}}{A_{Crys.only}} \quad (4)$$

$$pH = C^{Ca} + 13.9 \quad (5)$$

3. Leaching test of slag

The above model has been applied to estimate the elution behaviors of several synthetic and industrial slags. The elution behaviors of these slags were measured by the same method as that used in the previous study [2-4].

4. Results:

The calculated values of maximum pH and corresponding Ca content in leachate, for various slags are shown in **Fig.1a,1b** with the experimental results. The calculated values were similar to the experimental results. Therefore, this model can be considered as a useful tool to design the optimum composition of slag to suppress the alkali elution.

5.Conclusions:

A model has been proposed to simulate the dissolution behaviors of steelmaking slag. The simulated results agreed well with the experimental data.

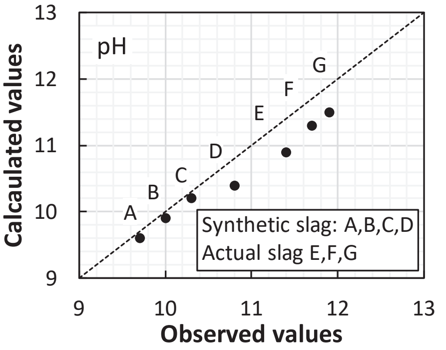

Fig.1a The comparison between calculated values of pH and observed ones

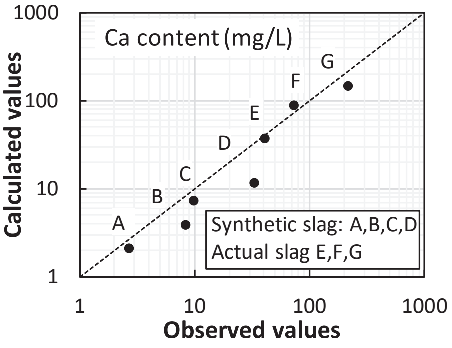

Fig.1b The comparison between calculated values of Ca content and observed ones

Reference

[1] K. Wada et. al, Seitetsu Kenkyu, 301 (1980), 13403. [2] Z.Zhu et. al., CAMP-ISIJ, 30(2017), 755. [3] Z.Zhu et. al., CAMP-ISIJ, 31(2018), 683. [4] Z.Zhu et. al., *ISIJ Inter*, 59(2019), 1908-1916.

Zuoqiao Zhu (School of Engineering, Tohoku University, Katahira2-1-1, Sendai 980-8577)

P-28

Micro-damage detection using backscattering method

Iichiro AIZAWA, Tsuyoshi MIHARA
Tohoku University Graduate School of Engineering Material Systems Engineering
6-6-6 Aramaki Aoba, Aoba-ku, Sendai,Miyagi

1.Background

While thermal power plants are required to operate with high efficiency, as for steam conditions, high temperature and high pressure have been promoted. Currently, thermal power generation is the mainstream in Japan, alloy steel with high creep strength and high chromium content is used for equipment used in ultra-supercritical coal-fired plants. However, it became clear that the creep strength of the high-chromium steel alloy sharply decreases with long-term use, and that a large number of creep voids are generated inside the thick welded part. Creep voids occur locally in the weld heat-affected zone (HAZ) fine grain area and are several µm in size. The power plant is regularly maintained for stable power supply and the equipment is replaced based on non-destructive evaluation (NDE). However the damaged welds of high-chromium steel equipment cannot be non-destructively inspected because that the creep voids are too deep in location and are too small in size, for conventional NDE methods. So these equipment have been replaced only according to the operating time based on the laboratory based material creep test without non-destructive damage monitoring. As a result, equipment with low damage has been replaced, resulting in uneconomical operation.

2.Purpose

Using ultrasonics, which is the core technique of industrial inner defects inspection method, we will develop the creep void evaluation system at the initial stage of creep damage.

3. Experimental results and discussion

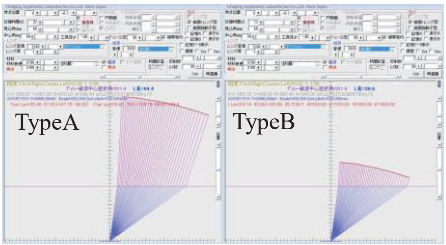

Fig.1 Aspherical angle focusing acoustic lens design

Although it has been thought that it is impossible to detect creep voids of several µm generated in the deep part of steel (30 mm) by ultrasonic measurement, the authors tried a method to evaluate using the ultrasonic backscattering method. Backscattered waves generated by microstructures are larger for high-frequency ultrasonic waves, and it is thought that the detection sensitivity of creep voids is higher. On the other hand, high-frequency ultrasonic waves also have large attenuation during propagation, which is disadvantageous for receiving transmitted waves and scattered waves to deep steel, and it is essential to ensure the sensitivity of transmitted and received signals. Based on simulations and preliminary experiments on the propagation of ultrasonic waves and the evaluability of creep voids, we examined the difference in creep void density detection in the deep part of steel due to the difference in ultrasonic focusing (large and small aperture) using a water immersion imaging device, which is a laboratory-based rigorous measurement device. The submerged imaging device mechanically scans the acoustic lens in the XY directions at a minute pitch to create an acoustic image that reflects the amplitude of the received signal at an arbitrary depth. The test piece cut out from the actual thermal power plant has a maximum of creep voids 900/mm^2 in the deep part of the steel. The ultrasonic frequency is 10 MHz, the XY scan is 1 µm pitch, and the scanning range is 1 mm × 1 mm. Since the creep void is expected to have a larger amplitude than the scattered wave of the fine structure, it is evaluated by extracting the number of bright points above a certain threshold in the acoustic image. As a result, it was suggested that it is possible to detect the degree of density of creep voids by focusing the ultrasonic waves more using a large-aperture acoustic lens. Next, assuming actual measurement, we designed and developed an aspherical oblique-angle focusing acoustic lens that emits ultrasonic waves at an oblique angle and efficiently focuses at a depth of 30 mm in order to avoid the effects of HAZ (Fig. 1). Two types of acoustic lenses were designed and fabiricated. Fig.2 and 3 show the comparison of acoustic images due to creep void using two acoustic lens. In both lens, damaged specimen (right image) observed many bright spots due to dense creep voids. Comparing to Fig.2 and 3, the thinner wedges of type B were more sensitive for creep voids. From the above results, it was suggested that the density of creep voids could be detected by evaluating the acoustic image based on the scattered wave amplitude produced by scanning a high-focus acoustic lens at a high-definition pitch. In the future, we will proceed with verification including measurement frequency, scanning pitch, and acoustic image processing method, and develop a system that can be used for equipment inspection of actual plant.

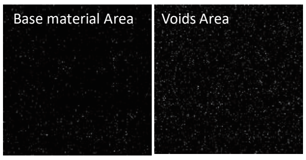

Fig.2 Acoustic image (type A)

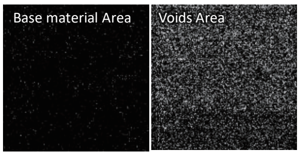

Fig.3 Acoustic image (type B)

P-29

Hydrogen Oxidation Reaction and Hydrogen Peroxide Generation Properties of Vacuum-Prepared Ru/Ir(111)

K. Hayashi*, K. Kusunoki, R. Sato, D. Kudo, N. Todoroki and T. Wadayama

Graduate School of Environmental Studies, Tohoku University, Sendai 980-8579

Prolonged lifetime is necessary for the wide-spread commercialization of polymer electrolyte membrane fuel cell (PEMFC), and thus, to prevent deterioration of the components under PEMFC operating conditions is crucial. From this viewpoint, development of the catalyst materials is of great importance because Pt nanoparticles supported on carbon black (Pt/C), which is generally used for both the cathode and anode catalysts, cause several types of degradation. For example, the Pt/C anode catalyst promotes not only hydrogen oxidation reaction (HOR); the anode reaction of PEMFC, but also H_2O_2 generation *via* a two-electron reduction of O_2 which comes from air. The generated H_2O_2 forms radical species of O* that deteriorate the PEM, leading to the degradation of PEMFC performance [1]. Thus, catalyst materials of less-active H_2O_2 generation with sufficient HOR activity are required for the anode catalyst. Recently, Ir-Ru catalysts are reported to show the Pt/C comparable HOR activity [2]. However, relation between the surface atomic compositions of the Ir-Ru and both the H_2O_2 generation and HOR properties are not clarified yet. We investigated in this work, the HOR and H_2O_2 generation properties of the well-defined Ru/Ir(111) bimetallic surfaces fabricated in ultra-high vacuum (UHV；~10^{-8}Pa).

Ru/Ir(111) bimetallic surfaces were prepared as Ir-Ru model catalysts by an arc-plasma deposition of 1 monolayer-thick Ru at a substrate temperature of T (T = 673, 773, 873 K) on UHV-surface-cleaned Ir(111) substrate. The topmost surface atomic compositions were estimated by low-energy ion scattering spectroscopy (LE-ISS) in UHV. The HOR and H_2O_2 generation properties were evaluated in respective solutions by using scanning electrochemical microscope (SECM).

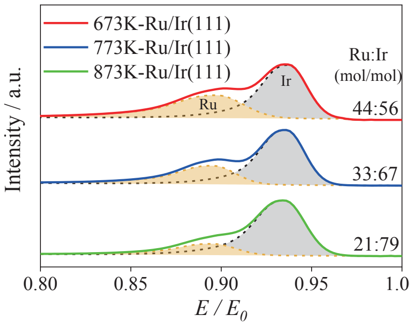

Fig. 1. LE-ISS spectra for the Ru/Ir(111).

LE-ISS spectra for the Ru/Ir(111) surfaces are shown in Fig. 1. Judging from the estimated top-surface atomic compositions, the surface Ru decreased with increasing the substrate temperatures through thermal diffusions of the Ru atoms into the substrate Ir. Fig. 2 presents the H_2O_2 generation properties evaluated in O_2-saturated 0.1 M $HClO_4$ by using SECM. In this method, the Pt micro tip electrode (φ ~ 20 μm) was hold about 40 μm above the sample surface at constant potential, and then the tip current, which corresponds to the detection of the H_2O_2 generated at the sample surfaces, was collected with sweeping sample potentials from 0.05 to 1.2 V vs. SHE. Throughout the measured potentials, all the Ru/Ir(111) and Ir(111) generated less amounts of H_2O_2 than Pt(111). Especially, 773 K-Ru/Ir(111) exhibited the lowest H_2O_2 generation property (@0.1V vs. SHE) among the tested samples. Thus, the topmost surface composition of Ir:Ru ~ 1:2 could be the most appropriate to suppress H_2O_2 generation for the Ir-Ru catalyst. The HOR activities of the samples will be also discussed.

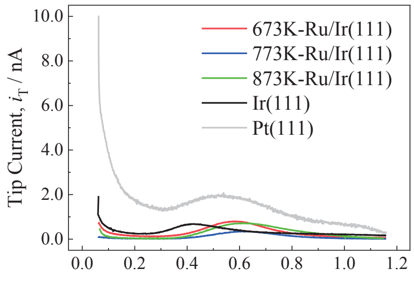

Fig. 2. H_2O_2 detection tip current vs. applied potentials.

[1] R. Borup et al., Chem. Rev. **107**, 3904 (2007).
[2] E. You, M. Min, S. Jin, T. Kim, and C. Pak, J. Electrochem. Soc. **165**, F3094 (2018).

Visible-light-induced antibacterial activity of TiO_2 layer formed by the two-step thermal oxidation of Ti

Ryusuke Koizumi[1], Kyosuke Ueda[1], Koyu Ito[2], Kouetsu Ogasawara[2], Takayuki Narushima[1,3]

[1]Department of Materials Processing, Tohoku University,
[2]Department of Immunobiology, Institute of Development, Aging and Cancer (IDAC),
Tohoku University,
[3]Research Center for Structural Materials, National Institute for Materials Science (NIMS)

Titanium and its alloys are widely used in biomaterials owing to their excellent corrosion resistance, bone compatibility, and mechanical properties. The benefits of Ti are widely recognized in dentistry; however, Ti dental implants possess the risk of infections caused by the adhesion of bacteria [1]. Therefore, surface treatments that impart antibacterial properties to Ti are necessary. The antibacterial activity of TiO_2, which is due to its photocatalytic activity, can be effectively utilized for biomedical applications [2]. Additionally, TiO_2 exhibits photocatalytic activity when exposed to ultraviolet (UV) light; however, UV radiation can potentially harm human body. Consequently, visible-light-induced antibacterial properties are essential. In our previous study, the carbon-added and anatase-rich TiO_2 layer formed through the two-step thermal oxidation of Ti showed antibacterial activity after visible-light irradiation for 14.4 ks [3]. The addition of nitrogen to the TiO_2 layer was expected to contribute the most to visible-light responsiveness. In this study, nitrogen-added TiO_2 layers were generated through the two-step thermal oxidation of Ti in a N_2-rich atmosphere and the antibacterial ability of these layers under visible-light irradiation was evaluated.

Commercially pure Ti (Gr. 2) plates with a diameter of 12 mm (single-side mirror-polished) were used as the substrate materials. First, the substrates were subjected to carbonitrization (N_2-1% CO, 1073 K, 3.6 ks). Subsequently, the materials were oxidized (N_2-1% O_2, 773–973 K, 10.8 ks and 973 K, 3.6–21.6 ks). The phases of the surface reaction layers were identified using X-ray diffraction, and the cross-section was observed using a scanning electron microscope. The chemical compositions of the reaction layers were analyzed through X-ray photoelectron spectroscopy. After oxidation, the antibacterial activity of the specimens under visible-light irradiation was evaluated by a glass adhesion method of *Escherichia coli* (*E. coli*), with JIS R 1752: 2013 as the reference.

During oxidation, an anatase-rich TiO_2 layer, a rutile-rich layer, and a rutile single-phase layer were produced at 773, 873, and 973 K, respectively. It was confirmed that nitrogen was dissolved in the TiO_2 layers. Furthermore, the TiO_2 layers irradiated with visible light had a significantly lower normalized number of viable bacteria (*E. coli*) than that of the TiO_2 layers kept in the dark. In particular, the rutile single-phase TiO_2 layer fabricated at 973 K for 7.2–10.8 ks showed the highest reduction after visible-light irradiation and had an antibacterial activity value of ~3.

[1] P.A. Norowski and J.D. Bumgardner, J. Biomed. Mater. Res. **88B**, 530–543 (2009).
[2] K. Sunada, T. Watanabe and K. Hashimoto, J. Photochem. Photobiol. **A156**, 227–233 (2003).
[3] T. Ueda, N. Sato, R. Koizumi, K. Ueda, K. Ito, K. Ogasawara, and T. Narushima, Dent. Mater, in press. (2020).

P-31

MnTe-based phase change memory with displacive polymorphic transformation

Shunsuke Mori[1*], Daisuke Ando[1] and Yuji Sutou[1]

[1] Dept. of Materials Science of Engineering, Tohoku Univ., Sendai, Japan

The phase change material (PCM) is known to show phase transition between amorphous and crystalline phases with large contrasts in optical and electrical properties [1]. $Ge_2Sb_2Te_5$ (GST225) is well known as a typical PCM. In optical disk or semiconductor memories, PCMs are used for a memory layer. Recently, new PCMs showing a transition between different two crystalline phases have much attention because of its melting-free process without amorphization, enabling very lower energy- and fast operation- memory. For example, $GeTe/Sb_2Te_3$ superlattice (GeTeSL) and single crystal In_2Se_3 are known to be melting-free PCMs showing very low energy operation [2,3].

MnTe is known as a polymorphic compound. According to Mn-Te binary phase diagram, β (wurtzite-type structure) and α (NiAs-type structure) phases are known to be stable phase in higher temperature region (more than 900 ℃) and at room temperature, respectively [4]. Recently we found that the sputtered MnTe films show the transformation from the β to stable α phase [5,6]. Moreover, the optical and electrical properties of the MnTe films changed upon the β→α polymorphic transformation drastically. In this study, we investigated the memory characteristics of the MnTe polymorphic film.

Mn-Te films on Si (725 μm) / SiO_2 (100 nm) substrates were prepared by radiofrequency magnetron sputtering at room temperature. MnTe-based memory device was fabricated using conventional photolithography and focus ion beam (FIB) technique. The memory device was annealed to obtain α-MnTe before the measurement. The memory characteristics of obtained devices were evaluated by a semiconductor parameter analyzer. In order to investigate the operation mechanism in memory devices, a cross-sectional image of a phase change region was observed using transmission electron microscopy (TEM). TEM samples were fabricated using FIB technique.

The MnTe-based memory devises showed a reversible resistive switching with increasing applied pulse voltage. Such a resistive switching behavior was observed even under the pulse width of 10 ns, indicating that the MnTe can show very fast transition speed. According to the calculation of the operation energy, the MnTe was found to achieve more than 90 % reduction of energy consumption in the conventional memory using GST225. Our TEM observation also revealed that the phase change region is a β' phase which has a wurtzite-type structure but the coordinates of the Te atoms are slightly different from the β phase. The atomic-column image at α/β' phase boundary revealed that the α/β' polymorphic change can be achieved by a displacive transformation without a long-range atomic diffusion. The atomic-displacement in MnTe polymorph enable the very fast and low energy memory operation [7].

[1] M. Wuttig, and N. Yamada, Nat. Mater. **6**, 824 (2007).
[2] R. E. Simpson, P. Fons, A. V. Kolobov, T. Fukaya, M. Krbal, T. Yagi, and J. Tominaga, Nat. Nanotechnol. **6**, 501 (2011).
[3] M. S. Choi, B. Cheong, C. H. Ra, S. Lee, J. Bae, S. Lee, G. Lee, C. Yang, J. Hone, and W. J. Yoo, Adv. Mater. **29**, 1703568 (2017).
[4] M.E. Schlesinger, J. Phase Equil. **19**, 591 (1998).
[5] S. Mori, Y. Sutou, D. Ando, and J. Koike, Mater. Trans. **59**, 1512 (2018).
[6] S. Mori, D. Ando, and Y. Sutou, Mater. Des. **196**, 109141 (2020).
[7] S. Mori, S. Hatayama, Y. Shuang, D. Ando, and Y. Sutou, Nat. Commun. **11**, 85 (2020).

Flow Stress Modeling of Alloy 720Li Using Internal State Variables Model

Jo Nakamura[1*], Nobufumi Ueshima[1] and Katsunari Oikawa[1]

[1]Department of Metallurgy, Graduate School of Engineering, Tohoku University
6-6-02 Aza-Aoba Aramaki, Aoba-ku, Sendai 980-8579, Japan

Alloy 720Li is a kind of precipitation strengthening Ni-based superalloy and is known as a forging material for turbine discs in aircraft engines. Hot forging not only improves workability by dynamic softening associated with microstructural changes such as dynamic recrystallization (DRX), but also brings out the mechanical properties by controlling the post-work structure [1]. Since flow stress and microstructure are closely related to each other, it is necessary to construct a flow stress model that takes these relationships into account in order to develop a manufacturing process that improves Workability and mechanical properties. The purpose of this study is to establish a flow stress model of Alloy 720Li by considering the effect of work hardening, dynamic recovery, DRX and grain-boundary strengthening by using internal state variables (ISV) model [2] based on the dislocation theory.

As-received Alloy 720Li cylindrical test specimens with a diameter of 8 mm and a height of 12 mm were homogenized at 1104 ℃ for 4 h and air cooled. Hot compression tests were carried out at temperatures of 1050 ℃, 1100 ℃ and 1150 ℃, strain rates of 0.001 s^{-1}, 0.01 s^{-1} and 0.1 s^{-1} and true strain of 0.5 and 0.7. Flow stress was modeled by optimizing parameters so that the sum of the squares of the differences between the flow stress values obtained from the hot compression tests and the calculated values by ISV model were minimized. The specimens were cut in the compression direction and their microstructure was observed by scanning electron microscope (SEM).

Fig. 1 shows the flow stress curves obtained by the compression tests and calculated by ISV model. The error between the experimental and calculated values was 6.6 % at 1100 ℃ and 1150 ℃ except for 0.001 s^{-1}, which shows flow behavior was well described by ISV model. However, at 1050 ℃, the constitutive equation used in this study did not work well. The results of microstructure observation are shown in Fig. 2. Tertiary γ' phase was observed before the compression test and in the compressed specimens at 1050 ℃ but was not observed in the compressed specimens at 1100 ℃ and 1150 ℃. These results suggest that the effect of precipitation on the constitutive equation is a possible reason for the deviation.

[1] F. Liu, J. Chen, J. Dong, M. Zhang and Z. Yao, *Mater. Sci. Eng. A* **561**, 102(2016).
[2] J. Lin, Y. Liu, D. C. J. Farrugia and M. Zhou. *Philos. Mag.* **85** 1967(2005).

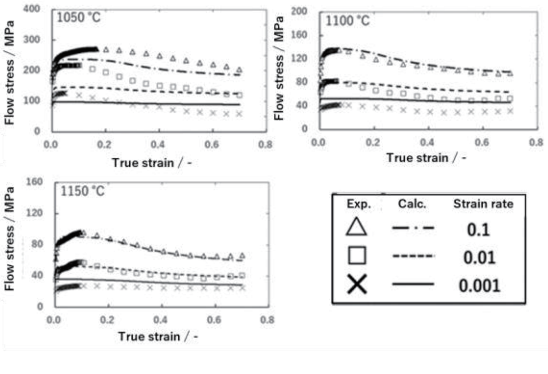

Fig. 1. Comparison of experimental and calculated flow stress curve

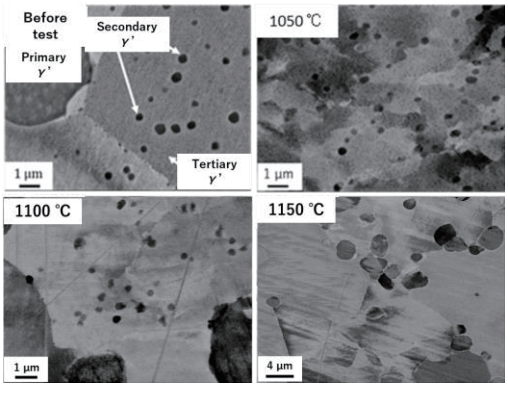

Fig. 2. BSE images for each condition.
Strain 0.5, Strain rate 0.01 s^{-1}

P-33

Thin-Film Properties of BTBT Derivatives with Oligo(ethylene oxide) Chains

Taichi Imai[1,2], Kohsuke Kawabata[1,2] and Kazuo Takimiya[1,2]

[1]Graduate School of Science, Tohoku University
[2]Center for Emergent Matter Science (CEMS), RIKEN

One of the important advantages of organic semiconductor materials is solution-processability, which enables low-cost fabrication of electronic devices. However, the materials with good charge transport properties such as 2,7-diphenyl[1]benzothieno[3,2-*b*][1]-benzothiophene (DPh-BTBT)[1] and dinaphtho[2,3-*b*:2′,3′-*f*]-thieno[3,2-*b*]thiophene (DNTT)[2] are difficult to apply to solution-processing due to their low solubilities. To improve the solubility, bulky alkyl substituents were introduced frequently[3]. However, such bulky substituents may change the crystal structures favorable for charge transport. Therefore, the search for soluble substituents with little steric hindrance is important for the development of soluble organic semiconductor materials with good charge transport properties.

In this study, we synthesized DPh-BTBT derivatives **1**, **2**, and **3** with oligo(ethylene oxide) and/or alkoxy groups (Fig. 1). Oligo(ethylene oxide) chains are known as soluble substituents with a linear structure[4]. **1** has low solubility in chloroform comparable to that of DPh-BTBT, while **2** and **3** have high solubilities enough for solution-processing. X-ray diffraction patterns of thin films of **2** and **3** fabricated by spin-coating indicated that the films have layer structures in the out-of-plane direction and the film of **2** has the herringbone arrangement in the in-plane direction (Fig. 2). Furthermore, organic field-effect transistors (OFETs) with **2** and **3** as active layers showed p-type charge transport properties, and the device based on **2** showed the hole mobility of up to 0.83 cm^2/Vs under vacuum (Fig. 3).

[1] K. Takimiya *et al.*, *J. Am. Chem. Soc.* **2006**, *128*, 12604−12605.
[2] T. Yamamoto *et al.*, *J. Am. Chem. Soc.* **2007**, *129*, 2224−2225.
[3] M. Sawamoto *et al.*, *ACS. Appl. Mater. Interfaces* **2016**, *8*, 3810−3824.
[4] J. Mei *et al.*, *Chem. Mater.* **2011**, *23*, 2285−2288.

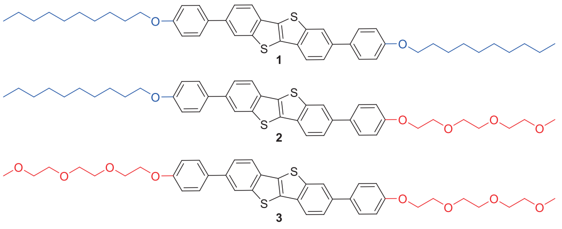

Fig. 1. Stuructures of DPh-BTBT derivatives

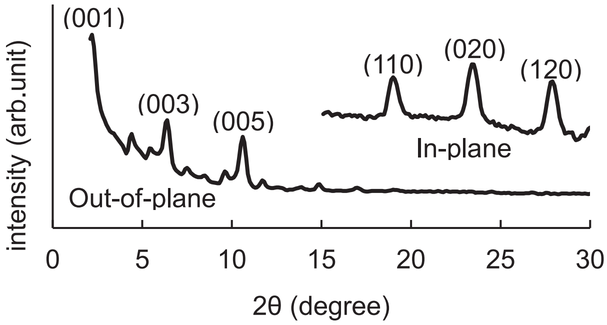

Fig. 2. XRD patterns of the film of **2**

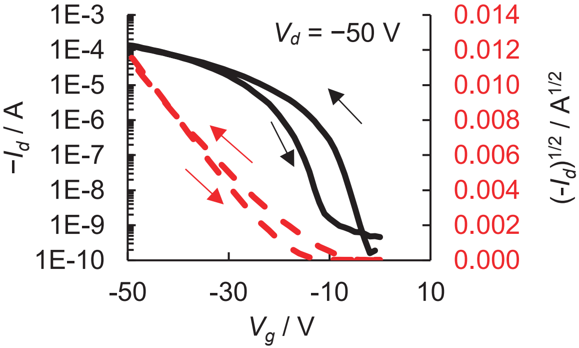

Fig. 3. Transfer curve of **2**

Exosome-targeting probe containing an environment-sensitive fluorophore introduced into amphipathic helix peptide

Kazuki Kuwahara[1], Kenta Mogami[1], Yusuke Sato[1,2] and Seiichi Nishizawa[1]

[1]Department of Chemistry, Graduate School of Science, Tohoku University, Sendai, Japan
[2]JST, PRESTO, Tokyo, Japan

Exosome, a kind of extracellular vesicles with about 30-150 nm in diameter, contains various nucleic acids and proteins inside, and it has been revealed that they are greatly involved in various diseases and cancers through intercellular communication. Hence, its functional analysis is indispensable for pharmaceutical applications [1]. While immunoassays like ELISA have been widely used for its quantification, some of them cannot be detected in principle [2]. Here, we report on the new class of exosome-binding fluorescent probe based on amphipathic helical peptide as a universal analytical tool for marker-free manner. This probe can be inserted hydrophobically into the lipid packing defects (LPDs) that can be commonly found in exosome-sized vesicles [3], which provides the detection of various kinds of exosomes without the bias from the surface protein diversity.

We selected C-terminal amphipathic region of human apolipoprotein A-I (ApoC) as the exosome recognition unit and Nile red (NR) was attached to N-terminal of ApoC. The resulting probe (ApoC-NR) was found to show the fluorescence enhancement response and the increase signal of CD at 208 and 222 nm, indicators of a-helicity, upon binding to K562 exosome. These results suggest that the ApoC unit binds to the LPDs on the exosome surface, and the NR unit is distributed inside the membrane. Though the fluorescence response was dependent on the exosome concentration and the detection limit was comparable to ELISA (Fig. 1), the detection sensitivity was not affected by different release cells (BPH-1, A549 and U87MG). Moreover, our method has a great advantage as an analysis tool that is extremely quick and simple (~5 min) over ELISA. Consequently, we found that ApoC-NR, the exosome-binding fluorescent probe based on our unique probe design, is useful as a new analytical tool that overcomes the problems of ELISA [4]. We envision that our approach will be powerful and helpful for practical medical applications.

[1] S. Mathivanan, H. Ji, and R, J. Simpson, J. Proteomics, 2010, **73**, 1907-1920.
[2] M. Jorgensen, R. Baek, S. Pedersen, E. K. L. Sondergarrd, S. R. Kristensen and K. K. Varming, J. Extracell. Vesicles, 2013, **2**, 20920
[3] S. Vanni, H. Hirose, H. Barelli, B. Antonny and R. Gautier, Nat. Commun., 2014, **5**, 4916.
[4] Y. Sato, K. Kuwahara, K. Mogami, K. Tahakashi, and S. Nishizawa, RSC Advances, 2020, DOI: 10.1039/d0ra07763a.

P-35

Electronic excitations in high-Tc superconducting cuprates by oxygen *K*-edge resonant inelastic X-ray scattering

Yukihiro Matsubayashi and Sumio Ishihara

Department of Physics, Tohoku University

In the resonant inelastic X-ray scattering (RIXS) processes, core electrons are resonantly excited by an incident X-ray, and then the X-ray is scattered when electrons are relaxed. It is widely recognized that the RIXS enables us to obtain information on the momentum- and energy-resolved elementary excitations of correlated materials, which are not accessible by other methods. Theoretical calculations play a large role for the interpretation for RIXS spectra, which are described by the second-order perturbation theory with respect to the electron-photon interaction. La_2CuO_4, the parent material of high-T_c superconducting cuprates, is a charge-transfer insulator and offers a starting point for understanding the origin and anomalous electronic states of the high-T_c superconductors. An experimental study of oxygen K-edge RIXS found that the Zhang-Rice singlet (ZRS) is formed by an electronic excitation from the oxygen to the copper atoms [1]. In order to reproduce the observed oxygen K-edge RIXS spectra, we need to take the oxygen orbitals into account. However, theoretical analyses of the detailed momentum dependence of the oxygen K-edge RIXS spectra have not been reported so far.

In this study, we analyzed the oxygen K-edge RIXS spectra on the basis of the Keldysh formalism [2]. We obtained the RIXS spectra shown in Fig. 1 by using the cluster perturbation theory (CPT), which reproduces the recent experimental results. There are the ZRS excitations from 1.5 to 3 eV and the charge-transfer excitations around 4 eV. These spectra are consistent with the results of a 2 by 2 cluster obtained by the exact diagonalization method as shown in Fig. 2.

[1] K. Okada and A. Kotani, Phys. Rev. **B65**, 144530 (2002).
[2] J. Igarashi and T. Nagao, Phys. Rev. **B88**, 014407 (2013).

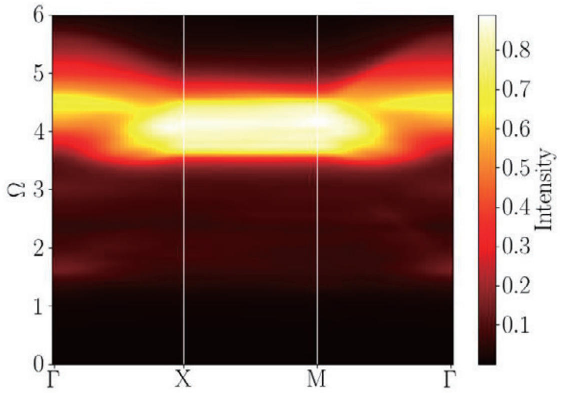

Fig. 1. Oxygen K-edge RIXS spectra calculated by the CPT method.

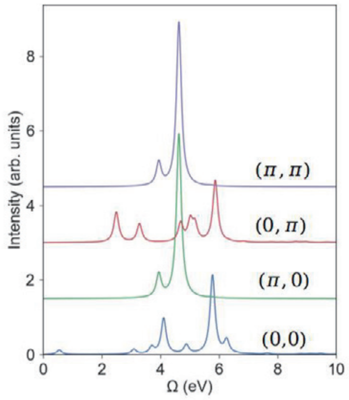

Fig. 2 Oxygen K-edge RIXS spectra calculated by the ED method.

P-36

High-Resolution ARPES Study on the Origin of High-Temperature Superconductivity in $FeSe_{1-x}Te_x/CaF_2$

K. Nakayama[1,2*], R. Tsubono,[1] G. N. Phan,[1] F. Nabeshima,[3] N. Shikama,[3] T. Ishikawa,[3]
Y. Sakishita,[3] S. Ideta,[4,5] K. Tanaka,[4,5] A. Maeda,[3] T. Takahashi,[1,6,7] and T. Sato[1,6,7]

[1] Department of Physics, Tohoku University
[2] Precursory Research for Embryonic Science and Technology (PRESTO),
Japan Science and Technology Agency (JST)
[3] Department of Basic Science, the University of Tokyo
[4] UVSOR Synchrotron Facility, Institute for Molecular Science
[5] School of Physical Sciences, The Graduate University for Advanced Studies (SOKENDAI)
[6] Center for Spintronics Research Network, Tohoku University
[7] WPI Research Center, Advanced Institute for Materials Research, Tohoku University

One of outstanding physical properties of iron-based superconductors is electronic nematicity characterized by spontaneous breaking of the rotational symmetry in the electronic structure. Since nematicity appears in the proximity of the high-temperature superconducting phase, the interplay between nematicity and superconductivity is a central issue in the current research of iron-based superconductors. Iron-chalcogenide superconductor $FeSe_{1-x}Te_x$ is an ideal system to investigate this issue, because (i) the parent FeSe ($x = 0$) shows unique nematicity without antiferromagnetic order [1] that complicates the electronic states and (ii) Te substitution leads to the highest T_c among non-carrier-doped FeSe system at ambient pressure [2]. However, the evolution of nematicity with Te substitution and the mechanism of high-temperature superconductivity have remained unresolved. In this study, by utilizing angle-resolved photoemission spectroscopy (ARPES), we have succeeded in determining the evolution of the electronic structure as well as nematicity in $FeSe_{1-x}Te_x$ across the critical Te concentration (x_c), above which the high-temperature superconductivity emerges. Our comprehensive study provides an important insight into the interplay between high-temperature superconductivity and nematicity in iron-chalcogenide superconductors.

[1] K. Nakayama, Y. Miyata, G. N. Phan, T. Sato, Y. Tanabe, T. Urata, K. Tanigaki, and T. Takahashi, Phys. Rev. Lett. **113**, 237001 (2014).
[2] Y. Imai, Y. Sawada, F. Nabeshima, and A. Maeda, Proc. Natl. Acad. Sci. USA **112**, 1937 (2015).

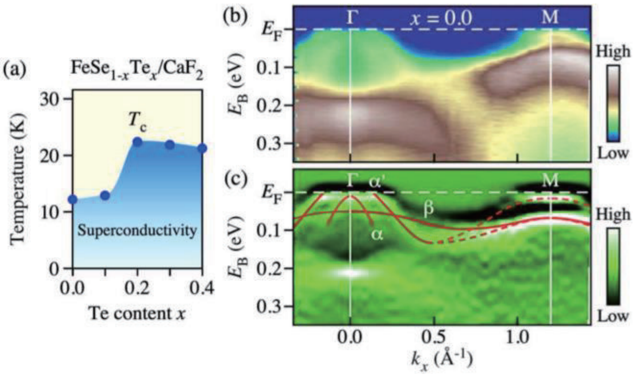

Fig. 1. (a) Phase diagram of $FeSe_{1-x}Te_x/CaF_2$. (b) Representative APRES-intensity plot and (b) corresponding second-derivative-intensity plot measured at $T = 30$ K for $FeSe/CaF_2$ ($x = 0$).

P-37

Electrical resistivity measurements under high pressure for iron-based ladder material $BaFe_2(S_{1-x}Se_x)_3$

R. Nojima, T. Aoyama, Y. Imai, and K. Ohgushi

Department of physics, Graduate School of Science, Tohoku University

The iron-based materials $BaFe_2X_3$ (X = S and Se), which exhibit pressure-induced superconducting transitions, are Mott insulators due to the strong electron correlation effect inherent in a quasi-one-dimensional ladder lattice at an ambient pressure [1, 2]. As in the case of iron-based superconductors with a two-dimensional square lattice, the orbital ordering derived from the multi-orbital nature of Fe^{2+} ions is observed in $BaFe_2X_3$; a slight anomaly in the electrical resistivity owing to the orbital ordering appears above the antiferromagnetic transition temperature. The antiferromagnetic/orbital ordering transition temperatures are 115 K/200 K for $BaFe_2S_3$ and 255 K/400 K for $BaFe_2Se_3$. The possible orbital-ordering pattern is a ferroic order of $d_{x^2-y^2}$ orbitals in $BaFe_2S_3$, and a staggered order of $d_{x^2-y^2}$ and d_{xz} orbitals in $BaFe_2Se_3$. In a solid solution $BaFe_2(S_{1-x}Se_x)_3$, the orbital-ordering pattern switches from the ferroic one into the staggered one at the critical concentration of the magnetic phase boundary, x_c= 0.23, where the ground-state magnetic structure switches from the striped-type one into the block-type one [3].

In this study, in order to clarify the details of the orbital ordering in the iron-based ladder compounds, we performed the electrical resistivity measurements under pressure for $BaFe_2(S_{1-x}Se_x)_3$. The measurements were performed up to 2.0 GPa using a piston-cylinder high-pressure cell.

As a result, we found a distinct temperature variation of the electrical resistivity below and above 0.25 GPa for $BaFe_2(S_{0.75}Se_{0.25})_3$ (Fig. 1); on cooling, the electrical resistivity sharply increases across the orbital ordering transition (210-190 K) below 0.25 GPa, while it shows a suppression of the divergent manner across the orbital ordering transition (183-180 K) above 0.5 GPa. By referring to electrical resistivity data at an ambient pressure, we conclude that the application of pressure to $BaFe_2(S_{0.75}Se_{0.25})_3$ induces the switching of the orbital-ordering pattern from the ferroic one into the the staggered one. In our poster presentation, we will show the details of experimental results, and discuss the origin of the pressure-induced orbital-switching behavior.

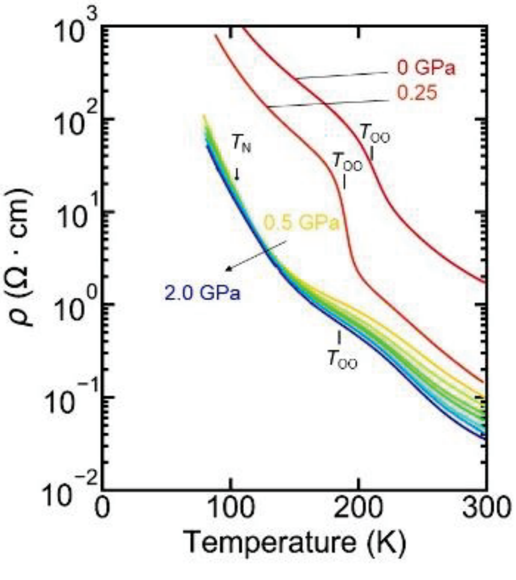

Fig. 1. The electrical resistivity of $BaFe_2(S_{0.75}Se_{0.25})_3$

[1] H. Takahashi, *et al*., *Nat. Mater.* **14**, 1008 (2015).
[2] J. Ying, *et al*., *Phys. Rev.* B **95**, 241109(R) (2017).
[3] S. Imaizumi, *et al*., *Phys. Rev.* B **102**,035104 (2020).

Dissipative particle dynamics approach to reaction-induced morphological changes in thermoplastic/thermosetting resin mixtures

Yoshinori Tomiyoshi[1*], Yutaka Oya[1,2], Toshihiro Kawakatsu[1] and Tomonaga Okabe[3]

[1] Department of Physics, Graduate School of Science, Tohoku University
[2] Department of Organic Materials Science, Graduate School of Organic Materials Science, Yamagata University
[3] Department of Aerospace Engineering, Graduate School of Engineering, Tohoku University

Control of microscopic structures of polymeric materials is of crucial importance in designing various material composites. We utilize phase separating polymers such as diblock copolymers as one of the promising tools to obtain a diversity of well-ordered microscopic structures. Progress in computational techniques to correctly predict these structures including molecular dynamics simulations or macroscopic continuum simulations is now strongly desired.

In experimental point of view, Lipic *et al.*[1] showed a possibility of controlling mesoscopic domain morphologies in thermoplastic/thermosetting resin mixtures. The morphological changes observed in this system can be explained by reaction-induced phase separation where the cross-linking of the matrix polymer leads to an instability of the microphase-separated structures with a large mean curvature. Although this mechanism is expected to be a key to the control of the microscopic structures, there have been few reports to understand the mechanism.

In the present study, we apply the dissipative particle dynamics (DPD) simulation, which was proposed by Groot and Warren[2] to simulate microphase separation, to homopolymer/diblock copolymer blends with a simple chemical reaction. In addition to their original methodology, we incorporate the chemical reaction where homopolymers are chemically connected with each other.

By conducting the simulation mentioned above, we reproduce the morphological changes of microscopic phase structures. Figure 1 shows a transition from cylindrical phase (Fig. 1 left) to lamellar phase (Fig. 1 right) due to the cross-linking of homopolymers. We also find that the rate of polymerization reaction affects the structural order of the finally-obtained microphase structures. This indicates the importance of the curing process in the control of domain morphology.

Acknowledgements: Financial support from Cross-ministerial Strategic Innovation Promotion Program (SIP) "Materials Integration for Revolutionary Design System of Structural Materials" (Funding agency: JST) is gratefully acknowledged.

[1] P. M. Lipic, F. S. Bates, and M. A. Hillmyer, J. Am. Chem. Soc. **120**, 8963 (1998).
[2] R. D. Groot and P. B. Warren, J. Chem. Phys. **107**, 4423 (1997).

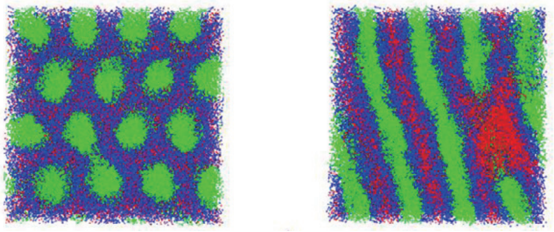

Fig. 1. Morphological change of the domain structure due to cross-linking reaction. (Left) Cylindrical phase as the initial structure. (Right) Lamellar phase as the final structure.

Solid Solution Strengthening and High-Temperature Strength in TiC–TaC–ZrC–NbC Ceramics

D. Demirskyi[1,2,3*], O. Vasylkiv[2] and K. Yoshimi[1,3]

[1] WPI-Advanced Institute for Materials Research (WPI-AIMR), Tohoku University
[2] National Institute for Materials Science, NIMS, Tsukuba
[3] Department of Materials Science and Engineering, Tohoku University

As an emerging concept in the field of metallic alloys, high-entropy (HE) materials combine multiple principal elements to create new single-phase materials. Over the past few years, the 'HE strategy' has been applied across various fields, including thermoelectricity, catalysis and structural ceramics [1]. The large configurational entropy is believed to enhance the simultaneous solubility of a large number of components, which can then be selected to optimize target properties. However, *medium*-entropy compounds may emerge if a fewer number of elements is being used. For these compounds, especially applied to ceramics, the good balance of strength and hardness is being anticipated [2], as a lattice distortion is not as severe as in HE case. Nevertheless, data on high-temperature strength is limited.

In this contribution, we explore synthesis of solid-solution of carbides, a *medium*-entropy $(Ti_{1/4}Ta_{1/4}Zr_{1/4}Nb_{1/4})C$ [3]. Bulk solid-solution or medium-entropy carbide ceramics have been obtained by two different thermal histories using the spark plasma sintering method.

The mechanical performance at room temperature for the (Ti,Ta,Zr,Nb) carbides is comparable to the best data for the TiC or TaC monolithic ceramics, reaching 600 MPa (**Figure 1**). This may be explained in terms of a solid-solution strengthening mechanism. In terms of the specific flexural strength or specific stiffness, *medium*-entropy carbide bulks are superior to the majority of the monolithic carbides, except the TiC. Importantly, at elevated temperatures, *medium*-entropy (Ti,Ta,Zr,Nb) carbides possess the strength of 300 or 500 MPa at 1600 °C where they fracture in an elastic manner [3]. The strength at high temperatures is quite sensitive to the consolidation conditions and is beyond a simple HE strategy and requires further research.

[1] C. Oses, C. Toher, S. Curtarolo, Nat. Rev. Mater. **5** 295–309 (2020).
[2] D. Demirskyi, H. Borodianska, T.S. Suzuki, Y. Sakka, K. Yoshimi, O. Vasylkiv, Scripta Mater. **164** [15] 12–16 (2019).
[3] D. Demirskyi, T.S. Suzuki, K. Yoshimi, O. Vasylkiv, Open Ceramics **2** 100015 (2020).

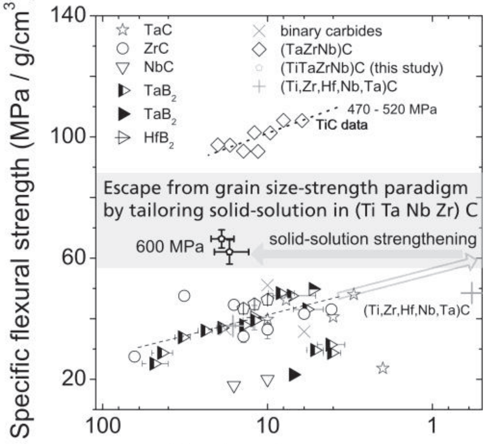

Fig. 1. Effect of the grain size and composition of selected UHTCs normalized strength values [3].

P-40

Electrochemical characterization of Magnesium Borohydride Ammonia Borane $Mg(BH_4)_2(NH_3BH_3)_2$ as a Magnesium Ionic Conductor

Kazuaki Kisu[1], Sangryun Kim[2], Munehiro Inukai[3], Hiroyuki Oguchi[4],
Shigeyuki Takagi[2], and Shin-ichi Orimo[1,2]

[1] WPI-Advanced Institute for Materials Research (WPI-AIMR), Tohoku University
[2] Institute for Materials Research (IMR), Tohoku University
[3]Tokushima University
[4] Shibaura Institute of Technology

All-solid-state Mg batteries are one of the promising candidates for solving the intrinsic drawbacks of Li-ion batteries, such as high cost and low abundance of Li sources, electrolyte leakage, and limited energy density [1]. For the development of all-solid-state Mg batteries, Mg ionic conductor as solid electrolytes are a key component because the conductivity and stability of the solid electrolyte determine battery performance. In this work, we investigated the Mg ionic conduction and electrochemical properties of the $Mg(BH_4)_2(NH_3BH_3)_2$ complex hydride [2] to establish its potential applicability in all-solid-state Mg batteries. Following the mechanochemical synthesis of $Mg(BH_4)_2(NH_3BH_3)_2$ from $Mg(BH_4)_2$ and NH_3BH_3, the Mg ionic conductivities were determined by impedance measurements as 1.3×10^{-5} S cm^{-1} at 30 °C and 8.4×10^{-5} S cm^{-1} at 40 °C, which are among the highest Mg ionic conductivities reported to date for solids without electron conduction as shown in Figure 1 right. In addition, cyclic voltammetry investigations of a cell based on this material combined with Mo and Mg electrodes showed that Mg stripping and plating occurred at 0 V (relative to the Mg metal electrode) as shown in Figure 1 left. These results therefore confirm that Mg ionic conduction can be achieved by the coordination of NH_3BH_3 to $Mg(BH_4)_2$, and it is expected that these observations will contribute to the development of all-solid-state Mg batteries [3].

This work was supported by MEXT, KAKENHI (JP18H05513 (Hydrogenomics), 19K15305, and 19K15666).

[1] J. Muldoon *et al., Chem. Rev.*, **114** (2014), 11683.
[2] X. Chen *et al., Dalton Trans.*, **42** (2013) 14365.
[3] K. Kisu *et al.*, *ACS Appl. Energy Mater.*, **3** (2020) 3174.

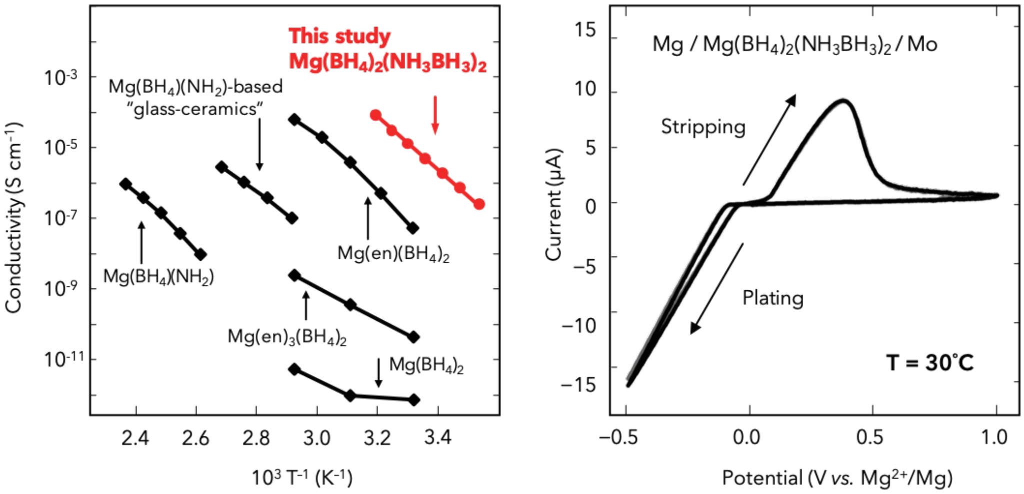

Fig. 1. Temperature dependence of the Mg^{2+} ionic conductivity of $Mg(BH_4)_2(NH_3BH_3)_2$ with those of previously reported complex hydride Mg-ion conductors (Left). Cyclic voltammograms of $Mg/Mg(BH_4)_2$-$(NH_3BH_3)_2/Mo$ at 30 °C, at a scan rate of 10 mV s^{-1}, and with use of a voltage range of −0.5 to 1.0 V *vs.* Mg^{2+}/Mg (Right).

P-41

Two dimensional bio-hybrid membranes based on self-assembly

Teng Ma[1]

[1] WPI-Advanced Institute for Materials Research (WPI-AIMR), Tohoku University

The bilayer lipid membrane (BLM), a basic structure in cell membranes, is a self-assembled structure of phospholipid molecules. Benefit from unique properties, such as ultrahigh resistance, thin thickness (3~4 nm), and amphiphilicity, BLMs have been widely used as platforms to explore physiological and pharmaceutical applications by monitoring transmembrane transport process. Recently, the combination of BLMs and nanocarbon materials has attracted significant attention as novel devices. In this work, we functionalized the BLMs using organic molecules such as [6,6]-phenyl-C_{61}-butyric acid methyl ester (PCBM), and Copper(II) 2,9,16,23-tetra-tert-butyl-29H,31H-phthalocyanine (CuPc), and demonstrated that the functionalized BLMs could be used as a platform for sensing devices.

Firstly, when free standing BLMs were doped with PCBM molecules, a photo-induced change in transmembrane conductance was observed [1]. The light illumination reversibly switched the membrane conductivity that was induced only when BLMs were doped with PCBMs. In order to further improve the performance of BLM-based devices, we introduced a “gate bias” to the free standing BLM system [2]. We fabricated a Si chip equipped with two metal electrodes as the support for BLMs. When the lateral bias was applied to the two electrodes on the Si chip, the PCBM-doped BLM showed photoresponse under light illumination and lateral bias. We were able to modulate the transmembrane current by changing the lateral bias. These results indicate that the BLM is a promising platform for hybrid nanodevices. To further expand the range of application of BLMs to solid-state devices, hybrid membranes consisting of lipid molecules and organic molecules, namely, CuPc were formed through self-assembly at a water/air interface [3]. We demonstrated that a hybrid membrane with a large area can be obtained by simply transferring the self-assembled membrane onto a Si substrate (Fig. 1). These results demonstrated that the hybrid BLM is a powerful and feasible platform for realizing sensing devices.

[1] K. Kanomata, T. Deguchi, T. Ma, T. Haseyama, M. Miura, D. Yamaura, D. Tadaki, M. Niwano, A. Hirano-Iwata, F. Hirose, J. Electroanal. Chem., **832**, 55 (2019).

[2] T. Ma, X. Feng, T. Deguchi, T. Ohori, D. Yamaura, R. Miyata, D. Tadaki, M. Komiya, K. Kanomata, F. Hirose, M. Niwano, A. Hirano-Iwata, ACS Omega, **4**, 18299 (2019).

[3] X. Feng, T. Ma, D. Yamaura, D. Tadaki, A. Hirano-Iwata, J. Phys. Chem. B, **123**, 6515 (2019).

[4] X. Feng, T. Ma, D. Tadaki, A. Hirano-Iwata, *J. Vis. Exp.* **159**. E60957 (2020).

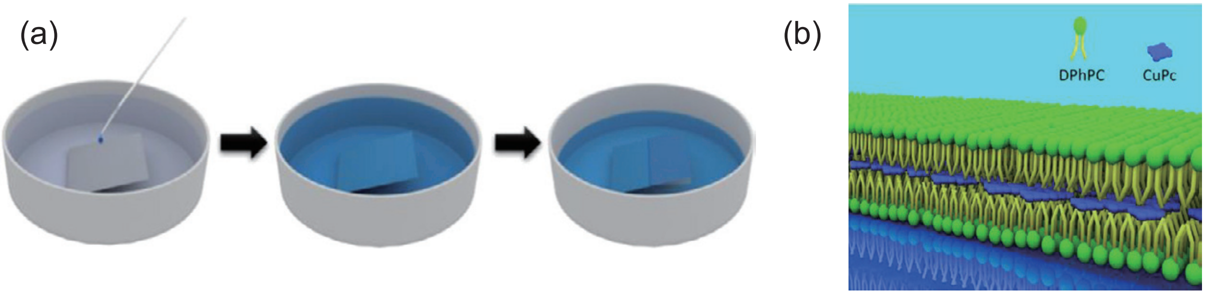

Fig. 1. Formation method (a) and structure illustration (b) of the CuPc-doped BLMs.

P-42

In-situ low-temperature scanning tunneling microscopy and spectroscopy studies of $SrVO_3$ and Pr thin films

Hirofumi Oka[1] and Tomoteru Fukumura[1,2]

[1] WPI-Advanced Institute for Materials Research (WPI-AIMR) and Core Research Cluster for Materials Science, Tohoku University
[2] Department of Chemistry, Graduate School of Science, Tohoku University

Nano-scale electronic materials, such as ultrathin films and nanostructures, are expected to exhibit novel quantum electronic properties paving the way to new functional electronic devices. In order to explore their novel electronic properties, it is crucial to characterize nano-scale materials on the atomic scale. Scanning tunneling microscopy and spectroscopy (STM and STS) are powerful techniques to investigate local atomic structures and electronic properties of nano-scale materials due to their high spatial resolution. Here, we report recent results of $SrVO_3$ ultrathin films on $SrTiO_3$ (001) and Pr thin films on CaF_2 (111) obtained using low-temperature STM equipped with pulse laser deposition (PLD).

Figure 1(a) shows a topographic STM image of $SrVO_3$ ultrathin films. Previously, we revealed that the surface reconstruction played an important role in the formation of metallic surface states of $SrVO_3$ [1]. We further investigated impact of dimensionality on the electronic states of $SrVO_3$ and revealed that the electronic states of $SrVO_3$ nanowires changed from metallic to insulating with decreasing the nanowire width [Fig. 1(b)]. We ascribed this new kind of a metal-insulator transition to dimensional crossover mechanism [2,3].

Another observation is concerned with fcc-structure Pr thin films on CaF_2 (111) deposited by PLD in vacuum, which is intriguingly one of high-pressure phases of Pr, probably exhibiting delocalized 4*f* electronic states. However, there has been no experimental report to directly corroborate delocalization of 4*f* electrons in high-pressure phase Pr. Figure 1(c) shows an STM image of the Pr thin films. We found a spatial modulation of differential conductance at step edges and around defects [Figs. 1(d) and (e)]. This is a clear indication of the existence of itinerant electrons in the high-pressure phase Pr, which is probably the first experimental evidence of delocalized 4*f* electronic states.

These studies are in collaboration with T. Hitosugi (AIMR, Tokyo Tech.), Y. Okada (AIMR, OIST), K. Kaminaga (AIMR), and D. Oka (Dept. Chemistry).

[1] H. Oka, Y. Okada, T. Hitosugi, and T. Fukumura, Appl. Phys. Lett. **113**, 171601 (2018).
[2] H. Oka, Y. Okada, K. Kaminaga, D. Oka, T. Hitosugi, and T. Fukumura, Appl. Phys. Lett. **117**, 051603 (2020).
[3] AIMResearch, 26 Oct. 2020.

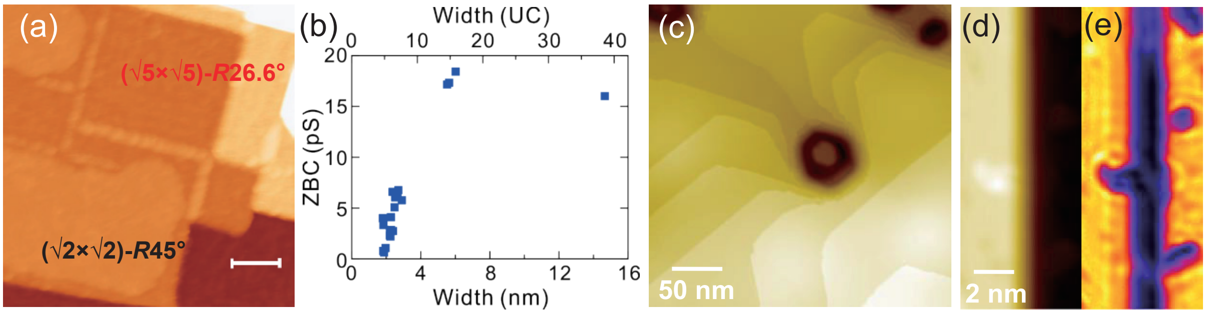

Fig. 1. (a) $SrVO_3$ ultrathin films deposited on $SrTiO_3$ (001). (b) Zero-bias conductance (ZBC) of nanowires as a function of the width. (c) Pr thin films deposited on CaF_2 (111). (d) and (e) Topographic and differential conductance maps around a step edge of Pr thin films (sample bias voltage $V = -10$ mV).

P-43

Phase Separation with Ordering in Aged Fe-Ni-(Al,Mn) Alloys

Fei Sun [1], Goro MIYAMOTO [2] and Tadashi FURUHARA [2]

[1] WPI-Advanced Institute for Materials Research (WPI-AIMR), Tohoku University
[2] Institute for Materials Research (IMR), Tohoku University

High entropy alloys (HEAs) are presently of great research interest in materials science and engineering. Stability of solid solution is affected by high entropy due to multi-component and high alloyed natures and also by complex mixing enthalpy due to various elemental interactions. This study aims to re-analyze effects of elemental interactions on decomposition of solid solution, such as ordering and phase separation, in model high alloys in ternary systems. Fcc based Fe-Ni alloys were selected since the most popular fcc HEA alloys contain both Fe and Ni as its constituents [1]. An additional third element, Mn or Al, was chosen. Mn is another element in the fcc HEA and Al gives a variety of phase separation [2].

The alloys Fe-35at.% Ni-10at.% Al and Fe-35at.% Ni-35at.%Mn were prepared by arc melting method. Hot forging and hot rolling were performed around 1300°C. Homogenization treatment was carried for 96h at 1150°C. Solution treatment was conducted for 1h at 1200°C. Aging treatments were performed at 400°C~800°C for various times. Atomic-scaled ordering and elements distribution behaviors were analyzed by Cs-corrected STEM and 3DAP.

Fe-35Ni-10Al alloys presented the peak hardening at 700°C and the hardness is slightly increased after aging at 500°C (Figure 1 (a)). Atomic structure of $L1_2$ ordered phases and elements slight fluctuations were presented in Figure 1 (b). Fe-35Ni-35Mn alloys showed the peak hardening after aging at 500°C (Figure 1 (c)). Atomic structure of $L1_0$ ordered phases were also detected after aging at 500°C for 96h in Figure 1 (d). Each particle is not distinguishable and composition fluctuation resembles spinodal decomposition. Furthermore, enrichment of Al/Mn and Ni and depletion of Fe at the same place are detected. High frequency of simultaneous depletion/enrichment of Al/Mn and Ni atoms also support co-segregation of Al/Mn and Ni atoms. Those results imply that fcc lattice is decomposed via spinodal ordering toward the formation of $L1_2$/$L1_0$ phases.

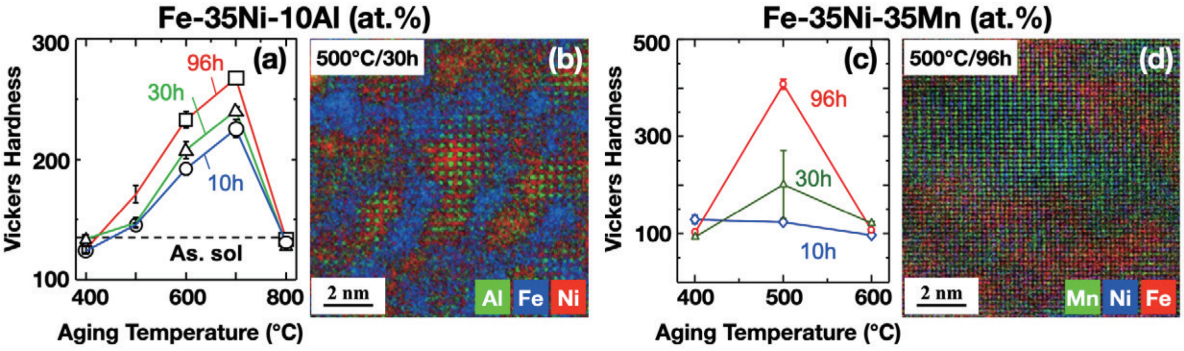

Figure 1. (a) Hardness after aging and (b) superposition of HAADF-STEM image and EDS mapping after aging at 500°C/30h of Fe-35Ni-10Al (at.%) alloys, (c) hardness after aging and (d) superposition of HAADF-STEM image and EDS mapping after aging at 500°C/96h of Fe-35Ni-35Mn (at.%) alloys.

[1] Cantor et al.: Mater. Sci. Eng. A, **375**, 213 (2004).
[2] He et al. : Acta Mater., **62**, 105 (2014).
[3] Sun et al.: JIM 2020 spring meeting abstract, S1.17.

Analysing ion conduction using persistent homology in lithium solid electrolytes

Joseph R. Nelson[1,2], Chris J. Pickard[1,2] and Kazuto Akagi[1,2]

1 WPI-Advanced Institute for Materials Research (WPI-AIMR), Tohoku University,
2-1-1 Katahira, Aoba-ku, Sendai, 980-8577 Japan
2 Department of Materials Science and Metallurgy, University of Cambridge,
27 Charles Babbage Rd, Cambridge CB3 0FS, United Kingdom

Topological data analysis (TDA) is a powerful technique in applied mathematics which allows insight into large data sets. In materials science in particular, persistent homology has been used in a number of applications, and has shed light on, for example, medium-range order in silica (SiO_2) glasses and in alloys [1], processes occurring in granular crystallization [2], and crazing phenomena (formation of a network of surface cracks) in polymers [3].

The examples [1-3] all feature systems with some type of disorder. Lithium solid electrolytes are ionic conductors with exceptionally high lithium mobility, and are sought after as materials for all-solid state batteries. These materials are expected to have disordered lithium ions. In this presentation, we use persistent homology to analyze fluorite-structured lithium oxide, Li_2O, a well-known lithium ion conductor. We show how this kind of TDA offers insight into ion conduction processes and conduction pathways.

[1] Y. Hiraoka, T. Nakamura, A. Hirata, E. G. Escolar, K. Matsue, and Y. Nishiura,
PNAS **113**, 7035-7040 (2016).
[2] M. Saadatfar, H. Takeuchi, V. Robins, N. Francois, and Y. Hiraoka,
Nat. Comm. **8**, 15082 (2017).
[3] T. Ichinomiya, I. Obayashi, and Y. Hiraoka,
Phys. Rev. E **95**, 012504 (2017).

Project Introduction of the Core Research Cluster for Materials Science

The Core Research Clusters for Materials Science
-Advanced Energy Material-

Shin-ichi Orimo[1,2] and Kazuaki Kisu[1]

[1] WPI-Advanced Institute for Materials Research (WPI-AIMR), Tohoku University
[2] Institute for Materials Research (IMR), Tohoku University

This project aims highly efficient energy conversion and storage systems for hydrogen energy based autonomous society. In this project, we systematically study the materials science relating to electricity generation from renewable energy using solar cell and spintronics materials, and that from hydrogen using high-performance fuel Cell materials, and also energy storage using some hydrogen Production/Storage Technologies and High-Safety Battery Materials (Fig.1). To realize the system and society, we are working on this project with all Tohoku university organizing by Prof. Orimo (AIMR・IMR), Prof. Samukawa (AIMR・IFS), Prof. Suito (AIMR), Prof. Mizuguchi (IMR), Prof. Amezawa (IMRAM), Prof. Honma (IMRAM), Prof. Tokumasu (IFS), Prof. Takamura (Graduate School of Engineering), Prof. Wadayama (GSES), and Prof. Yumoto (IMR). As recent achievements, we reported papers regarding lithium-ion solid electrolyte [1], proton conductors [2, 3], electrochemical CO2 reduction reaction [4], biocompatible batteries [5], and low-temperature plasma science and technology [6]. While continuing to look at applications for practical devices and systems, we will aim to develop leading-edge energy materials for energy generation, storage, conversion, and use.

[1]. S. Kim, H. Oguchi, N. Toyama, T. Sato, S. Takagi, T. Otomo, D. Arunkumar, N. Kuwata, J. Kawamura and S. I. Orimo, *Nat. Comm.*, **10**, 1081 (2019).
[2]. H. Takahashi, I. Yashima, K. Amezawa, K. Eguchi, H. Matsumoto, H. Takamura, S. Yamaguchi, *Chem. Mater.*, **29**, 1518 (2017).
[3]. T. Nakamura, S. Mizunuma, Y. Kimura, Y. Mikami, K. Yamauchi, T. Kuroha, N. Taniguchi, Y. Tsuji, Y. Okuyama and K. Amezawa, *J. Mater. Chem. A*, **6**, 15771 (2018).
[4]. N. Todoroki, H. Tei, H. Tsurumaki, T. Miyakawa, T. Inoue, T. Wadayama, *ACS Catalysis*, **9**, 1383 (2019).
[5]. S. Stauss and I. Honma, "Bull. Chen. Soc. Jpn. (Accounts & Reviews)", **91**, 492 (2018).
[6]. W. Mizubayashi, S. Noda, T. Nishi, A. Kikuchi, H. Ota, PH. Su, YM. Li, S. Samukawa, and K. Endo, *Appl. Phys. Express,* **10**, 26501 (2017).

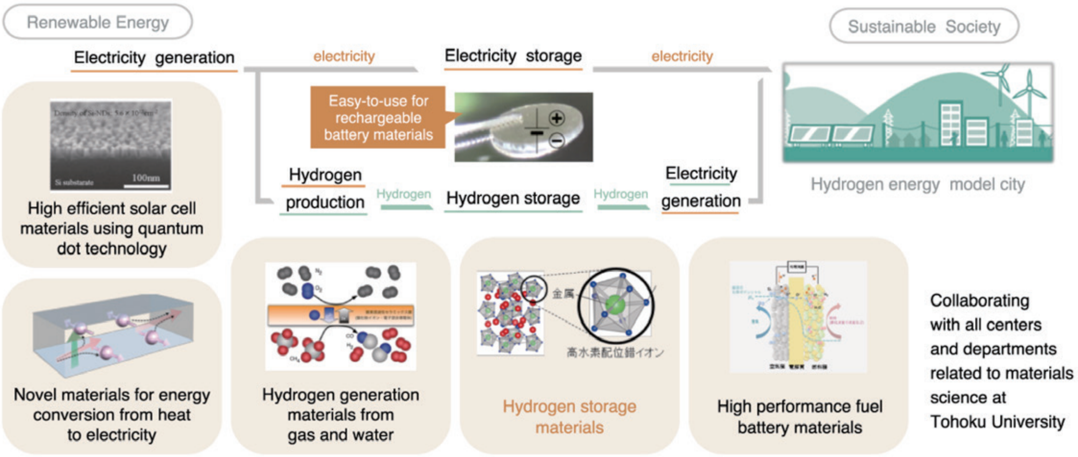

Figure 1. High-Efficient Energy Conversion & Storage Systems for Hydrogen-Energy Based Autonomous Society

P-46

Advanced Electronic Materials Project in Core Research Cluster of Material Science

Tomoteru Fukumura[1,2] and Hirofumi Oka[1]

[1] WPI-Advanced Institute for Materials Research (WPI-AIMR) and Core Research Cluster,
Tohoku University
[2] Department of Chemistry, Graduate School of Science, Tohoku University

In this project, new scientific principles and novel materials/properties/functionalities in advanced electronic materials are explored via state-of-the-art material synthesis and measurement techniques for bulk crystals, thin films, nanostructures, and heterointerfaces of inorganic/organic/hybrid compounds. Through these researches, we aim to develop new research fields as well as applications such as energy saving, generation, and storage.

Our recent achievements are concerned with elucidation of crystal growth dynamics of GaSb crystal [1], discovery of near-room temperature ferromagnetic semiconductor [2], thin film growth of quantum spin honeycomb IrO_6 structure [3], synthesis of hazardous element-free quantum dot phosphors [4], development of highly efficient n-type organic thermoelectric [5], electronic/ionic conduction switching in n-type organic semiconductor [6], and development of vacuum process for ionic liquid nano-gel film [7], in addition to construction of electronic phase diagram for ladder type iron based superconductor [8], enhancement of Curie temperature in 2D topological material [9], and transformation of conventional superconductor into topological superconductor [10].

This project members are currently composed of Profs. Yong P. Chen (WPI-AIMR/Purdue Univ.), Takafumi Sato (WPI-AIMR/Physics), Kenya Ohgushi (Physics), Kazuo Takimiya (Chemistry), Yuji Matsumoto (Applied Chemistry), Atsushi Tsukazaki (IMR), Kozo Fujiwara (IMR), Tomoyuki Akutagawa (IMRAM), Takahisa Omata (IMRAM), and Hiroshi Suito (WPI-AIMR). By strengthening intra-university network, advanced electronic materials are to be developed.

[1] K. Shiga, M. Kawano, K. Maeda, H. Morito, and K. Fujiwara, Scr. Mater. **168**, 56 (2019).
[2] T. Yamamoto, K. Kaminaga, D. Saito, D. Oka, and T. Fukumura, Appl. Phys. Lett. **117**, 052402 (2020).
[3] K. Miura, K. Fujiwara, K. Nakayama, R. Ishikawa, N. Shibata, and A. Tsukazaki, Commun. Mater. **1**, 55 (2020).
[4] S. Tsukuda and T. Omata, J. Soc. Inf. Disp. **28**, 680 (2020).
[5] Y. Wang and K. Takimiya, Adv. Mater. **32**, 2002060 (2020).
[6] H. Abe, A. Kawasaki, T. Takeda, N. Hoshino, W. Matsuda, S. Seki, and T. Akutagawa, ACS Appl. Mater. Interf. **12**, 37391 (2020).
[7] H. Watanabe, R. Takazawa, R. Takahaashi, S. Maruyama, and Y. Matsumoto, ACS Appl. Nano Mater., accepted (2020).
[8] S. Imaizumi, T. Aoyama, R. Kimura, K. Sasaki, Y. Nambu, M. Avdeev, Y. Hirata, Y. Ikemoto, T. Moriwaki, Y. Imai, and K. Ohgushi, Phys. Rev. B **102**, 035104 (2020).
[9] H. Idzuchi, A. E. Llacsahuanga Allcca, X. C. Pan, K. Tanigaki, and Y. P. Chen, Appl. Phys. Lett. **115**, 232403 (2019).
[10] C. X. Trang, N. Shimamura, K. Nakayama, S. Souma, K. Sugawara, I. Watanabe, K. Yamauchi, T. Oguchi, K. Segawa, T. Takahashi, Y. Ando, and T. Sato, Nature Commun. **11**, 159 (2020).

Next-generation medical diagnosis and treatment based on bio-hybrid materials and devices

Teng Ma[1,2], Ayumi Hirano-Iwata[1,3]

[1] WPI-Advanced Institute for Materials Research (WPI-AIMR), Tohoku University
[2] Core research cluster for materials, Tohoku University
[3] Research Institute of Electrical Communication (RIEC), Tohoku University

As one of the five core materials research clusters of the Designated National University programme in Tohoku University, the goal of the biomaterial research cluster is to achieve basic technologies in support of leading-edge medical care, and to create highly functional biomaterials and devices. By fusing biomaterials and nanotechnology, we seek to create bio-hybrid materials and devices equipped with advanced functions, which are not possible with biomaterials or artificial materials on their own, and to extend these to technologies for diagnosis and treatment. We will contribute to the realization of future medical care from the viewpoint of materials science by forming alliances with researchers in related areas in Japan and abroad, and through collaboration with mathematical science. We seek to create new functional biomaterials for future medical care with the aim of realizing SDG 3, “Good health and well-being,” as well as to contribute to SDG 9, “Industry, innovation and infrastructure,” and SDG 12, “Responsible consumption and production.”

In the past two years, we devoted to realize the former mentioned goal of the core research cluster of biomaterials and made significant progresses. For example, we developed totally organic stretchable electrochromic to realize skin patch for wound healing and drug dosing [1], fabricated honeycomb films by the breath figure technique and examine their applications in various fields [2], and investigated the impact of modular organization on dynamical richness in cortical networks and its effect on neural networks [3]. Toward the final goal of this programme, we are marshaling the comprehensive research capability of Tohoku University as a whole to develop unprecedented highly functional biomaterials.

[1] H. Kai, W. Suda, S. Yoshida, M. Nishizawa, Biosensors. Bioelectron. **123**, 108 (2019).
[2] H. Yabu, Sci. Technol. Adv. Mater. **19**, 803 (2018).
[3] H. Yamamoto, S. Moriya, K Ide, T. Hayakawa, H. Akima, S. Sato, S. Kubota, T. Tanii, M. Niwano, S. Teller, J. Soriano, A. Hirano-Iwata, Sci. Adv. **4**, eaau4914 (2018).

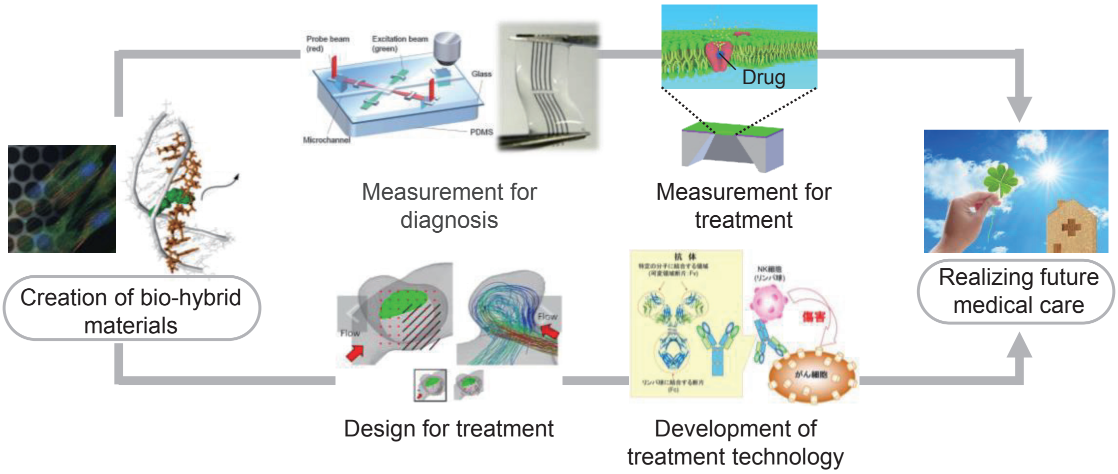

Fig. 1. The main goal and approaches of the core research cluster of biomaterials.

P-48

Strengthening by metastable solute clustering/precipitation in low-alloy nitrogen steels

Tadashi Furuhara[1,2], Mitsutaka Sato[2] and Goro Miyamoto[2, 3]

[1] Core Research Clusters for Materials Science, Tohoku University
[2] Institute for Materials Research, Tohoku University
[3] Research Center for Structural Materials, National Institute for Materials Science

Nitrogen (N), another major interstitial element other than carbon (C), can be utilized in strengthening of steels. When nitrogen has a strong attractive interaction with substitutional solute element in iron, precipitation of nanoscale solute clusters prior to alloy nitride precipitation, resulting in extraordinary large strengthening [1, 2]. Such metastable solute clusters are formed by phase separation coupled with ordering interstitial element (i) and substitutional element (s). However, the process of N-s solute cluster formation and transition to stable alloy nitride is not clearly understood in atomic scale. In our group, advanced nanoscale characterization techniques, such as Cs-corrected HAADF-STEM and 3-Dimenional Atom Probe, have been applied to examine precipitation behaviors in nitriding of ferritic steels or tempering of martensitic steels containing substitutional solute elements.

During the high-temperature tempering of Fe-0.3mass%N martensite with addition of Cr, Mo, or Mn by 1mass%, resistance to temper softening is clearly observed [3]. In particular, secondary hardening occurs with Cr or Mo addition. In early stage of tempering, monolayer metastable clusters are formed within the martensite as well as heterogeneous precipitation of stable B1-type alloy nitride at defects such as grain boundaries. As tempering is prolonged, the alloy cluster increase its thickness and changed to B1-type nitride, resulting in further increase of hardness. With Mn addition, B1-type Mn nitride was detected, which presumably changes to stable η-Mn_3N_2 having a larger hexagonal unit cell by thickening.

Large strengthening with nanosized precipitation of alloy nitrides, which are hard particles, implies operation of Ashby-Orowan dispersion strengthening mechanism. We are now examining the relationship between strengthening and metastable clustering in nitrided Fe-Ti alloys [4] and results obtained will be also discussed.

[1] T. Furuhara: Ferrum, 25(2020), pp. 506-512.
[2] G. Miyamoto et al., Mater. Sci. Technol. , 27(2011), 742.
[3] S. -W. Young et al: submitted to Acta Materialia, 2020.
[4] K. Itasaka et al.: CAMP-ISIJ, 33(2020), 587.

Overview of the High-Strength Materials Project

D. Demirskyi[1,2*], and K. Yoshimi[1,2]

[1] 1WPI-Advanced Institute for Materials Research (WPI-AIMR), Tohoku University
[2] Department of Materials Science and Engineering, Tohoku University

This contribution introduces the high-strength materials project which was initiated in the framework of the research activities of the Tohoku University.

We consider the advanced control over synthesis, evaluation, and testing technologies and their fusion with modeling as the main idea behind the project. Fulfilment of these ideas are required to enhance and pioneer new class of ultra-high temperature materials with improved strength and ultimate heat-resistant properties as result of flexible microstructure control.

Crucially, by extending interdisciplinary nature of the graduate school educational system with ideas, methods and technologies developed within the project, we attempt to establish a world premier research and educational center for high-strength materials drawing on the history and traditions of Tohoku University.

Currently, our joint efforts [1–3] are being devoted to fusion of ideas between metallurgy and ceramic science in order to create and characterize novel high-temperature alloys, high-temperature ceramics, and composites.

[1] D. Demirskyi, T.S. Suzuki, K. Yoshimi, O. Vasylkiv, Open Ceramics **2** 100015 (2020).
[2] H. Fukuyama, M. Ohtsuka, R. Sawada, H. Nakashima, Y. Ohishi, N. Hirao, M. Tanaka, K. Yoshimi, Materialia **13** 100867 (2020).
[3] W. Zhou, K. Kikuchi, N. Nomura, K. Yoshimi, A. Kawasaki, Materialia **10** 100655 (2020).

P-50

Endothelial Cells Distribution on the Stent Strut with Surface Treatment after the Flow Exposure

Zi Wang[1,2], Narendra Kurnia Putra[3], Kako Yamasaki[4], Naofumi Ohtsu[4], Hisatoshi Kobayashi[5], and Makoto Ohta[1]

[1]Institute of Fluid Science, Tohoku University, Japan
[2]Graduate School of Biomedical Engineering, Tohoku University, Japan
[3]Instrumentation and Control Research Group, Faculty of Industrial Technology, Institut Teknologi Bandung
[4]School of Earth, Energy and Environmental Engineering, Kitami Institute of Technology, Japan
[5]WPI-MANA, National Institute for Materials Science, Japan

With the rapid development of stent technology, stent implantation is now becoming one of the main treatments for cardiovascular diseases, such as stenosis and aneurysm [1]. However, the damage on the endothelial cells (ECs) layer could lead to chronical complications such as in-stent restenosis (ISR), neointimal hyperplasia and thrombosis are because of the intravascular blood flow disturbed by the structure of stent struts [2].

Previous studies found that ECs could response to the wall shear stress (WSS) sensitively by causing their morphological and physiological changes [3]. And ECs could suppress the neointima formation. Therefore, the clinical complications after stent deployment could be considered as the endothelial cells dysfunction around the stent struts or insufficient endothelialization.

In this study, to observe whether the surface treatment method could promote the endothelialization. Moreover, many researches were conducted under static state. Because ECs are sensitive to flow and WSS, ECs distribution on the stent strut with different surface treatment is necessary to investigate under the flow exposure.

A parallel flow chamber was designed to produce constant WSS on ECs monolayer to make the flow effect clear. A straight NiTi stent strut with surface treatment of collagen coating or anodizing was placed above the ECs layer. ECs were exposed to flow for 24 h under 2 Pa WSS condition, which is a normal condition in human. Then, ECs distribution on the surface of stent strut were observed. To understand the WSS distribution inside the flow chamber, computational fluid dynamics (CFD) simulation was used.

After 24 h exposure to the flow, ECs density on the downstream surface of stent strut is higher than the density on the upstream surface. ECs density on the stent strut with surface treatment is higher than the stent strut without any surface treatment. CFD results show the flow recirculation near the downstream side of stent strut.

The stent with surface treatment such as collagen coating and anodizing may could promote the process of endothelialization.

[1] W. S. Aronow and J. A. Mcclung, Translational Research in Coronary Artery Disease: Pathophysiology to Treatment (Academic Press, 2015).
[2] J. E. Cohen, J. M. Gomori, S. Moscovici, R. R. Leker, and E. Itshayek, Delayed Complications after Flow-Diverter Stenting: Reactive in-Stent Stenosis and Creeping Stents, Journal of Clinical Neuroscience 21, 1116 (2014).
[3] H. Anzai, T. Watanabe, X. Han, N. K. Putra, Z. Wang, H. Kobayashi, and M. Ohta, Endothelial Cell Distributions and Migration under Conditions of Flow Shear Stress around a Stent Wire, Technol Health Care 28, 345 (2020).

Evaluation and Sensing Project - support through collaboration between microscopic analysis, measurements and evaluation infrastructure-

Masami Terauchi*

* Institute of Multidisciplinary Research for Advanced Materials, Tohoku University.

To aid development of advanced materials going beyond traditional performance limits, we are aiming to form a measurement and evaluation infrastructure network around the core technologies of microscopic analysis and three-dimensional visualization.

Figure 1. Core members of Evaluation and Sensing Project.

In support of effective and efficient materials development, we will facilitate collaboration between researchers involved in development and application of analysis technologies, with microscopic analysis as core, and technical staff managing the shared equipment infrastructure for measurement and evaluation, while having coordinators match measurement and analysis technologies to the needs of those engaged in development of materials.

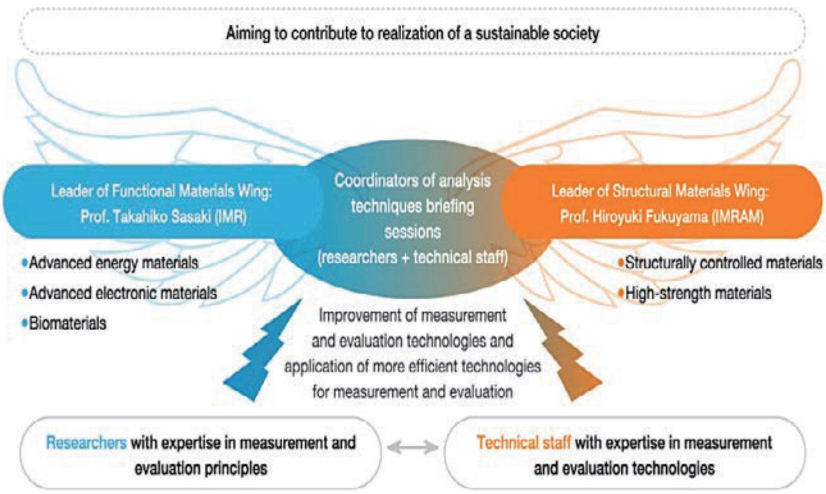

Figure 2. Evaluation and Sensing Project Concept.

Briefing sessions on analysis techniques and matching consultations have been held sometime according to demands of materials scientists [1]. Pushing the limit of an evaluation method [2] and collections on experimental data of new analysis applications as a data base are ongoing [3].

[1] H. Morito, S. Shibano, T. Yamada, K. Ikeda, M. Terauchi, R.V. Belosludov and H. Yamane, *Solid State Sciences* **120,** 106166-1-5 (2020).

[2] M. Terauchi, T. Hatano, M. Koike, A.S. Pirozhkov, H. Sasai, T. Nagano, M. Takakura and T. Murano, *IOP Conf. Series: Materials Science and Engineering* **891,** 012022-1-11 (2020).

[3] M. Terauchi, H. Takahashi, M. Takakura, T. Murano, and S. Koshiya, "*Handbook of Soft X-ray Emission Spectra ver.6.0*" (Aug. 2020).

P-52

Process Science Toward Design and Control of Nanomaterials

Akira Yoko[1], Gimyeong Seong[2], Takaaki Tomai[3], Tadafumi Adschiri*[1,2,3]

[1] WPI-Advanced Institute for Materials Research (WPI-AIMR), Tohoku University
[2] New Industry Creation Hatchery Center, Tohoku University, Sendai 980-8579, Japan
[3] Institute of Multidisciplinary Research for Advanced Materials, Sendai 980-8577, Japan,
*Email: tadafumi.ajiri.b1@tohoku.ac.jp

To achieve fine control and design of nanomaterials, processing of nanomaterials are focused on. Process science [1] toward the construction of platform for the nanomaterial engineering is introduced.

Nanoparticles behave as monomers like molecules in various processes, and it is crucial to establish "thermodynamics of nanoparticles" including the phase behavior (dispersive and aggregative) and transport property (diffusion, viscosity, thermal conductivity). Dispersive behavior of organic modified nanoparticles in organic solvents was studied using solubility parameter. Microscopic phenomenon such as incorporation of solvent molecules into organic modifier layer was found to affect the dispersibility of nanoparticles. Transport properties of nanoparticles such as diffusion, viscosity, and thermal conductivity was studied relating to its phase behavior. Structural formation such as nucleation, growth, and crystallization can be understood based on these fundamental properties and analogy of conventional molecular system.

Toward engineering of nanomaterials, unit operations of nanomaterials such as synthesis, separation, and assembly of nanoparticles should be considered as conventional chemical processes of molecular system. Progress of "Process Science" project is introduced in this presentation.

[1] A. Yoko, G. Seong, T. Tomai, T. Adschiri, Acc. Mater. Surf. Res. **5 (3)**, 43-50 (2020).

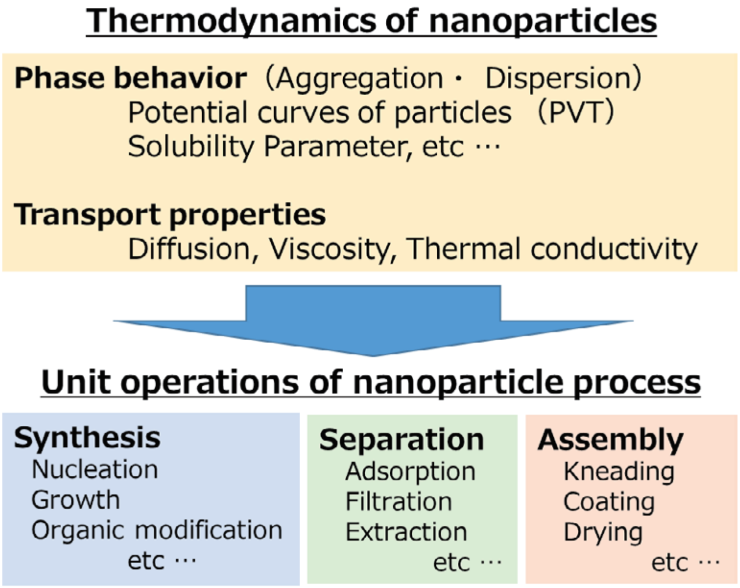

Fig. 1. Schematic diagram of "Process Science" project [1]

P-53

Formation of the global human resources development base - Introduction of International Joint Graduate Program in Materials Science -

K. Katagiri[1*], Y. Yoshioka[1] and K. Oikawa[1]

[1] International Joint Graduate Program in Materials Science, Tohoku University

The aim of our group will develop the global human resources development base in the Core Research Cluster for Materials Science together with the International Joint Graduate Program in Materials Science (GP-MS) as shown in Fig. 1. In this presentation, we will introduce about the details of GP-MS. GP-MS program offers opportunities to study leading research and technologies in the world in order to develop researchers and engineers capable of leading innovations in global material science and engaging powerfully with the international community. Students in this program will take 4 main subjects; Material Science International, Materials Science Practice, Practical language skills and Materials Science Special Seminar which give them valuable learning and experiences. This program also has various assistance, such as financial support and support for travelling overseas, so that students can concentrate on their studies.

Fig.1 The structure of Education and Human Resources development in Materials science

POSTER ABSTRACTS:
GP-MS

Properties of Primitive Membrane and Optimization of Biopolymers in Life Evolution

Akiko Baba[1*], Ulf Olsson[2] and Masayuki Imai[1]

[1] Department of Physics, Tohoku University
[2]Depertment of Physical Chemistry, Lund University

Fatty acid, one of simplest component of cellular membrane, is thought to be a key material bridging material world and biological world. In this study, we show various patterns of growth of fatty acid vesicle, which is cellular membrane-like spherical structure, under continuous supply of material resources [2]. A life is a system that (i) taking in material and energy sources from environment, (ii) synthesizing proteins based on genetic information molecules and (iii) replicating the information molecules and biological membrane using functional protein. Concerning from non-living molecular assemblies to cellular life, **interplay between biopolymers** such as proteins and information molecules and **vesicles** that are container of biopolymers is essence. In the prebiotic era, it is likely that oligonucleotides or oligopeptides encourage growth and division of primitive fatty acid vesicles. **Fatty acid** is a carboxylic acid with a long hydrocarbon chain, and is thought to have worked as membrane in the birth of life. Decanoic acid, one of fatty acid, stably forms vesicles around at pH 7 in aqueous solution [3]. In previous researches, it has been reported that certain amino acids and bases bind to decanoic acid, and enhance stability of vesicles against salt [4][5]. However, the properties of fatty acid as vesicle and interplay between fatty acid and prebiotic materials in prebiotic self-reproduction system are still unclear.

Therefore, we investigated **the effect of primitive molecule**s on the growth of vesicle, and then **clarified them by the growth rate**. The vesicle growth rate probably depends on the sequence of nucleotides or amino acids, which determine “fitness landscape” toward the cellular life (**Fig.1**). Our results imply that gene and protein expression might have been a result of s**elective linked sequence** and polymerization degree of bases and amino acids toward superior catalyst to the growth.

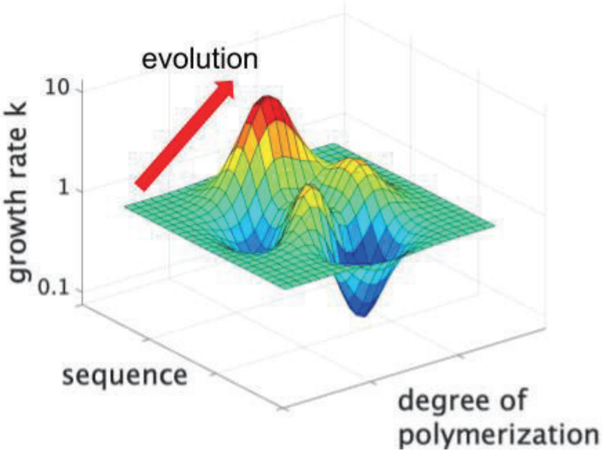

Fig. 1. Illustration of Fitness Landscape

[2] T.F. Zhu, and J. W. Szostak, J. Am. Chem. Soc. **131**, 15, 5705-5713 (2009).
[3] R. Wick, P Walde, and P.L. Luisi, J. Am. Chem. Soc. **117** , 1435-1436 (1995).
[4] C.E. Cornell, R. Black, M. Xue, H.E. Litz, A. Ramsay, M. Gordon, A. Mileant, Z.R. Cohen, J.A. Williams, K.K. Lee, G.P. Drobny, and S.L. Keller, Proc. Natl. Acad. Sci. U.S.A. **116**, 17239-17244 (2019).
[5] R.A. Black, M.C. Blosser, B.L. Stottrup, R. Tavakley, D.W. Deamer, and S.L. Keller, Proc. Natl. Acad. Sci. U.S.A. **110**, 13272-13276 (2013).

P-56

Development of Microfluidic Device for Planar Assembly of Giant Vesicles

T. Chiba[1], H. Sugiyama[2], T. Toyota[2] and M. Imai[1]

[1] Graduate School of Science, Tohoku University
[2] Graduate School of Arts and Science, The University of Tokyo

In multi-cellular organism, cellular membrane morphology plays a key role that connects between cell shape mechanics and cellular functions. To extract minimal essence of the relationship, we have investigated morphology of the giant vesicle (GV: shell structure composed of lipid bilayer) assemblies as a model of multi-cellular organism [1, 2]. The GV doublet, the simplest GV assembly, shows characteristic morphology transitions by varying the volume to area ratio and adhesion strength. In this study, we extend this result to larger-scale GV assemblies composed of tens GVs. For this purpose, we have been developing a microfluidic device that extracts GVs having the same size from polydisperse mother GV suspension and forms planar and monodisperse GV assemblies. Design of our microfluidic device is based on a deterministic lateral displacement technique developed by Huang's group. [3, 4]. In preliminary experiments, we have succeeded in forming the planar assemblies composed of ~ 20 GVs with a 20 μm radius. This is a first step to construct the biomimetic platform for multi-cellular organism.

[1] Y. Sakuma, M. Imai, M. Yanagisawa and S. Komura, Eur. Phys. J. E, **25**, 403-413 (2008)
[2] K. Murakami, R. Ebihara, T. Kono, T. Chiba, Y. Sakuma, P. Ziherl and M. Imai, Biophys. J. (2020) DOI: https://doi.org/10.1016/j.bpj.2020.09.030
[3] L. R. Huang, E. C. Cox, R. H. Austin and J. C. Sturm, Science., **304**, 987-990 (2004)
[4] Y. Kazayama, T. Teshima, T. Toshihisa, S. Takeuchi and T. Taro, Anal. Chem., **88**, 1111-1116 (2016)

Promotion of DNA Synthesis by Liposome Surface

Yuto Hachiya[1*], Hikaru Hatori[1] , Shoichi Toyabe[2] Steen Rasmussen[3] and Masayuki Imai[1]

[1]Department of Physics, Tohoku University*,
[2]Department of Applied Physics, Tohoku University
[3]Department of Physics, Chemistry and Pharmacy, University of South Denmark
6-3 Aoba, Aramaki, Aoba, Sendai 980-8578, Japan

DNA is a molecule which can retain information by 4 kinds of bases and accurate DNA synthesis is very important for many fields. Templated ligation reaction is the connection of two DNAs which bind to one DNA called template strand and base sequences can be produced exactly by this reaction. But the reaction proceeds ineffectively in bulk because each DNA diffuses 3-dimensionally in random direction.

To solve this problem, We propose the way to accelerate templated ligation reaction of DNA which have hydrophobic segment on liposome surface. Liposome is the spherical lipid bilayer like cell membrane and on liposome surface, hydrophobic molecules aggregate and diffuse 2-dimensionally due to the high fluidity of liposome surface. So it is expected that hydrophobically-modified DNAs become dense and collide each other frequently on liposome surface and reaction is promoted (Fig.1). To confirm this hypothesis, we estimated the rate of DNA synthesis on liposome surface by fluorescent dye and compared it to the mathematical model we made. As a result, it was unveiled that liposome surface promotes the DNA synthesis highly.

This method is very effective and reasonable way to synthesize DNA and even make it possible to create new material. In fact, DNA-liposome complex is used as a nanomaterial in bioengineering, pharmacy and so on and liposome performs various functions depending on the functional molecules on it [1,2]. Therefore, liposome can be functionalized by synthesizing chemically-modified DNA on the surface on demand.

This strategy of DNA synthesis is expected to be applied to various fields.

[1] B.Zhao, Q Tian, Y.Bagheri and Mingxu You, Curr. Opin. Biotechnol. 13:76-83 (2020)
[2] Philipp M.G. Löffler, Oliver Ries, Alexander Rabe, Anders H. Okholm, Rasmus P. Thomsen, Jørgen Kjems, Stefa Vogel, Angewandte Chemie, 56-43(2017)

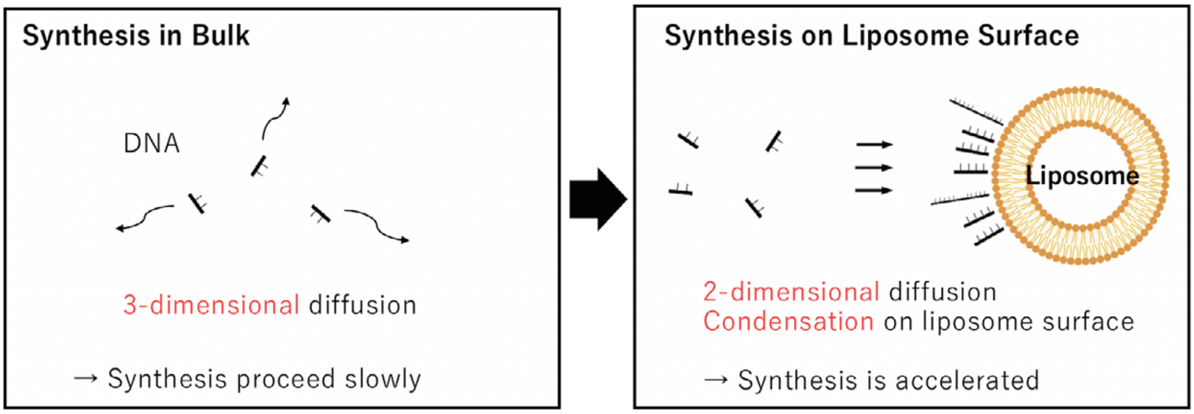

Fig.1. Comparison of DNA synthesis between in bulk and on liposome surface

P-58

Phase stabilities of magnesiated MnO_2 polymorphs as cathodes for magnesium rechargeable batteries

Takuya Hatakeyama[1], Hongyi Li[1], Norihiko L. Okamoto[1] and Tetsu Ichitsubo[1]
[1] *Institute for Materials Research, Tohoku University, Sendai 980-8577, Japan*

Magnesium rechargeable batteries that employs magnesium metal anodes are potential alternatives to currently available lithium-ion batteries. The major advantages of magnesium metal anodes are derived from its natural abundance, high capacity, and non-dendritic nature. Abundance of magnesium in earth crust ensures low material cost. Magnesium metal anode processes a high theoretical capacity (2205 mAh/g) that is greater than that of lithium-inserted graphite (339 mAh/g) and comparable to that of lithium metal (3860 mAh/g). Additionally, magnesium metal tends to be plated uniformly during electrodeposition, thereby ensuring safe operation, in contrast to Li metal that easily forms hazardous dendrites.

One of huge challenges in developing magnesium rechargeable battery is to establish high capacity cathode materials. Capacity of 3d-transition-metal-oxide cathodes comes to be strongly influenced by slow kinetics of magnesium intercalation. To obtain inherent capacity, the intercalation kinetics must be promoted by reducing the particle size of cathode materials and elevating cell temperature, etc. Moreover, even if the kinetics is improved, capacity of most oxide cathodes gradually fades in several cycles of magnesium intercalation/deintercalation. Such a capacity fade implies irreversible change of cathode material caused by magnesium intercalation. Deep understanding of the mechanism of irreversible process is essential to prevent capacity fade.

The stability of Mg-extracted (i.e., defective) crystal structure is a key factor to enable reversible magnesiation cycling. According to our previous research, which investigated the possibility of magnesium deintercalation from spinel family $MgTM_2O_4$ (TM= Co, Mn, Fe, Cr), magnesium deintercalation from $MgTM_2O_4$ (redox of TM^{3+}/TM^{4+}) can be markedly observed in the Mn spinel. This result agrees with the fact that Mg-deintercalated structure Mn_2O_4 (λ-MnO_2) is relatively stable compared to the other transitional metals. In fact, several stable polymorphic structures known for MnO_2, while stable dioxides of Co, Fe, Cr are difficult to be produced.

In this study, phase stability of magnesium-intercalated polymorphic MnO_2 structure ($\alpha, \beta, \gamma, \delta$ and λ) has been investigated experimentally and theoretically. The present electrochemical experiments demonstrate that α and γ type structures allow topotactic magnesium intercalation up to $x = 0.16$ in Mg_xMnO_2, corresponding to a capacity of 100 mAh/g. X-ray characterization suggests that capacity fade mechanism lies in over-magnesiation that induces transformation from original MnO_2 framework into rocksalt-structured $Mg_{\sim 0.5}MnO_2$. This fundamental understanding of phase stability will advance further optimization of MnO_2-based cathode for magnesium batteries.

[1] T. Hatakeyama, N. L. Okamoto, K. Shimokawa, H. Li, A. Nakao, Y. Uchimoto, H. Tanimura, T. Kawaguchi and T. Ichitsubo, Phys. Chem. Chem. Phys., 2019, 21, 23749–23757.

[2] S. Okamoto, T. Ichitsubo, T. Kawaguchi, Y. Kumagai, F. Oba, S. Yagi, K. Shimokawa, N. Goto, T. Doi and E. Matsubara, Adv. Sci., 2015, 2, 1500072

P-59

Effect of Minor alloying elements on Microstructural and mechanical properties changes in Ti-Fe Alloy

YeonBeom Jeong[1*] and Hidemi Kato[2]

[1]Graduate school of engineering, Tohoku University, 980-8577, Sendai, Japan
[2]Institute for Materials Research, Tohoku University, 980-8577, Sendai, Japan

Generally, eutectic alloys show very high yield strength because of their large number of interfaces [1]. However, they offer limited plasticity at room temperature. To improve plasticity, the development of ultrafine eutectic alloys containing micron-scale dendrites in the lamellar structure has been highlighted. The primary mechanism for improving the plasticity of these alloys is the rotational motion of the eutectic colony. So, these alloys effectively diminish the localization of the shear stress, thus improving the plasticity. Similarly, the formation of chemical heterogeneity in the eutectic alloy increases the ductility because the formation of different constituent phases in the eutectic colony boundaries prevents catastrophic failure. In this study, the microstructure alternation and change of mechanical property are investigated as adding Bi-In eutectic alloy in the Ti65Fe35 hypereutectic alloy. With the addition of Bi-In, the microstructures of $(Ti_{65}Fe_{35})_{100-x}(Bi_{53}In_{47})_x$ (X= 0, 1, 3, 5, 7) alloys exhibit the dendritic phases having different compositions in the eutectic matrix. Especially in case of the addition of 3at. % (Bi-In), the TiFe dendritic phase changes to the β-Ti dendritic phase. This phase deformation leads to implementing the plasticity about four times compared with non-added alloy. To identify the evolution of the dendritic phase's chemical composition, more exactly EDX analysis was conducted. Also, to reveal the reason for enhancing the plasticity fractured surfaced was measured.

[1] Y. B. Jeong et. al. Mater. Des. 175 107814 (2019)

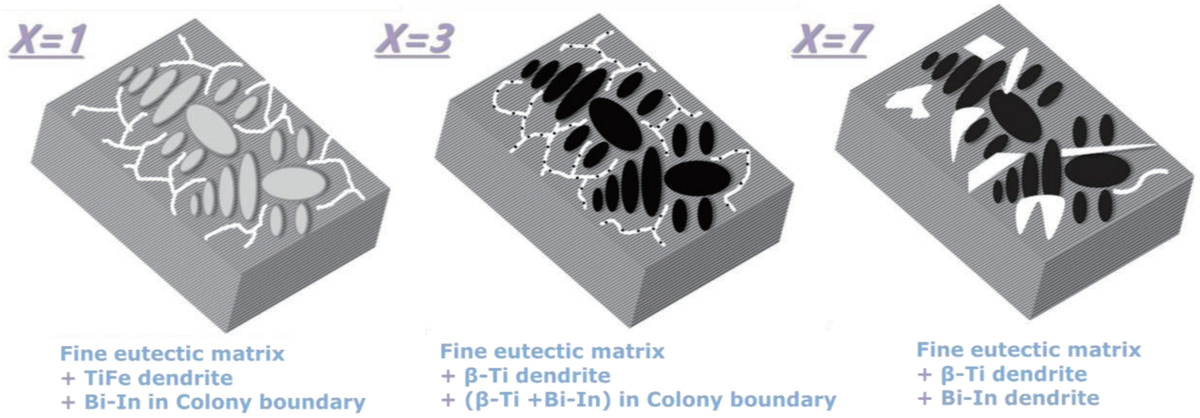

Fig. 1. Influence of (BiIn) on TiFe fine eutectic alloy

P-60

Revealing the Reaction Mechanism of Li-O_2 Battery by *in-situ* Surface-Enhanced Raman Scattering (SERS)

Koki KANNARI, Aimin GE, Ken-ichi INOUE and Shen YE

Department of Chemistry, Graduate School of Science, Tohoku University

Lithium-Oxygen battery (Li-O_2 battery) has attracted much research attention due to its high theoretical specific energy density, which is much higher than that of practical lithium-ion batteries [1]. Therefore, Li-O_2 battery is expected as one of the next-generation secondary batteries for electric vehicle's power source.

The main electrode reactions of Li-O_2 battery are shown in below. On the cathode surface, oxygen reduction reaction (ORR) occurs during the discharging process, and oxygen evolution reaction (OER) proceeds in the charging process.

Anode : $Li \rightleftarrows Li^+ + e^-$ (1)

Cathode : $O_2 + 2Li^+ + 2e^- \rightleftarrows Li_2O_2$ (2)

Li-O_2 battery is promising but still has many problems. Especially, high charge over-potential on the cathode, which causes electrolyte decomposition, becomes a bottleneck in Li-O_2 battery development. However, the origin of the problem is still unclear because understanding the reaction mechanism on the cathode surface is not enough. In the present study, surface-enhanced Raman scattering (SERS) has been employed to investigate the ORR/OER on a cathode surface made of nanostructured gold materials. SERS measurement enables us to selectively observe the species on the surface during the electrode reactions [2]. Combining SERS technique with cyclic voltammetry measurements, the reaction mechanisms of ORR / OER process on the cathode surface were investigated *in situ* to make a strategy to understand the origin for the high charge over-potential.

The *in-situ* SERS measurements show that the lithium peroxide (Li_2O_2) is formed on the cathode as the cathodic currents flows in the discharge process. The SERS signals for the Li_2O_2 quickly disappear as soon as the anodic current starts to flow, although the anodic current still flows until the potential becomes higher than 4.0 V (vs. Li^+/Li). Based on the observation, it is reasonable to conclude that Li_2O_2 is initially decomposed from the interface between Li_2O_2 and the cathode surface (Figure 1). A higher charge over-potential is required to decompose Li_2O_2 remaining away from the electrode surface. Detailed discussions will be given during the presentation.

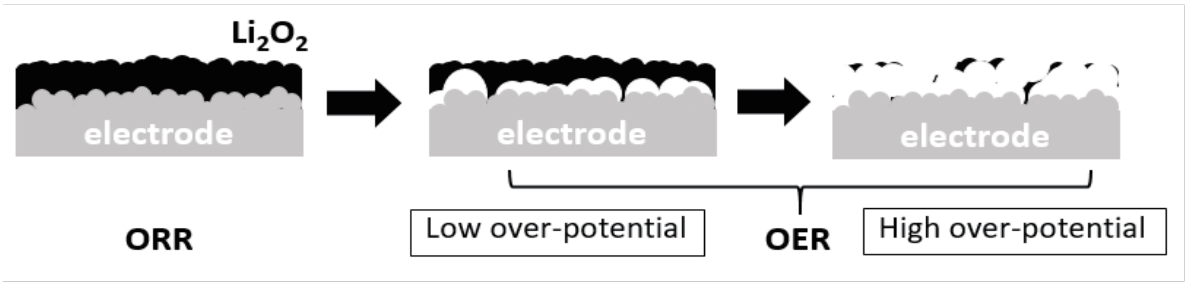

Fig. 1. Schematics of the reaction mechanism for OER during charging process

[1] D. Aurbach, B.D. McCloskey, L.F. Nazar, and P.G. Bruce *Nat. Energy*, **2016**, *1*, 16128
[2] X.-B. Han, K. Kannari, S. Ye *Curr. Opin. Electrochem.*, 2019, 17, 174

P-61

High-Pressure Synthesis and Defect Chemistry of Hydrated Ba-Sc-Based Perovskites

Hiroaki Kawamori[1], Itaru Oikawa[1] and Hitoshi Takamura[1]

[1] Department of Materials Science, Tohoku University,
hiroaki.kawamori.s2@dc.tohoku.ac.jp

Hydrogen energy has been highly demanded for sustainable society. Hydrogen generation, storage, transportation, and conversion to electricity are keys for its practical application. Proton (H^+)-conducting solid-oxide fuel cells have high energy conversion efficiency. Many efforts have been made to develop proton-conducting electrolytes. Acceptor-doped perovskite-type oxides (ABO_3) are expected as the electrolyte because of their high proton conductivity. Acceptor-ions are charge compensated by oxygen vacancies and protons depending on atmosphere, especially relative water vapor pressure. Increase in the proton concentration is demanded to achieve high conductivity.

In this study, Ba-Sc-oxide was focused on. It has oxygen-deficient perovskite structure under conventional synthesis condition. Although it has large amount of oxygen vacancies for hydration reaction, the reports of hydrated Ba-Sc-oxide are limited [1]. Now, we synthesized hydrated Ba-Sc-oxide by using high-pressure method and investigated its structure, composition and proton concentration.

$Ba(OH)_2 \cdot H_2O$ and Sc_2O_3 are heated up to 1200°C under 8 GPa within Au sealant. The obtained sample had orthorhombic perovskite-type structure with the ratio Ba:Sc of 3:2. This implies that a large amount of Sc vacancies are formed on *B* sites. The weight change by dehydration that indicates its proton concentration is shown in Fig. 1. The large weight loss can be hardly discussed without taking Sc vacancies into account. It showed good agreement with the amount of protons that are required for compensation of Sc vacancies. The *B*-cation deficient hydrous perovskite was also obtained from hydrogarnet-type $Ba_3Sc_2(OH)_{12}$ whose vacant cation sites are known to be compensated by protons. Their structural relationship is shown in Fig. 2. The compensation mechanism of Sc vacancies in perovskite structure seems to resemble that of vacant cation site in hydrogarnets.

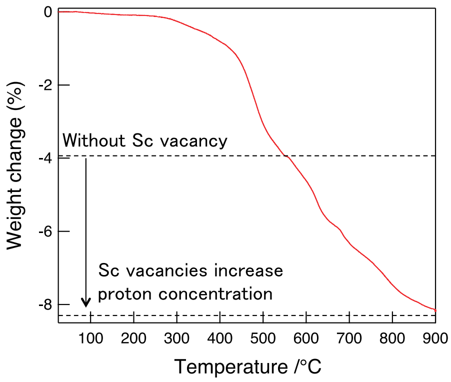

Fig. 2 Weight change of Ba-Sc based *B*-cation deficient hydrous perovskite by dehydration.

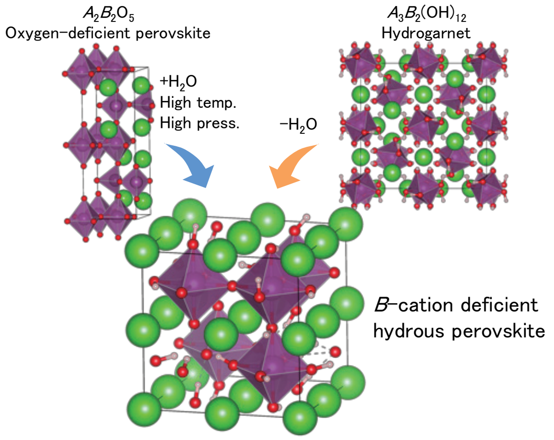

Fig. 2 Crystal structures of *B*-cation deficient hydrous perovskite and related compounds.

[1] Rinlee B. Cervera, Shogo Miyoshi, Yukiko Oyama, Youssef E. Elammari, Takehiko Yagi, and Shu Yamaguchi, Chem. Mater. **25**, 1483–1489 (2013).

P-62

Mixed Conduction and Local Structural Analysis of Y and Al co-doped $BaZrO_3$

Koya Kimura[1*], Itaru Oikawa[1] and Hitoshi Takamura[1]

[1] Department of Metallurgy, Materials Science and Materials Processing, Tohoku University

Mixed proton-hole conductor is expected to be a cathode material for proton conducting solid oxide fuel cells (PCFCs). Accepter-doped $BaZrO_3$ has oxygen vacancies that can be either proton defects in wet condition or holes in oxydizing condition. Mixed proton-hole conduction is achieved when both proton and hole concentration are high. Takahashi *et al.* investigated the relationship between local structural distortion and hydration energy of accepter-doped $BaZrO_3$[1]. It was suggested that large Y^{3+} prefers the compensation by proton defects; on the other hand, small Al^{3+} does holes or oxygen vacancies. Thus, by doping Y and Al into $BaZrO_3$, we expect to achieve mixed proton-hole conduction. In this study, the local structure around dopants, especially around Al, is focused on. Nuclear magnetic resonance (NMR) spectroscopy is a powerful tool to investigate the local structure around nuclei. We can evaluate the coordination number of oxygen around Al, and it can be converted to the amount of oxygen vacancies. We therefore evaluated the defect equilibrium of Y and Al co-doped $BaZrO_3$ from the view point of local structure, and its mixed conductivity.

$BaZr_{0.8}Y_{0.2-x}Al_xO_{3-\delta}$ (BZYA) was prepared by solid state reaction method. Proton concentration was evaluated by thermogravimetric analysis at 350ºC. AC impedance measurement was performed to evaluate the conductivity of BAYA in dry Ar or wet Ar. Proton transport number was measured at 600ºC by using water vapor concentration cell. ^{27}Al Magic-Angle Spinning (MAS) NMR was performed to investigate the configuration around Al. Proton concentration of BZY10A10, BZY15A5 was 0.6 mol%, 1.8 mol% (Fig. 1). They were much smaller than that of BZY20, 18.6 mol%. This indicates that Al substitution led to decrease in proton concentration. Meanwhile, BZYA showed proton conduction and high proton transport number, 0.84. This is due to the unique oxygen configuration around Al. In this poster session, we discuss the local structure around Al from NMR spectra (Fig. 2) and its effect on proton concentration and mixed conduction.

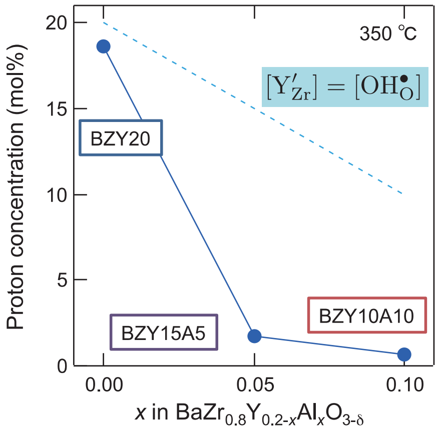

Fig. 1 Proton concentration of BZYA at 350ºC

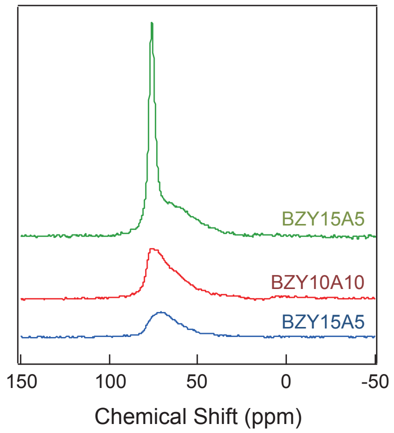

Fig. 2 ^{27}Al MAS NMR spectra of BZYA

[1] H. Takahashi *et al.*, *Chem. Mater.* **29**, (2017) 1518.

Effect of Anodizing Time on Galvanic Corrosion Resistance on Localized Corrosion Initiated at IMP of Al Alloys

Takumi Kosaba[1*], Izumi Muto[1] and Yu Sugawara[1]

[1]Department of Materials Science, Tohoku University

As global warming become serious problems, the demand for weight reduction of automobiles is increasing these days: then the multimaterial structures, which is one of the methods to achieve the weight reduction, attract great interest. Because of low cost and high stiffness, Al alloys and steels joints are especially anticipated to utilize in the structures. However, galvanic corrosion is expected to occur on anode (less noble potential metals) such as Al alloys when dissimilar metals are contacted.

In our previous research, the effect of anodizing on galvanic corrosion resistance of pure Al coupled to pure Fe or Type 430 stainless steel was studied, and it was obtained that more than 400 nm thickness of anodic oxide film is needed to prevent galvanic corrosion damage of pure Al coupled to pure iron. It was expected that thicker anodic oxide film was needed to enhance galvanic corrosion resistance for Al alloys because Al alloys has lower corrosion resistance than pure Al due to existence of intermetallic particles. The intermetallic particles containing Fe or Cu increase the mechanical strength of Al alloys. In contrast, the boundary between Al matrix and the particles is likely to become initiation sites of localized corrosion on Al alloys because electrode potential of the particles is higher than that of Al matrix. Consequently, it is needed to control the anodic oxide film on Al matrix and intermetallic particles to prevent galvanic corrosion of Al alloys.

In this study, we investigated the effect of anodizing time on galvanic corrosion resistance of Al alloys coupled to pure Fe or Type 430 stainless steel in diluted synthetic seawater. This electrolyte is suitable for simulating the corrosion behavior in atmospheric environments. AA5083 (Al alloy containing Mg) was used as the specimens. In this alloy, $Al_6(Fe, Mn)$ and Mg_2Si particles were contained as intermetallic particles. The galvanic corrosion tests were carried out by zero resistance ammeter techniques. Anodizing was performed in sulfuric acid in applied voltage of 16 V for 18 to 180 s. The relationship between galvanic corrosion resistance of A5083 and the thickness of anodic oxide films was determined.

P-64

Giant Vesicle of AOT: New Material for Soft Microscale Compartment and its Dynamic Property

Minoru Kurisu[1*], Ryosuke Katayama[1], Yuya Takashima[1], Peter Walde[2] and Masayuki Imai[1]

[1] Department of Physics, Tohoku University
[2] Department of Materials, ETH Zürich

Microscale vesicles composed of amphiphilic molecules have attracted much interdisciplinary interests as promising soft materials especially in the field of molecular robotics, microreactor and artificial cell research. Here we report the promising properties of AOT giant vesicles for these research fields in comparison with conventional vesicles composed of phospholipid and fatty acid. In aqueous solution, amphiphilic molecules such as phospholipid and fatty acid are known to form **vesicle** (cell membrane-like closed spherical membrane) spontaneously. These vesicles can separate aqueous solution into two regions by membrane: small volume of solution inside the membranes and large volume of bulk solution outside the membranes. Therefore, vesicles have attracted much interests in the fields of microscale chemistry and engineering. For example, one can realize localized chemical reaction inside vesicle. Another example is molecular robot that load functional molecules such as protein, enzyme and molecular motor on vesicles. For those applications of vesicles, the physical and chemical properties of vesicles such as membrane elasticity, permeability and stability deriving from membrane-forming molecules are necessary. AOT, i.e., sodium bis-(2-ethylhexyl) sulfosuccinate, is amphiphilic molecule, and we invented fabrication method of 10-20 μm size giant vesicles of AOT. Critical vesicle concentration of AOT is dependent on temperature and concentration of sodium ion, and utilizing these properties, it is possible to fabricate AOT giant vesicle with simpler way than gentle hydration method. In addition, giant vesicle of AOT might have large potential for application that requires membrane deformation. In comparison with widely used phospholipid giant vesicle, AOT membrane is thinner and rougher in molecular scale [1], which enables higher permeability and following osmotic swelling (**Fig.1**). Furthermore, coupled with a vesicle membrane surface-confined polymerization reaction, AOT based giant vesicles show growth/division cycles as we previously reported (**Fig.2**) [2]. In this poster, we show how to fabricate giant vesicle of AOT and the recent results of a series of investigations on physical and chemical properties of AOT membrane. Our investigations imply that AOT giant vesicles have higher transmembrane permeability even for relatively large molecules such as glucose, and concerning the deformation properties, AOT vesicles might be promising soft materials for molecular robot and artificial cell.

[1] K. Junker et. al., *ACS Catalysis*, **4**, 10 (2014)
[2] M. Kurisu et. al., *Communications Chemistry,* **2,** 117 (2019).

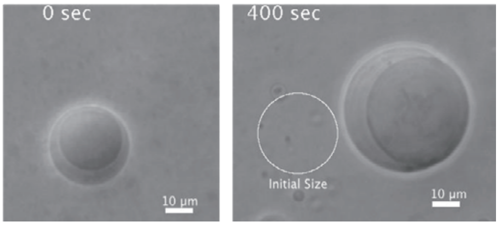

Fig. 1. Swelling of AOT vesicles caused by uptake of water.

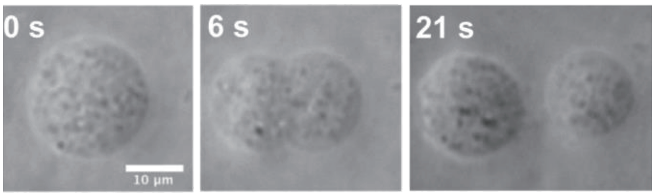

Fig. 2. Division of AOT base giant vesicles.

P-65

Synthesis and n-type thermoelectric application of pyranylidene-substituted heteroaromatics with extremely high electron-donating ability

Takaya Matsuo[1], Kohsuke Kawabata[1,2] and Kazuo Takimiya[1,2]

[1]Department of Chemistry, Graduate School of Science, Tohoku University
[2]RIKEN Center for Emergent Matter Science

Thermoelectric conversion is a technology that can convert unused thermal energy to electric power. Although inorganic thermoelectric materials exhibit high device performance and robustness, organic counterparts offer advantages such as low cost, large-area deposition, high elasticity, material abundance, and low weight.

In thermoelectric device, doping is a key process to optimize the thermoelectric conversion efficiency. In the prototypical n-type dopants (e.g. *N*-DMBI), a doping process is composed of the initial thermal cleavage of C-H bond to produce a radical species, which then donates electron from its SOMO (Fig. 1a) [1]. However, the radical species may react with host materials undesirably. On the other hand, electron donation from HOMO of closed-shell molecules dose not accompany such undesired reactions. However, it is challenging to realize a compound with HOMO energy levels higher than the LUMO energy levels of commonly used n-type organic semiconductors. Therefore, a design strategy for increasing the HOMO energy levels is a key to develop superior dopants to improve thermoelectric properties.

In this context, pyranylidene-substituted heteroaromatics, which have been previously reported to have high-lying HOMO energy levels, is a promising platform for n-type dopants [2]. In this study, to further improve electron-donating ability, we introduced electron-donating groups, namely, methoxy and dimethylamino groups, on the pyranylidene rings, and thus developed **1a**, **1b**, **2a** and **2b** (Fig. 1b) are examined as n-type dopants on N2200, which is one of representative host materials in n-type organic thermoelectric devices.

The HOMO energy levels of **1a**-**2b** calculated by DFT methods are approximately −3.7 eV below the vacuum level, which suggests that the compounds have extremely high electron-donating ability. Upon doping with **1a-2b**, the electrical conductivity of doped N2200s were increased, and the Seebeck-coefficient measurement confirmed that they show n-type thermoelectric performance. In this presentation we also report the power factors of doped N-2200 depending on the dopants (**1a-2b**, and *N*-DMBI) and their concentration.

[1] P. Wei, J. H. Oh, G. Dong, and Z. Bao, *J. Am. Chem. Soc.* **132**, 8852 (2010).
[2] K. Takimiya, T. Otsubo, F. Ogura, H. Ashitaka, K, Morita, and T. Suehiro, *Chem. Lett.* **23**, 255 (1994).

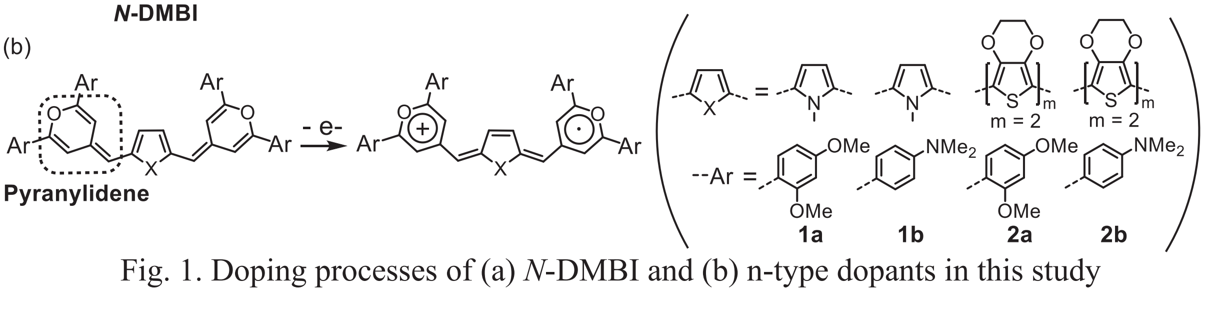

Fig. 1. Doping processes of (a) *N*-DMBI and (b) n-type dopants in this study

Anomalous magnetoresistance of antiferromagnetic semiconductor $BaMn_2Bi_2$

Takuma Ogasawara[1*], Kim-Khuong Huynh[2] and Katsumi Tanigaki[3]

[1] Dept. of Phys., Grad. School of Sci., Tohoku Univ.*, Miyagi, Japan
[2]WPI-Advanced Institute for Materials Research (WPI-AIMR), Tohoku Univ., Miyagi, Japan
[3]Beijing Academy of Quantum Information Sciences (BAQIS), Beijing, China

Recently, the antiferromagnetic (AFM) materials have been studied intensly due to the potential for spintronics material as well as physical viewpoint because AFM device resolve the vulnerability issue of the conventional spintronics memory device consisted of ferromagnet against strong magnetic field and stray field. Simultaneosly, such a robustness makes it difficult to manipulate and read the magnetic ordering of AFM. Although some successful studies reported that the AFM ordering was manipulated via inverse spin galvanic effect and read by anisotropic magnetoresistance [1,2], they are still far from application due to the fewness of candidate materials due to the requirement of extraordinal symmetry, odd for both space inversion and time reversal operation, and requirement for high current-density. Further research for sphisticated physical phenomena in antiferromagnetic materials is needed for more progress.

In this poster, we present the anomalous magnetoresistance in the antiferromagnetic material $BaMn_2Pn_2$ (*Pn*: As, Sb, Bi) [4] that is cllasified to specific magnetic point group, that is odd for both space inversion and time reversal operation similar to antiferromagnetic materials refered in [1,2], predicted to drive some intriguing physical phenomena such as inverse spin galvanic effect [3]. Their magnetoresistance become significant, whose sign changes depending on temperature and strength of magnetic field, when the magnetic field applid perpendicular to AFM ordering [5]. Although the relationship between this magnetoresistance and theoretical analysis of symmetry is unclear, no siguniture of phase transition in other physical properties i.e. heat capacity and magnetization under strong magnetic field suggests that magnetoresistance in $BaMn_2Pn_2$ is not caused by conventional magnetic field induecd phase transition such as spin-flop transition.

In the session, I show the details of these data and discussed some possibilities of magnetoresistance.

[1] P. Wadley, B. Howells, J. Železný et al., Science 351, 587 (2016).
[2] S. Y. Bodnar, Šmejkal et al., Nature Communications 9, 348 (2018).
[3] H. Watanabe and Y. Yanase, Phys. Rev. B 96, 064432 (2017).
[4] K.-K. Huynh, T. Ogasawara et al., Phys. Rev. B 99, 195111 (2019).
[5] T. Ogasawara, K.-K. Huynh et al., ArXiv:2010.00807 [Cond-Mat] (2020).

Effect of the Alkyl Linker of Thiazole Orange Base Surrogate in the Peptide Nucleic Acid-DPQ Conjugate on the Binding and Fluorescence Sensing of the Promoter Region of Influenza A Virus RNA

Okeke Chioma Uche, Hiromasa Miura, Yusuke Sato, Seiichi Nishizawa

* Department of Chemistry, Graduate School of Science, Tohoku University, Sendai, Japan

New class of drug candidates targeting the influenza A virus (IAV) has been highly desirable considering the emergence of drug resistant IAV strains. In this context, much attention has been paid to RNA-binding molecules for the promoter region of IAV RNA as this region is not involved in the genetic variations associated with pathogenesis and antiviral resistance. In an early attempt, aminoglycosides antibiotics were shown to work as useful binders. However, given some inherent problems such as promiscuous binding to various RNA structures and the risk of adverse effects, their clinical use would be severely limited. We recently developed the conjugate of triplex-forming peptide nucleic acid (TFP) carrying thiazole orange (TO) base surrogate with small molecule (DPQ) as the promising candidates for the promoter region. Here, TFP unit can recognize the double-stranded structure. Meanwhile, DPQ unit can bind selectively to the internal loop of the promoter region. The binding of the conjugate can be monitored by the light-up response of TO base surrogate that is connected with the peptide nucleic acid (PNA) backbone through an acetyl linker. This conjugate was demonstrated to strongly and selectively bind to the IAV RNA promoter region.

In this work, we examine the effect of TO base surrogate on the binding and fluorescence functions of the conjugate for IAV RNA promoter region. Based on our previous findings, we explored the use of a propyl linker in the conjugate. TO base surrogate in the conjugate was almost non-fluorescent, but its fluorescence was greatly enhanced upon binding to the model RNA containing the promoter region, although the light-up response is moderate compared to the acetyl-linker containing conjugate that was previously developed by us. This can be explained by the intercalation of the TO unit into the triplex structure that can be formed between the target RNA and the TFP unit of the conjugate. However, we found that the conjugate carrying the propyl linker showed the enhanced binding affinity for target RNA compared to the acetyl linker-containing one. These results indicate the favorable effect of the propyl linker on the binding affinity of the conjugate for the IAV RNA promoter region. Further details of the present conjugates will be discussed in the presentation.

[1] T. Sato, Y. Sato, and S. Nishizawa, J. Am. Chem. Soc. **138**, 9397-9400 (2016).
[2] M.-K. Lee, A. Bottini, M. Kim, M. F. Bardaro Jr., Z. Zhang, M. Pellecchia, B.-S. Choi, and G. Varani, Chem. Commun. **50**, 368-370 (2014).
[3] T. Sato, Y. Sato, and S. Nishizawa, Chem. Eur. J. **23**, 4079-4088 (2017).

P-68

Fabrication of Type 304L Stainless Steel Containing Mo-rich Phases By Spark Plasma Sintering and Its Corrosion Resistance in 0.1 M NaCl

Haruka Saito [1*], Izumi Muto [1] and Yu Sugawara [1]

[1] Department of Materials Science, Tohoku University, 6-6-02, Aza-Aoba, Aramaki,
Aoba-ku, Sendai 980-8579, Japan

It is well known that the corrosion resistance of stainless steels is improved by addition of Mo [1]. The role of Mo has been investigated for long time. It was proposed that Mo forms Mo-oxides and inhibits corrosion attack [2]. In addition, it is suggested that Mo changes the structure of the Cr oxide layers on stainless steels [3].

In this study, we fabricated type 304L containing Mo-rich phases by Spark Plasma Sintering (SPS), and the corrosion resistance was assessed in 0.1 M NaCl.

Type 304L containing Mo-rich phases was fabricated by SPS. As the starting materials, pure Mo powders and type 304L stainless steel powders were used. Table 1 shows the chemical composition of type 304L powders. Sintering was performed at 1373 K for 20 min. After sintering, the specimen was heat-treated at 1573 K for 5 h and quenched in water. After that, the solution treatment (1373 K, 30 min) was conducted and water quenched. The specimen surface was polished down to 1 μm using a diamond paste. Sintered type 304L and type 316L were used as reference materials. The same SPS procedure and solution treatment (1373 K, 30 min) were applied to prepare those.

The surface of type 304L containing Mo-rich phases was inspected using an optical microscope. specimens were also analyzed using a scanning electron microscope (SEM) equipped with an electron probe micro analyzer (EPMA).

Potentiodynamic polarization was conducted in 0.1 M NaCl. Specimens were covered by epoxy resin, with the exception of the electrode area (5 mm × 5 mm).

On the basis of the surface observations, it was suggested that the steel matrix of type 304L containing Mo-rich phases is austenite, but many voids were generated. Mo-rich phase were observed on the entire surface.

In polarization measurements, the passive current density of type 304L containing Mo-rich phases and type 316L was unstable, because of the presence of voids. However, the pitting potentials of type 304L containing Mo-rich phases were higher than those of type 316L. The existence of Mo-rich phases inhibited pitting growth.

[1] M. Nishimoto, I. Muto, Y. Sugawara, and N. Hara, *J.Electrochem.Soc.*, **166**(11) (2019), C3081-C3089.
[2] K. Hashimoto, K. Asami, and K. Teramoto, *Corros. Sci.*, **19** (1979), 3-14.
[3] M. F. Montemor, A. M. P. Simões, M. G. S. Ferreira, M.D.C. Belo, *Corros. Sci.*, **41** (1999), 17-34.

Table 1 Chemical composition of type 304L gas atomized powders (mass%)

C	Si	Mn	P	S	Ni	Cr	Mo	Cu	Ti	Al	Nb
0.01	0.22	0.17	0.012	0.0025	11.13	19.01	0.01	0.01	0.001	0.002	0.007

Elucidation of the Initiation of Pitting Corrosion and the Growth of Filiform Corrosion of AZ91D Die-cast Mg Alloy

Shao Zheng[1 *], Muto Izumi[1], Sugawara Yu[2]

[1]Tohoku University Graduate School of Engineering,6-6, Aramaki Aza Aoba, Aoba-ku, Sendai, Miyagi 980-8579, Japan

[2] Tohoku University Graduate School of Engineering,6-6, Aramaki Aza Aoba, Aoba-ku, Sendai, Miyagi 980-8579, Japan

1 Introduction

Mg-Al-Zn alloys such as AZ91 (Mg-9% Al-1% Zn) are very lightweight, and expected to be used in transportation equipment (*e.g.*: automotive and aerospace). Mathieu *etal.* studied the effect of elements and phase compositions of AZ91 alloy on corrosion behavior 1)-2), and they revealed that the content of aluminum and the distribution of $Mg_{17}Al_{12}$ have the significant effect on the corrosion resistance of the alloy. However, the corrosion mechanism is still not perfectly figured out. In this study, the aim is to elucidate the initiation of localized corrosion of die-cast AZ91D.

2 Experimental

2.1 Macro-scale electrochemical measurements

Open circuit potentials and potentiodynamic polarization curves were measured at 298 K. The specimen surfaces were coated with an epoxy resin and subsequently with paraffin. Measurements were performed in a conventional three-electrode cell: the counter electrode was a Pt wire, and the reference electrode was Ag/AgCl (3.33 M KCl). The electrolyte used were naturally aerated 0.1 M and 0.01M NaCl (pH 8.0, adjusted with NaOH). The size of the electrode area was *ca.* 1cm^2.

2.2 Micro-scale electrochemical measurements

To elucidate the pit initiation sites, potentiodynamic polarization curves for a small electrode area for AZ91D die-cast were measured. The electrode area was *ca.* 0.25 mm^2 or *ca.* 0.01 mm^2. The specimen surfaces, with the exception of the electrode area, were masked with a silicone sealant, and the sealant was dried for 24 h. To preserve the electrolyte, a small acrylic cell was put on the specimen. Before the potentiodynamic polarization, the reference and counter electrodes were connected with a small droplet of the electrolyte. The electrolyte used were naturally aerated 0.1 M NaCl (pH 5.46) and 0.01M NaCl (pH 8.0, adjusted with NaOH). After polarization, corrosion morphology was characterized using a laser microscope, optical microscope, and FE-SEM.

3 Conclusion

In macro-scale measurements, the open circuit potential was approximately -1.5 V but oscillating during the immersion. The oscillations were due to the competition of corrosion initiation and repassivation. After immersion, it was observed that filiform corrosion occurred.

In micro-scale polarization, regardless of the size of the sample area, pitting tended to occur underneath the coating. The discoloration occurred on the eutectics. Some eutectics discolored, and some did not transform. The discolored eutectics might be close to the grain boundaries. The initiation of pitting was seen at the eutectic phase adjacent of β phase. Pitting caused the initiation of filiform corrosion. After the pit initiation, hydrogen gas bubbles were generated. During the growth of filiform corrosion, hydrogen was also continuously produced.

[1] S. Mathieu, C. Rapin, J. Steinmetz, and P. Steinmetz, Corros. Sci. **45**, 27412755(2003)

[2] Y. Li, T. Zhang, F. Wang, Electro Acta, **51**, 28452850(2006)

P-70

Oxidation Mechanism of the Unsaturated Phospholipid Monolayer in the Low-level Ozone Studied by HD-SFG

Chunji TAKADA, Ken-ichi INOUE, Aimin GE and Shen YE

Department of Chemistry, Graduate School of Science, Tohoku University, Japan

Pulmonary surfactant is known to reduce the surface tension at air-water interface of the alveoli. Both saturated and unsaturated phospholipids are included in the pulmonary surfactant and play essential roles in lung function. Ozone is one of the most oxidative compounds and exists in ambient air at a low-level (20~40 ppb). During respiration, ozone reaches the alveoli and reacts with pulmonary surfactant. In our previous study, it was found that the unsaturated alkyl chain of phospholipids was selectively oxidized in the low level ozone by using conventional sum frequency generation (SFG) spectroscopy and Langumuir monolayer technique. SFG spectroscopy (Fig. 1) provides information of molecular structure on the interface at molecular level while Langmuir monolayer technique does macroscopic information of the monolayer by measuring π-A isotherms (surface pressure-area per molecule).[1,2] However, the results could not give enough information to identify the oxidized compounds and their amount. This is because conventional SFG can only provide the square of the second-order nonlinear susceptibility, $\left|\chi^{(2)}\right|^2$ information. Since $\left|\chi^{(2)}\right|^2$ is heavily distorted due to the interference among the resonant peaks, the accurate interpretation is very difficult. In the present study, heterodyne-detected sum frequency generation spectroscopy (HD-SFG) was used to measure the imaginary part of $\chi^{(2)}$ which directly reflects the vibrational resonance and can be interpreted more straightforwardly. In *situ* HD-SFG study revealed that the unsaturated phospholipid, 1-palmitoyl-2-oleoyl-glycero-3-phosphocholine (POPC) was rapidly decomposed by the low-level (20~40ppb) ozone and the oxidized compounds from POPC were mostly consist of 1-palmitoyl-2-(9'-oxononanoyl)-*sn*-glycero-3-phosphocholine (POnPC), in which the C=C bond in an unsaturated alkyl chain of POPC is cleaved and replaced by aldehyde[3]. The mixed monolayer's structure of POPC and a major saturated lipid of pulmonary surfactant (1,2-dipalmitoyl-*sn*-glycero-3-phosphatidyl-choline (DPPC)), which is a better mimic of alveoli's surface, was also examined. The detailed results will be discussed in the poster.

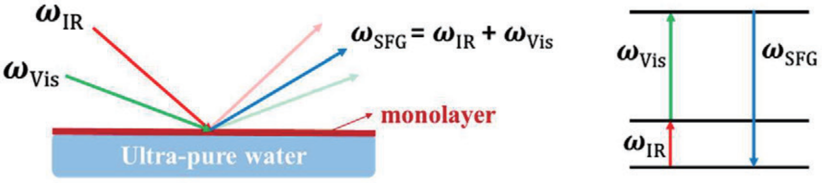

Fig.1 Brief concept of sum frequency generation spectroscopy

[1]L.Qiao, A.Ge, M.Osawa, and S.Ye, *Phys. Chem. Chem. Phys.* 2013, 15, 17775 .

[2]L.Qiao, A.Ge, Y.Liang, and S.Ye, *J. Phys. Chem. B*, 2015, 119, 14188 .

[3] K.Inoue, C.Takada, L.Wan, A.Morita and S.Ye, *J. Phys. Chem. B*, **124**, 5246 (2020)

P-71

Surface oxygen dissociation reaction rates of Co-containing oxides

Toma Tazawa[1*], Yuto Tomura[1], Itaru Oikawa[1] and Hitoshi Takamura[1]

[1] Department of Materials Science, Graduate school of Engineering, Tohoku University*
Sendai 980-8579, Japan
*Email: tazawa@ceram.material.tohoku.ac.jp

While solid oxide fuel cell (SOFC) shows the highest efficiency among fuel cells, there is a serious problem that operating temperature is as high as 750 °C. Oxygen surface exchange reaction, which takes place on cathode surface, is a rate-determining step and prevents SOFC from reducing its operating temperature. It is therefore necessary to develop oxides showing high exchange reaction rates and to understand the reaction mechanism. Co-containing oxides such as BSCF and LSC are well-known oxides with high exchange reaction rates. However, the roles of Co on the surface exchange reaction have not been understood yet. In this study, we prepared Co-doped MgO, which has low defects concentration, and investigate the effects of Co content on oxygen surface exchange reaction, especially dissociation reaction rates. In addition, Ni-doped MgO, which is also a 3d transition metal oxide, was examined.

Co- and Ni-doped MgO were fabricated by the Pechini method and confirmed to be a single phase and cubic rock salt-type structure. A modified pulsed isotopic exchange (PIE) was used to quantitatively evaluate their oxygen surface exchange reaction and dissociation reaction rates [1]. No incorporation of oxygen into Co-doped MgO was observed because of very limited oxygen vacancy due to the donor-type defects, Co^{3+}, on surface. As shown in Fig. 1, dissociation rate increased with increasing concentration of the Co ion. Meanwhile, decrease in activation energy with increasing Co content was confirmed. For Ni-doped MgO, increase in the catalytic activity was observed only in a range of higher concentration of Ni. These trends suggest that not only cations act as activation site on surface, but also their electronic structure strongly affects the catalytic activity.

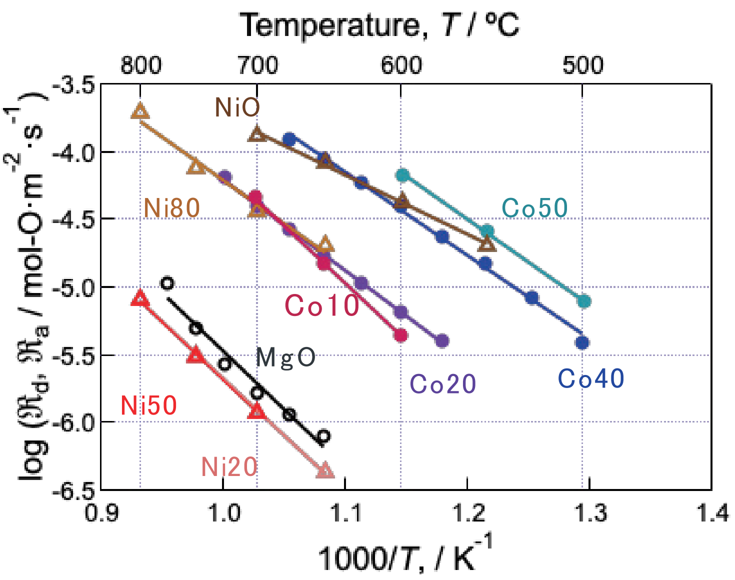

Fig. 1 Arrhenius-type plot of oxygen surface dissociation rates of Co- and Ni-doped MgO

[1] Y. Tomura, T. Tazawa, I. Oikawa and H. Takamura, *J. Mater. Chem. A*, in press.

P-72

Local structure and mixed conductivity of Co-doped $BaZr_{0.9}Sc_{0.1}O_{3-\delta}$

Hiroki Uehara [*], Itaru Oikawa, Hitoshi Takamur

Department of Materials Science, Graduate School of Engineering, Tohoku University,
Sendai 980-8579, Japan, uhiroki@ceram.material.tohoku.ac.jp

Proton-conducting solid oxide fuel cell (pc-SOFC) is expected to be one of the most efficient, highly stable, and cost-effective SOFCs. As a cathode material for the pc-SOFC, a composite cathode system comprising of both electron- and proton-conducting materials has been examined and developed. In such case, the reaction area is limited to the triple phase boundary, and resultant cathode performance is poor. On the other hand, for a mixed proton-hole conductor (MphC), the reaction area will be expanded to the whole surface of cathode; the efficiency of the cell will be significantly enhanced[1]. However, almost no practical MphC material has been developed because the effect of the proton-hole correlation on the carrier conductivity is unclear. In this study, we investigate the effect of proton-hole correlation on mixed conduction from a local structural viewpoint.

To fabricate proton-hole mixed conductor for a pc-SOFC cathode, two kinds of metal were doped to $BaZrO_3$. One is cobalt with valence state +3, which create holes, and the other is lanthanide, Sc, around which protonic defects can be formed [2-4]. $BaCo_xZr_{0.9-x}Sc_{0.1}O_{3-\delta}$ ($x = 0, 0.01, 0.04, 0.1, 0.2$) was prepared by solid-state reaction. All the samples were confirmed to be a single phase and cubic perovskite structure. Thermogravimetric analysis was carried out under dry/wet N_2 to calculate the amount of proton in the sample. Co-doped samples showed lower proton content than that of a sample without Cobalt. The main carrier was suggested to be hole based on EMF and P_{O2} dependence of total conductivity. The conductivity of $x = 0.04$ sample under wet Ar was higher than the conductivity under dry Ar whereas the conductivity measured under dry oxidizing atmospheres was higher than that under wet atmospheres. This implies that the conductivity is decreased by proton introduction when the hole concentration is high. ^1H and ^{45}Sc magic angle spinning (MAS) nuclear magnetic resonance (NMR) spectroscopy were carried out for $x = 0.01$ and 0.04 samples annealed under wet Ar/O_2 or vacuum condition. It was suggested that proton was incorporated in all of the samples annealed under wet atmospheres. Comparing the ^{45}Sc MAS NMR spectra of samples annealed under wet Ar and O_2, it was implied that the proton amount in the sample decreases when hole concentration of sample increases (P_{O2} of heat-treatment condition increases), in spite of constant Sc concentration ([Sc] = 0.1). In summary, it is suggested that proton-hole correlation appears to have a negative effect on both hole and proton conduction. In order to decrease the correlation, separation of proton/hole conducting path is important for development of practical proton-hole mixed conducting materials for pc-SOFC cathode.

[1] E. Fabbri, A. Magrasó, and D. Pergolesi, MRS Bull. **39**, 792 (2014).
[2] V.P. Gorelov, V.B. Balakireva, Y.N. Kleshchev, V.P. Brusentsov, Inorg. Mater. 37 (2001) 535-538.
[3] I. Oikawa and H. Takamura, Chem. Mater. 27 (2015) 6660-6667.
[4] Y. Rao, S. Zhong, F. He, Z. Wang, R. Peng, Y. Lu, Int. J. Hydrog. Energy 37 (2012) 12522-12527.

Black Titanium Oxynitride Thin Films Prepared by Ion-Beam-Assisted Pulsed Laser Deposition

Mina Yamaguchi, Akihiro Ishii, Itaru Oikawa, Hitoshi Takamura

Department of Materials Science, Graduate School of Engineering, Tohoku University,
Sendai, Japan, mina.yamaguchi.q1@dc.tohoku.ac.jp

Preference for a classy black turn-off appearance and for distinct dark colors on flat-panel displays has led to a high demand for optically black materials. The black materials are required to have a large optical density (i.e. high magnitude of absorbance), have absorption which is less wavelength-dependent in the visible range ($\lambda = 400$–700 nm), and also be homogeneous at the micro scale to avoid light scattering. It is difficult to satisfy these three requirements simultaneously. In this study, we focused on the Ti-O-N materials since the flat and constant absorption in visible range can be expected due to coexisting of both of interband absorption (cf. nitrogen doping in TiO_2) and free-carrier absorption (cf. TiN).

Titanium oxynitrides and tungsten-doped oxynitrides were prepared using nitrogen plasma assisted pulsed laser deposition, and their optical absorption properties were investigated. A selection of Ti-O-N films were prepared with different compositions by controlling the emission current (I_e) and discharge voltage (V_d) of the ion source. It was found that the nitrogen content of the $Ti(O,N)_x$ could be adjusted by controlling the I_e. The large, flat absorption coefficient of approximately 40 μm^{-1} in the visible range (400–700 nm) attained for the samples deposited at high V_d (300 V) was attributed to tungsten doping from a W filament in the ion source. The 4.1 mol%W-doped $Ti(O,N)_x$, which had a rock-salt-type structure, was optically jet-black. The origin of the flat wavelength dispersion in the W-doped $Ti(O,N)_x$ was attributed to the coexistence of semiconducting absorption and metallic absorption mechanisms. DFT calculations suggest that the 5d states achieved when using doped tungsten provide high absorption in the mid-wavelength range, whereas undoped- $Ti(O,N)_x$ was characterized by weak absorption.

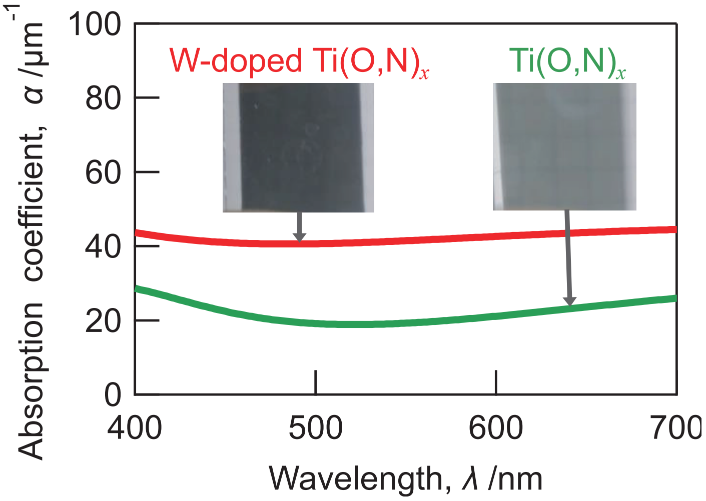

Fig. 1. Absorption coefficient of the undoped and tungsten doped titanium oxynitride thin films and the appearances

[1] M. Yamaguchi, A. Ishii, I. Oikawa and H. Takamura Applied Surface Science. **534**, 147616 (2020).

P-74

Synthesis of anti-ThCr_2Si_2-type La_2O_2Bi epitaxial thin film by multilayer solid-phase epitaxy method

Yuki Yamamoto[1], Hideyuki Kawasoko[1] and Tomoteru Fukumura[1,2]

[1] Department of Chemistry, Graduate School of Science, Tohoku University
[2] WPI-Advanced Institute for Materials Research (WPI-AIMR) and Core Research Cluster, Tohoku University

Anti-ThCr_2Si_2-type RE_2O_2Bi (RE = rare earth) composed of Bi square nets and RE_2O_2 layers shows metal-insulator transition by substituting RE elements, and La_2O_2Bi is an insulator [1]. Recently, La_2O_2Bi bulk polycrystals have demonstrated metallic conduction with high hole mobility by expanding *c*-axis length via excess oxygen intercalation [2]. Accordingly, highly crystalline La_2O_2Bi is intriguing for the further development of the transport properties. In this study, we synthesized La_2O_2Bi epitaxial thin films by multilayer solid-phase epitaxy method.

Multilayer precursors were deposited on MgO(001) substrate at room temperature by magnetron sputtering in Ar gas atmosphere. The structure of multilayer precursors was $[\mathrm{Bi}\ (3.0\ \mathrm{nm}) / \mathrm{La}\ (7.2\ \mathrm{nm})]_{10}$ (nominal composition: $La_{2.0}Bi_{1.0}$) with Si_3N_4 capping layer (4 nm). Subsequently, the multilayer precursors were *in situ* heated at 750 °C, 850 °C and 950 °C for 11 minutes in the Ar gas atmosphere.

From X-ray diffraction θ-2θ measurements, $00l$ oriented La_2O_2Bi was synthesized at all heating temperatures in addition to La_2O_3 and Bi impurities (Fig. 1), indicating that the oxidation reaction was caused by residual oxygen. The epitaxial growth of La_2O_2Bi thin films was confirmed by ϕ scan measurement. The *c*-axis length of La_2O_2Bi epitaxial thin films was linearly expanded from 13.934 Å to 13.995 Å with increasing heating temperature (Fig. 2), suggesting that high heating temperature realized large amount of excess oxygen. The full width at half maximum (FWHM) of rocking curve for the 006 diffraction of La_2O_2Bi monotonically decreased from 1.9° to 0.9° with increasing heating temperature (Fig. 2), indicating that high heating temperature improved film crystallinity. In the poster, we will discuss film synthesis using other structure precursors.

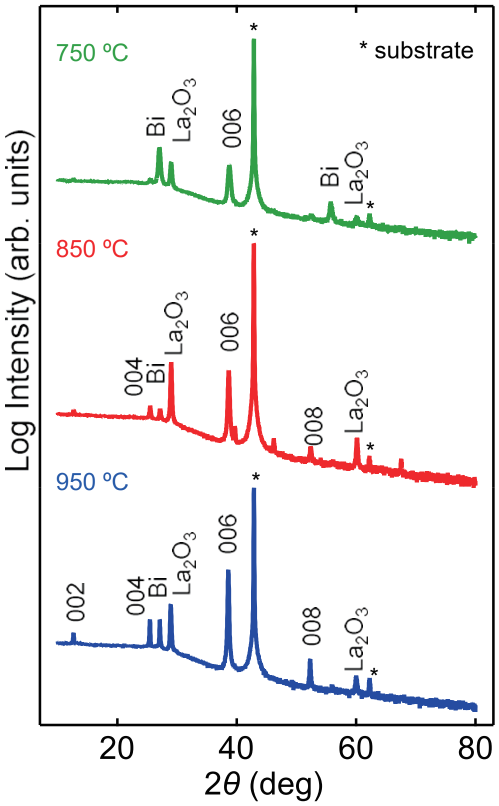

Fig. 1. X-ray diffraction θ-2θ patterns of thin films after heating treatment.

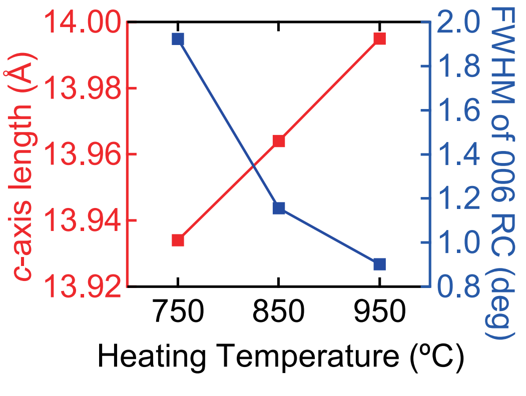

Fig. 2. Heating temperature dependence of *c*-axis length and FWHM of rocking curve (RC) for La_2O_2Bi epitaxial thin films.

[1] H. Mizoguchi *et al.*, *J. Am. Chem. Soc.* **133**, 2394 (2011).
[2] K. Matsumoto *et al.*, *Appl. Phys. Lett.* **116**, 191901 (2020).

Tohoku University

2-1-1 Katahira, Aoba-ku, Sendai, Miyagi, 980-8577, Japan
Phone: +81-22-217-5971
Fax: +81-22-217-5129

Symposium Secretariat
International Affairs Center(IAC）

iac@grp.tohoku.ac.jp
https://www.wpi-aimr.tohoku.ac.jp/iac/indexE.html